

Cronin effect and high- p_{\perp} suppression in the nuclear gluon distribution at small x

E. Iancu, K. Itakura, and D. N. Triantafyllopoulos

*Service de Physique Théorique, CEA/DSM/SPhT, 91191 Gif-sur-Yvette Cedex,
France*

Abstract

We present a systematic, and fully analytic, study of the ratio \mathcal{R}_{pA} between the gluon distribution in a nucleus and that in a proton scaled up by the atomic number A . We consider initial conditions of the McLerran–Venugopalan type, and quantum evolution in the Color Glass Condensate, with both fixed and running coupling. We perform an analytic study of the Cronin effect in the initial conditions and point out an interesting difference between saturating effects and twist effects in the nuclear gluon distribution. We show that the distribution of the gluons which make up the condensate in the initial conditions is localized at low momenta, but this particular feature does not survive after the quantum evolution. We demonstrate that the rapid suppression of the ratio \mathcal{R}_{pA} in the early stages of the evolution is due to the DGLAP-like evolution of the proton, whose gluon distribution grows much faster than that in the nucleus because of the large separation between the respective saturation momenta. The flattening of the Cronin peak, on the other hand, is due to the evolution of the nucleus. We show that the running coupling effects slow down the evolution, but eventually lead to a stronger suppression in \mathcal{R}_{pA} at sufficiently large energies.

Contents

1	Introduction	3
2	Cronin effect in the initial conditions	12
2.1	Generalities	12
2.2	The McLerran–Venugopalan model: Fixed & running coupling	15
2.3	Cronin effect in the McLerran–Venugopalan model	23
2.4	A sum rule and its consequences	27
3	Non-linear gluon evolution in the Color Glass Condensate	32
3.1	Non-linear evolution at low k_{\perp} : Saturation and universality	33
3.2	Linear evolution at high k_{\perp} : Fixed coupling	34
3.3	Linear evolution at high k_{\perp} : Running coupling	42
4	High- k_{\perp} suppression from quantum evolution: The general argument	47
4.1	A general argument on the y -dependence	48
4.2	A general argument on the k_{\perp} -dependence	51
4.3	A general argument on the A -dependence	52
5	The evolution of the Cronin peak with increasing y	53
5.1	The suppression of the peak: Fixed coupling	54
5.2	The suppression of the peak: Running coupling	58
5.3	The flattening of the Cronin peak	62
6	High- k_{\perp} suppression in the nuclear gluon distribution at small x	68
6.1	Fixed coupling	69
6.2	Running coupling	74
A	Appendix	79
	References	84

1 Introduction

Motivated especially by the recent experimental results for gold–gold (Au–Au) [1, 2] and deuteron–gold (d–Au) collisions at RHIC [3–6], there is currently a large interest in the physics of collective phenomena in the wavefunction of an energetic nucleus, which could explain, for instance, why the gluon distribution of a large nucleus (with atomic number $A \gg 1$) is not simply the incoherent sum of the gluon distributions of the A constituent nucleons. For sufficiently high energies (and, marginally at least, also for the energies at RHIC), one expects these collective phenomena to be associated with non–linear effects favored by the high gluon density, which rises rapidly with the energy, and also with A [7–12]. Thus, these effects are expected to be more pronounced in a (large) nucleus as compared to a proton, and this difference should be particularly important at not so high energies, where the proton is still in a linear regime.

This difference could explain some of the remarkable regularities observed in the results for d–Au collisions at RHIC, like the Cronin enhancement in particle production at central rapidity ($y = 0$) [3], and the ‘high- k_{\perp} suppression’ in the particle yield at ‘forward rapidities’ ($y = 2 - 3$ in the deuteron fragmentation region) [4–6]. Specifically, the Cronin peak [13] can be understood as the result of Glauber–like multiple scattering off the gluon distribution produced by uncorrelated “valence quarks” [14] (as described, e.g., by the McLerran–Venugopalan model [10], see also [15]), whereas the high- k_{\perp} suppression can result from non–linear effects in the quantum evolution with increasing energy [16]. (See also [17] for alternative interpretations of these results.) On the other hand it is most likely that a similar suppression seen in Au–Au collisions at central rapidity [2] is due to jet quenching through final state interactions [18].

More precisely, the experimental results are used to construct the ratio $R_{dAu}(k_{\perp}, y)$ between the number of particles produced in a d–Au collision (with a given transverse momentum k_{\perp} and at a given rapidity y) and the corresponding number for a proton–proton collision scaled up by the number of collisions. The deviation of this ratio from one — like a Cronin peak ($R_{dAu} > 1$ at intermediate momenta), or the high- k_{\perp} suppression ($R_{dAu} < 1$ at generic, hard, momenta) — can be attributed to the difference between the gluon spectrum (or “unintegrated gluon distribution”) in the nucleus, and that in the proton scaled up by A . In turn, this difference is measured by the ratio:

$$\mathcal{R}_{pA}(k_{\perp}, y) \equiv \frac{\varphi_A(k_{\perp}, y)}{A^{1/3} \varphi_p(k_{\perp}, y)}, \quad (1.1)$$

between the gluon occupation factors (see Eq. (2.1)) in the nucleus and the proton¹.

¹ Our conventions are such that the more standard “unintegrated gluon distribution” is equal

Previous studies in the literature show that it is indeed possible to compute the cross-section for particle production in terms of the gluon distributions in the target and the projectile [7, 14, 19–22], and, moreover, any qualitative trend seen in the ratio (1.1) of the gluon distributions gets transmitted to the corresponding ratio for the cross-sections [16, 23–25], which is the quantity relevant for RHIC.

Motivated by this observation, and also by the conceptual importance of the ratio (1.1) as a direct measure of collective effects in the nuclear wavefunction, we shall devote this work to a systematic analysis of this quantity within the effective theory for the Color Glass Condensate (CGC) [26], which is the appropriate framework to describe non-linear effects in the gluon distribution within QCD.

Although inspired by the RHIC phenomenology, our analysis does not aim to the description of the data (for such attempts, see e.g. [27, 28]), but is rather oriented towards the fundamental understanding of phenomena like the emergence of the Cronin peak in the ratio \mathcal{R}_{pA} and the suppression of this peak with increasing energy. Our main objective is to present a calculation for such phenomena from **first principles**, and which is **fully analytic**. These requirements entail strong constraints on the kinematical range which is accessible to our analysis, and also a significant loss of accuracy, due on the one hand to the limited accuracy of the perturbative framework that we shall use, and on the other hand to the additional approximations that we shall perform within this framework, to allow for analytic calculations. In particular, our focus on the gluon distribution, rather than on the cross-section for multiparticle production, is also motivated by the requirement of (analytic) calculability, together with our concern to avoid theoretical uncertainties as much as possible.

As already mentioned, our theoretical framework will be the CGC effective theory [10, 26, 29–36] (see also [11, 12] for recent review papers), which is a lowest-order (in α_s) formalism in QCD, although obtained after elaborate resummations: These resummations include only those diagrams of perturbative QCD in which the powers of α_s are enhanced by either large logarithms of the energy (i.e., by powers of $y \sim \ln s$), or by high density effects (e.g., by the gluon occupation factor, which at saturation is of order $1/\alpha_s$). Still, it should be emphasized that this formalism becomes more and more accurate with increasing energy because, first, it does include the leading effects at large y , and, second, the **saturation momentum** $Q_s(y)$ — the typical momentum of the gluons which make the condensate — increases very fast with y [7, 37–42], so the relevant coupling constant decreases at high energy: $\alpha_s(Q_s(y)) \propto 1/\sqrt{y}$ at large y . Thus, the results that we shall obtain here represent the actual prediction of QCD for sufficiently large y .

This discussion also shows that the inclusion of running coupling effects in the formalism is crucial in order for the asymptotic freedom of QCD to become operative at high energies.

to $S_A \varphi_A(k_\perp, y)$, with S_A the area of the nuclear disk.

The running of the coupling is a higher order effect in α_s , so its inclusion in a leading order formalism is by definition ambiguous. But physical intuition about the typical scales involved in the interactions, and also the experience with BFKL equation [43] — which in the context of the CGC formalism is the linear equation describing the approach towards saturation, and is presently known to next-to-leading order in α_s [44, 45] —, will permit us to effectively use a one-loop running coupling, with the scale for running set either by the gluon transverse momentum k_\perp , or by the saturation momentum.

As mentioned above, another source of accuracy loss are the further approximations needed to make the CGC formalism tractable via analytic calculations. Whereas the initial condition that we shall use at low energy — namely, the McLerran–Venugopalan model [10] — is sufficiently simple to allow for exact (analytic) calculations, the subsequent evolution with increasing y is described by complicated non-linear equations which couple n -point correlations with any number of points n [26, 32, 34]. This is similar to the infinite hierarchy of Schwinger–Dyson equations, and within the CGC theory it can be summarized into a closed functional equation for the generating functional of the correlations [26, 31, 34], also known as the JIMWLK equation. Exact numerical solutions to this functional equation have recently become available [46], but these are still difficult to handle, so most numerical analyses (including that of the \mathcal{R}_{pA} -ratio in Ref. [25]) have instead focused on a simpler non-linear equation, the Kovchegov equation [33], which is a kind of mean field approximation to the general JIMWLK equation [47, 48], and is expected to work reasonably well for a large nucleus at not so high energies (for numerical analyses of the Kovchegov equation, see [49–52]).

But whereas the numerical calculations are undoubtedly important, they cannot fully supplant the analytic studies as far as our physical insight and fundamental understanding are concerned. The numerical results in Ref. [25] have revealed very interesting features — notably, an extremely fast suppression of the ratio $\mathcal{R}_{pA}(k_\perp, y)$ at generic momenta with increasing y , and also the complete disappearance of the Cronin peak after only a short evolution —, but these observations have also raised new questions, since the precise mechanism behind such a rapid evolution has remained unclear. In particular, it was not clear whether the two effects alluded to above (the high- k_\perp suppression and the flattening of the Cronin peak) were caused by the same mechanism, or not. Also, the specific roles played by the proton and by the nucleus during evolution have not been elucidated.

The previous analytic investigations in the literature appeared before the numerical results in Ref. [25], and cannot fully explain the latter. For instance, while the arguments in Refs. [16, 24] do explain the suppression at relatively large y and for high k_\perp , they cannot explain why this suppression is so rapid in the early stages of the evolution, or why the Cronin peak flattens out so fast. Indeed, the approximations used in these previous studies do not apply for transverse momenta in, or near, the nuclear saturation region, nor for very small values of y . Besides, running coupling effects have never been considered in

the previous studies, either analytic or numerical. As we shall see, these effects lead to important changes, especially for the evolution at late stages. More generally, what seems to be still missing is a coherent, qualitative and quantitative, picture explaining what are the specific features of the MV model which imply the emergence of a well pronounced peak at low energies, and also what are the generic features of the quantum evolution which lead to the rapid flattening of this peak and to a general suppression in the ratio \mathcal{R}_{pA} at all non-asymptotic momenta.

Our subsequent analysis is intended to fill this gap, through a systematic study of the ratio \mathcal{R}_{pA} in the MV model and of its evolution with y , for both fixed and running coupling. Being systematic, our analysis has necessarily some overlap with previous studies in the literature, especially with Ref. [24], with which we share some results and conclusions, notably about the high- k_{\perp} suppression. In our opinion, what distinguishes the present analysis from such previous investigations, in addition to its aim to completeness and the treatment of the running coupling case, is the constant effort towards elucidating the fundamental reasons for the observed behavior, and also the use of a coherent scheme of approximations, which will be carefully justified, and whose limitations will be discussed.

In what follows, we shall briefly describe the picture which emerges from these calculations when increasing y from $y = 0$, and at the same time present the structure of the paper :

i) Initial conditions at $y = 0$: Cronin peak in the MV model (cf. Sect. 2)

Although a Cronin peak in the ratio $\mathcal{R}_{pA}(k_{\perp})$ has been clearly seen in numerical simulations of the MV model [22–25, 53, 54], its analytic study has been hindered so far by the non-linear aspects of the problem, which must be treated exactly. In Sect. 2, we shall present a complete, analytic, study of the nuclear gluon distribution in this model, which will enable us to compute the magnitude and the location of the peak, and clarify the conditions for its existence: The emergence of a well pronounced peak in the MV model reflects the peculiar redistribution of gluons in transverse phase space, under the influence of the non-linear effects responsible for saturation. In turn, this issue has two aspects:

The very existence of a peak can be anticipated on the basis of very general arguments (like the sum rule introduced in Ref. [24]; see also Refs. [23, 25] and Sect. 2.4 below), which reflect two basic properties of the MV model: (a) the fact that the gluon distribution saturates, at a value of order $1/\alpha_s$, for low momenta $k_{\perp} \leq Q_s(A)$, and (b) the fact that, at large momenta $k_{\perp} \gg Q_s(A)$, the nuclear gluon distribution is simply the incoherent sum of the individual distributions of the A nucleons (so that $\mathcal{R}_{pA}(k_{\perp}) \rightarrow 1$ when $k_{\perp} \rightarrow \infty$). As we shall see in Sect. 2.3, these two properties alone imply the existence of a peak at intermediate momenta. The height of the peak is of order $\rho_A \equiv \ln Q_s^2(A)/\Lambda_{\text{QCD}}^2 \sim \ln A^{1/3}$, and thus is parametrically enhanced at large A .

Moreover, the fact that the peak is so pronounced, and located in the vicinity of the saturation

momentum $Q_s(A)$, is the consequence of the fact that the distribution of the saturated gluons which make up the condensate is **compact**, in the sense that it **vanishes exponentially at momenta above the saturation scale**. This feature has not been recognized in previous studies of the MV model. Of course, on top of this compact distribution there is also a **power-law tail**, which represents the sum of the ‘twist’ contributions usually mentioned when discussing the high- k_\perp behavior of the distribution. But as we shall see, for momenta $k_\perp \lesssim Q_s(A)$, the sum of the twist terms is **parametrically suppressed at large A** as compared to the compact distribution which represents the condensate. Because of that, the overall distribution has a rapid, exponential, fall-off at momenta just above $Q_s(A)$, leading to the pronounced peak seen in numerical simulations [22, 23, 25, 53, 54].

ii) $y > 0$: Non-linear quantum evolution in the CGC (cf. Sect. 3)

In Sect. 3 we shall present our approximations to the solution to the non-linear equations which describe the evolution of the gluon occupation factor with y .

In the saturation region at low momenta, physics is fully non-linear, but for $k_\perp \ll Q_s(A, y)$ the solution can be constructed in a mean field approximation [35, 36]. The result is an universal, and slowly varying, function of $z \equiv k_\perp^2/Q_s^2(A, y)$: $\varphi_A \propto (1/\alpha_s) \ln 1/z$ for $z \ll 1$ [35–37, 55]. The solution in the transition region around $Q_s(A, y)$ is not known in general (see however Sect. 5.3), but we do know that, along the **saturation line $k_\perp = Q_s(A, y)$** , φ_A is constant and of order $1/\alpha_s$.

At high momenta $k_\perp \gg Q_s(A, y)$, the gluon density is low, and the general evolution equations reduce to the BFKL equation [43], which, although linear, is still sensitive to saturation effects, through its boundary conditions [7, 37–41]. The solution to this equation in the presence of saturation has attracted much attention in the recent literature [38–41, 48], where analytic approximations have been constructed for both fixed and running coupling. Here, we shall simply summarize the relevant results, and discuss their range of applicability. Still, a few steps in the construction of these approximations will be outlined, to clarify some subtle points and reveal the generic features of the evolution which will be needed in the subsequent discussion of the ratio \mathcal{R}_{pA} .

We shall quite generally distinguish between two physical regimes, which are described by different approximations: (I) a “DLA” (“double-log accuracy”) regime at very large momenta $k_\perp \gg Q_g(A, y)$, in which the evolution is dominated by the transverse phase-space $\rho(A, k_\perp) \equiv \ln k_\perp^2/Q_s^2(A)$, and (II) a “BFKL regime” within the range $Q_s(A, y) \ll k_\perp \ll Q_g(A, y)$, where physics is linear but influenced by saturation, and the gluon distribution preserves the **geometric scaling** [56] property characteristic of saturation: it depends upon the kinematical variables k_\perp and y only through the ratio $z = k_\perp^2/Q_s^2(A, y)$ [38, 39]. Here, $Q_g(A, y)$ is the “geometric scaling momentum”, which grows faster than the saturation momentum with y , and marks the upper bound of the geometric scaling region [38] (see also [39–41, 48]). With a running coupling, the discussion of the physical regimes becomes

slightly more involved, and will be presented in Sect. 3.3.

The approximations described in this section will be sufficient to study the suppression in the ratio $\mathcal{R}_{pA}(k_\perp, y)$ with increasing y at generic momenta. On the other hand, they are not sufficient to describe the flattening of the Cronin peak (see below).

iii) $y > 0$: The general argument for high- k_\perp suppression (cf. Sect. 4)

In Sect. 4 we shall identify and characterize the general features of the quantum evolution which are responsible for the suppression of the ratio \mathcal{R}_{pA} at generic momenta.

The rapid suppression of the ratio $\mathcal{R}_{pA}(k_\perp, y)$ with increasing y is shown to be the consequence of the strong dissymmetry between the quantum evolution of the nucleus and that of the proton, which in turn reflects the large separation of scales between the respective saturation momenta. Physically, it is so because, for the same values of y and k_\perp , the transverse phase-space available for the evolution, namely $\rho(A, k_\perp) \equiv \ln k_\perp^2 / Q_s^2(A)$, is larger for the proton than for the nucleus (since $Q_s(A) \gg Q_s(p)$). In more technical terms, the proton evolves faster because of general properties of the kernel of the BFKL equation, like the convexity of its eigenvalue $\chi(\gamma)$, which accelerate the evolution with increasing ρ .

Moreover, the **suppression rate** $d \ln \mathcal{R}_{pA} / dy$ is largest at small y and for not so large transverse momenta (as compared to the nuclear saturation momentum), since in this regime the difference between the evolution of the proton and that of the nucleus is most pronounced. This explains the rapid suppression observed in the early stages of the evolution in the numerical results in Ref. [25]: This is the consequence of the DGLAP [57] evolution of the proton (as described here by DLA), while the nucleus evolves comparatively little (except at extremely large momenta).

The general properties of the evolution equations can also be used to show that, for fixed y with $\alpha_s y \gtrsim 1$, the ratio $\mathcal{R}_{pA}(k_\perp, y)$ is **monotonously increasing** with k_\perp . Thus, the Cronin peak flattens out during the first $1/\alpha_s$ units of rapidity.

Another interesting consequence of the evolution is a **reversal in the A -dependence of the ratio \mathcal{R}_{pA} when increasing y** (see also Refs. [23, 24]) : Whereas at $y = 0$, the height of the Cronin peak — and, more generally, the ratio $\mathcal{R}_{pA}(k_\perp)$ at generic momenta around $Q_s(A)$ — is (logarithmically) **increasing** with A , this tendency is rapidly reversed by the evolution: after only a small rapidity increase $\alpha_s y \sim 1/\rho_A$, $\mathcal{R}_{pA}(k_\perp, y)$ becomes a **decreasing** function of A for any k_\perp . This property could be related to a similar change of behavior in the centrality dependence of the ratio R_{dAu} measured at RHIC [4–6].

iv) The flattening of the Cronin peak (cf. Sect. 5)

The evolution of the proton alone produces a rather uniform suppression in the \mathcal{R}_{pA} -ratio at all momenta. Thus, by itself, this cannot wash out any structure present in the initial conditions, like the Cronin peak. Therefore, the disappearance of the peak is necessarily related to the evolution of the nucleus.

In order to study this phenomenon, we shall use the Kovchegov equation to compute the evolution of the nuclear gluon distribution in the first step Δy in rapidity, with $\alpha_s \Delta y \ll 1$. This calculation allows us to follow the evolution of the peak at least up to the rapidity y_0 , with $\alpha_s y_0 \sim (\ln^2 \rho_A)/\rho_A \ll 1$, where the height of the peak becomes of order one. As the calculation shows, the effect of the evolution is to generate power law tails which progressively replace the original exponential tail of the gluon distribution at saturation. Because of that, the peak flattens out, and moves up to larger momenta.

The flattening is related to the difference in the nuclear evolution at momenta below and, respectively, above the saturation momentum $Q_s(A, y)$. For $k_\perp < Q_s(A, y)$, the gluons in the nucleus are saturated, and evolve only slowly. For $k_\perp > Q_s(A, y)$, the nucleus is in the linear, BFKL, regime, and the corresponding gluon distribution increases much faster (although not so fast as the proton distribution at the same k_\perp). Because of this dissymmetry, the Cronin peak gets tilted up, and flattens out very fast. Although we cannot control analytically this evolution until the complete disappearance of the peak, we shall check that the peak has flattened out when $\alpha_s y \sim 1$.

v) High- k_\perp suppression: the detailed picture (cf. Sects. 5 and 6)

In Sect. 6, we shall give the detailed picture of the phenomenon of “high- k_\perp suppression” in the kinematic plane $y - \ln k_\perp^2$. (Previously, a similar analysis will be presented in Sect. 5, but only for the evolution along the nuclear saturation line $k_\perp = Q_s(A, y)$.) In fact, the suppression will be seen to occur at all momenta, and not only at those which are “high” in the sense of the present analysis (and which are such that $k_\perp \gg Q_s(A, y)$). Still, the suppression is stronger for momenta above the proton saturation scale $Q_s(p, y)$ — since this is where the proton evolves faster — but below the nuclear geometric scale $Q_g(A, y)$, since for even larger momenta, both the proton and the nucleus are in the DLA regime, and their respective evolutions almost compensate in the ratio $\mathcal{R}_{pA}(k_\perp, y)$. Thus, not surprisingly, the ratio is found to asymptotically approach one from the below when increasing k_\perp at fixed y . But since $Q_g(A, y)$ increases rapidly with y , it is clear that, for $\alpha_s y \gtrsim 1$, a strong suppression will be visible at all non-asymptotic momenta.

The explicit analysis in Sect. 6 will confirm the general trend of the evolution anticipated in Sect. 4: For generic momenta k_\perp (such that the nucleus is either at saturation, or in the BFKL regime), the suppression in the ratio $\mathcal{R}_{pA}(k_\perp, y)$ is very fast in the early stages of the evolution, when the proton is in the DLA regime, but with increasing y it slows down, and eventually \mathcal{R}_{pA} stabilizes at a very small value, proportional to an inverse power of $A^{1/3}$. Besides, for fixed y (with $\alpha_s y \gtrsim 1$), the ratio is monotonously increasing with k_\perp ,

from a very small value $\sim 1/A^{1/3}$ for $k_\perp \sim \Lambda_{\text{QCD}}$ to $\mathcal{R}_{pA} \simeq 1$ when $k_\perp \rightarrow \infty$.

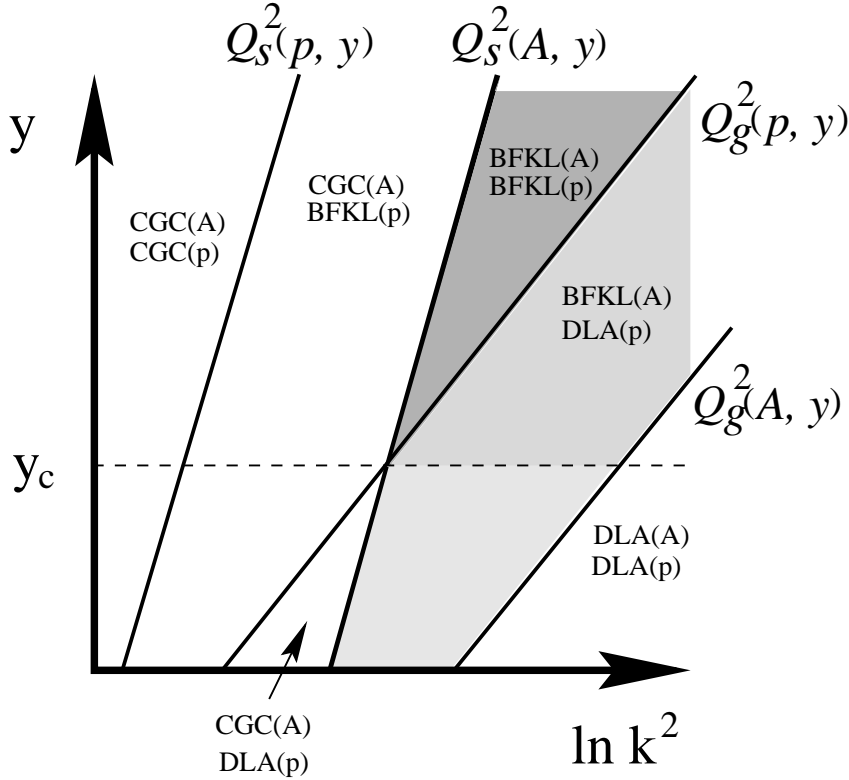


Fig. 1. *Physical regimes for evolution in the kinematic plane $y - \ln k_\perp^2$ (for fixed coupling, for definiteness; see Fig. 10 for the corresponding picture with a running coupling). Both the saturation momentum $Q_s(A)$ and the ‘geometric scale’ momentum $Q_g(y)$ rise exponentially with y (for both the proton and the nucleus), and thus are represented by straight lines in the logarithmic scale of the plot. As visible on this plot, the geometric scale rises faster (its logarithmic slope is roughly twice as large as that of the saturation momentum).*

In order to describe this evolution in more detail, it is convenient to follow a line which is parallel to the saturation line in the kinematic plane $y - \ln k_\perp^2$ (see Fig. 1). That is, we simultaneously increase y and k_\perp in such a way to keep the ratio $z \equiv k_\perp^2/Q_s^2(A, y)$ fixed. If $z = \mathcal{O}(1)$, then when increasing y from zero, the proton starts in the DLA regime, because $Q_g(p, y) \ll Q_s(A, y)$ at sufficiently small y . But with increasing y , $Q_g(p, y)$ grows faster than $Q_s(A, y)$, so at some ‘critical’ value y_c the proton changes from the DLA to the BFKL regime. The value of y_c is however different for fixed or running coupling, and so is also the evolution for larger rapidities $y > y_c$, as we explain now:

(a) With fixed coupling, $\alpha_s y_c \sim \rho_A$, and most of the suppression is achieved already for $y \lesssim y_c$. For $y > y_c$, the suppression slows down significantly because the BFKL evolutions of the proton and of the nucleus almost cancel in the ratio (1.1) (due to the fact that the respective saturation momenta evolve in the same way with y [42]). Thus, at large y , the

ratio $\mathcal{R}_{pA}(z, y)$ decreases only slowly, and eventually stabilizes, when $\alpha_s y \gtrsim \rho_A^2$, at a small value $\mathcal{R}_{pA} \sim 1/(A^{1/3} \rho_A)^{1-\gamma}$, which shows a weak dependence on z . Here, $\gamma \approx 0.63$ is the BFKL saddle point (or ‘anomalous dimension’) near saturation [38, 39].

(b) With running coupling, y_c is parametrically larger, $y_c \propto \rho_A^2$, but the suppression is pursued within a significant range of y above y_c , because in that range the proton and nuclear saturation momenta evolve differently with y [42] : The proton saturation momentum $Q_s(p, y)$ grows initially faster, and catches up with that of the nucleus when $y \sim \rho_A^4$. For larger y , $Q_s(A, y) \approx Q_s(p, y)$, and the ratio stabilizes at the constant value $\mathcal{R}_{pA} \simeq 1/A^{1/3}$ which is even smaller than the corresponding limit for fixed coupling. In fact, this limiting value is simply the factor of $A^{-1/3}$ introduced by hand in Eq. (1.1). This reflects the **universality** of the gluon distribution which, within a wide range of k_\perp , depends upon the hadron species only via the saturation momentum.

It should be also stressed that, although the suppression in \mathcal{R}_{pA} is eventually stronger with running coupling, the evolution leading to this suppression is **slower** in that case, in the sense that it takes a considerably larger interval of rapidity before the final limiting value is reached. Besides, all the intermediate stages of the evolution (like changing from the DLA to the BFKL regime with increasing y at fixed z) require a longer rapidity evolution with a running coupling than with a fixed one.

To conclude this introductory discussion, let us emphasize that all the phenomena discussed so far — the Cronin peak in the initial condition, its disappearance with increasing y , and the high- k_\perp suppression — are **hallmarks of saturation**, which however reflect **different aspects of saturation**, and of the quantum evolution towards saturation : The Cronin peak reflects **classical saturation**, i.e., the saturation via non-linearities in the classical field equations, whereas the color sources in these equations (the ‘valence quarks’) are uncorrelated. (Alternatively, this reflects **incoherent**, Glauber-like, multiple scattering.) This is, of course, the content of the MV model, but it could also be a reasonable approximation for a large nucleus at not so high energies, where the effects of quantum evolution are negligible. Furthermore, the driving force towards both high- k_\perp suppression and the flattening of the Cronin peak is the linear evolution (either DGLAP, or BFKL). But notwithstanding this, these phenomena are still a signal of saturation, since they occur only because of the **mismatch between various regimes of evolution**, which is made possible by saturation : For the flattening of the peak, this is the mismatch between the nuclear evolution below and above the saturation scale, whereas for the high- k_\perp suppression, this is the mismatch between the (linear) evolutions of the proton and of the nucleus, which originates in the difference between the respective saturation momenta.

2 Cronin effect in the initial conditions

2.1 Generalities

By the “unintegrated gluon distribution” we shall more precisely understand in what follows the **gluon occupation factor**, i.e., the number of gluons of given spin and color per unit phase-space in a nucleus with atomic number A :

$$\varphi_A(k_\perp, y) \equiv \frac{(2\pi)^3}{2(N_c^2 - 1)} \frac{dN_A}{dy d^2k_\perp d^2b_\perp}. \quad (2.1)$$

Here, y denotes the rapidity (related to the longitudinal momentum fraction x of the gluons via $y = \ln(1/x)$), k_\perp is the transverse momentum, and b_\perp is the gluon position in transverse space. For simplicity, we shall consider a hadron which is homogeneous in the transverse plane, and we shall suppress the b_\perp -dependence in all the formulae. Within light-cone quantized QCD, the gluon occupation factor (2.1) is related to a gauge-invariant 2-point function of the color fields, which can be computed within the CGC effective theory [12, 26]. More precisely, the evolution of this quantity with y can be computed within perturbative QCD (to the accuracy of the effective theory), but the initial conditions at $y = 0$ remain non-perturbative, and require a model. It turns out that the choice of this model has a strong influence on the physical problems that we would like to address, especially as far as the existence of a Cronin peak [13] is concerned.

Physically, the initial conditions that we are interested in correspond to a large nucleus ($A \gg 1$) in a regime of intermediate energies. The initial energy should be high enough for the gluons with the smallest values of x to be coherent with each other, but low enough for the quantum effects in the gluon distribution to be negligible. These conditions require $x_0 \lesssim 1/A^{1/3}$, but at the same time $\alpha_s \ln 1/x_0 \ll 1$, where x_0 denotes the longitudinal fraction of the slowest gluons within the nucleus at the initial energy. For instance, for a gold nucleus and with $\alpha_s \approx 0.2$, these requirements can be satisfied by choosing $x_0 \sim 10^{-1}$. (From now on, the rapidity variable will be understood to represent the difference from this original rapidity: $y = \ln(x_0/x)$.) Under these conditions, the gluon distribution in the nucleus is simply the result of classical radiation from the valence quarks. But if A is large enough — which is what we assume here —, the resulting gluon density can be still very high, and thus favor non-linear effects which lead to **gluon saturation** at sufficiently low k_\perp , below some characteristic scale $Q_s(A)$.

A simple model which encompasses these physical conditions is the McLerran–Venugopalan (MV) model [10, 12], in which the total color charge in the nucleus is the incoherent sum of the individual color charges of the valence quarks, and the corresponding saturation mo-

momentum scales like $Q_s(A) \sim A^{1/6}$ (since $Q_s^2(A)$ is proportional to the color charge squared per unit transverse area). If A is large enough, this scale is hard ($Q_s^2(A) \gg \Lambda_{\text{QCD}}^2$), and the matter made of the gluons (the CGC) is weakly coupled.

In what follows we shall adopt the MV model as our initial condition at $y = 0$. The remaining part of this section is devoted to a study of the gluon distribution in this model, with emphasis on the Cronin peak, and, more generally, on the role of non-linear effects in rearranging the gluons in momentum space. Although this model has been extensively studied in the literature [10, 12, 14, 29, 30] (in particular, in relation with the Cronin peak [23–25, 53, 54]), our analysis below will bring some new results and conceptual clarifications, and will reveal some novel, and perhaps surprising, features, which to our knowledge have escaped to previous investigations.

Specifically, in Sect. 2.2, we shall provide a complete, analytic, study of the gluon distribution in the MV model, that we shall generalize on this occasion to include running coupling effects, in such a way to be compatible with the quantum evolution to be discussed later. The results obtained in this analysis will permit us to clarify the conditions for the emergence of the peak, and explicitly compute properties like the location of the peak and its magnitude (in Sect. 2.3). Then, in Sect. 2.4, we shall reexamine a global argument in favor of the Cronin peak, based on a sum-rule [24], that we shall use in order to better understand the origin of the gluons which make up the condensate.

A rather surprising feature which will emerge from this analysis refers to the redistribution of gluons in momentum space under the influence of the non-linear effects : Whereas it has been since long appreciated that the effect of the repulsive interactions is to push the gluons towards the modes at larger momenta, and thus provide a spectrum which is infrared-safe [12, 14, 30], it has not been recognized so far that the dominant part of this spectrum — the one which is parametrically enhanced for large A , and provides a plateau of order $1/\alpha_s$ at saturation ($k_\perp \lesssim Q_s(A)$) — is actually **compact**, i.e., it falls off exponentially with increasing k_\perp above $Q_s(A)$. In fact, as we shall see, it is precisely this exponential decrease in $\varphi_A(k_\perp)$ for momenta just above $Q_s(A)$ which explains why a pronounced peak appears in the ratio \mathcal{R}_{pA} when computed in the MV model.

To conclude this general discussion, let us mention two alternative definitions for the unintegrated gluon distribution which are used in the literature. These definitions have in common the fact that they relate the gluon distribution to a scattering operator: the scattering amplitude $\mathcal{N}_A(r_\perp, y)$ for a color dipole with transverse size r_\perp which scatters off a hadronic target with atomic number A at relative rapidity y . Under suitable approximations, this quantity obeys a closed, non-linear, evolution equation (a generalization of the BFKL equation), originally derived by Kovchegov [33].

Specifically, in Ref. [38], the following definition has been proposed (the color dipole is taken to be made off two gluons):

$$\varphi_A(k_\perp, y) \equiv \int \frac{d^2 r_\perp}{\pi r_\perp^2} e^{-ik_\perp \cdot r_\perp} \frac{\mathcal{N}_A(r_\perp, y)}{\alpha_s N_c}. \quad (2.2)$$

This definition has no deep motivation, but is simply based on the analogy with a formula for the true occupation factor (2.1) which holds within the MV model (see Sect. 2.2 below). In fact, the quantities in Eqs. (2.2) and (2.1) are very similar to each other: They coincide with each other in the linear regime at high momenta $k_\perp \gg Q_s(A, y)$, where they both obey the BFKL equation, and they also show a similar behavior at low momenta $k_\perp \ll Q_s(A, y)$, so they differ, at most, in the transition region towards saturation. The approximations that we shall develop in this paper are not sensitive to the details of this transition region, nor to the differences [47, 48] between the Kovchegov equation and the general, functional, evolution equation for the CGC, so all the results that we shall obtain apply literally to both definitions. Thus, our results are directly comparable to the numerical calculations in Ref. [25], which are based on Eq. (2.2) together with the Kovchegov equation.

A different definition, with a deeper physical motivation, has been introduced in Ref. [19], and reads

$$h_A(k_\perp, y) \equiv \frac{1}{4} k_\perp^2 \nabla_k^2 \varphi_A(k_\perp, y) = k_\perp^2 \int \frac{d^2 r_\perp}{4\pi} e^{-ik_\perp \cdot r_\perp} \frac{\mathcal{S}_A(r_\perp, y)}{\alpha_s N_c}, \quad (2.3)$$

where in this context $\varphi_A(k_\perp, y)$ is the function defined in Eq. (2.2), and $\mathcal{S}_A(r_\perp, y) \equiv 1 - \mathcal{N}_A(r_\perp, y)$ is the S -matrix element for dipole-hadron scattering. The quantity (2.3) enters a factorized formula for the cross-section for gluon production in proton-nucleus collisions [14, 20–22], and as such it is directly relevant for the phenomenology of d-Au collisions at RHIC. Note that its interpretation as a ‘gluon distribution’ is only conventional (this is based on an analogy with the k_\perp -factorization which holds in the linear regime at not so high energies), and should not give rise to confusion: There is a priori no reason why the (canonical) gluon distribution should enter the calculation of observables for high energy scattering. Indeed, in the high-density environment at high energy, the scattering operators are non-linear in the color field in the target (the non-linear effects describe **multiple scattering**), so, unlike what happens at low energy, they are not simply proportional to the 2-point function which defines the gluon distribution.

The results that we shall obtain for φ_A later in this paper do not directly apply to h_A , although they could be easily translated for it (at least, in the case of a fixed coupling), by using $h_A \propto k_\perp^2 \nabla_k^2 \varphi_A$. The numerical analysis in Ref. [25], which considers both definitions (2.2) and (2.3), shows that the ratio \mathcal{R}_{pA} is qualitatively the same when computed with any of these two definitions. But important quantitative differences persist, especially at low momenta, where the functions φ_A and h_A are very different. In view of this, it would be interesting to repeat for h_A , and also for the convolution yielding the cross-section for gluon production, the analysis that we shall give below in this paper for φ_A . A potential

difficulty that we foresee with such an analysis is the fact that the generalization of Eq. (2.3) to the case of a running coupling is ambiguous (unlike for the other definitions, Eqs. (2.1) and (2.2), for which a natural generalization exists; see below).

2.2 The McLerran–Venugopalan model: Fixed \mathcal{E} running coupling

The color sources which generate the small- x gluons in the McLerran–Venugopalan (MV) model [10, 12] are the $3A$ valence quarks (from the A nucleons), which are assumed to be uncorrelated with each other except for the long-range correlations associated with confinement. The gluon occupation factor $\varphi_A(k_\perp) \equiv \varphi_A(k_\perp, y = 0)$ at momenta $k_\perp \gg \Lambda_{\text{QCD}}$ is then obtained as [14, 30]

$$\varphi_A(k_\perp) = \int d^2 r_\perp e^{-ik_\perp \cdot r_\perp} \frac{1 - \exp\left\{-\frac{1}{4} r_\perp^2 Q_A^2 \ln \frac{4}{r_\perp^2 \Lambda^2}\right\}}{\pi \alpha_s N_c r_\perp^2}, \quad (2.4)$$

where Λ is a non-perturbative scale of order Λ_{QCD} (the only trace of confinement), $N_c = 3$ is the number of colors, and $Q_A^2 = \alpha_s N_c \mu_A \propto A^{1/3}$ is proportional to the color charge squared μ_A of the valence quarks per unit transverse area. The factor of 4 within $\ln(4/r_\perp^2 \Lambda^2)$ is only a matter of choice. The integration in Eq. (2.4) must be restricted to $r_\perp < 2/\Lambda$, for consistency with the approximations leading to this formula [12], and also to avoid that the logarithm in the exponent changes sign. But as long as $k_\perp \gg \Lambda$, the value of the integral is very little sensitive to the precise value of the upper cutoff.

Since the MV model is a classical approximation, Eq. (2.4) is a priori written for a fixed coupling α_s . Later, we shall consider quantum evolution with a running coupling, and at that stage we shall also need a generalization of Eq. (2.4) which includes running coupling effects to one-loop order (i.e., for a running coupling $\alpha_s(Q^2) \equiv b_0/\ln(Q^2/\Lambda_{\text{QCD}}^2)$). The generalization that we shall consider reads (from now on, we shall not distinguish between the scales Λ and Λ_{QCD})

$$\varphi_A(k_\perp) = \int d^2 r_\perp e^{-ik_\perp \cdot r_\perp} \frac{1 - e^{-\frac{1}{4} r_\perp^2 Q_A^2}}{\pi b_0 N_c r_\perp^2} \ln \frac{4}{r_\perp^2 \Lambda^2}, \quad (2.5)$$

where $Q_A^2 \equiv b_0 N_c \mu_A$ has now a slightly different meaning as compared to the fixed coupling case, but is still proportional to $A^{1/3}$. Formally, Eq. (2.5) is obtained from Eq. (2.4) by replacing in the latter $\alpha_s \rightarrow \alpha_s(4/r_\perp^2)$ within the denominator of the integrand, and also within Q_A^2 . In contrast to Eq. (2.4), there is no need for an upper cutoff in Eq. (2.5): the integral is convergent as written, and for any $k_\perp \gg \Lambda$ it is dominated by perturbative sizes $r_\perp \ll 1/\Lambda$.

Since the choice of a running in the absence of a complete one-loop quantum calculation is a priori ambiguous (especially in the presence of several scales, like in Eq. (2.4)), it is important to justify in more detail our choice leading to Eq. (2.5). Note first that (a) the coupling α_s which is explicit in Eq. (2.4) (in the denominator) and the one which is implicit in the definition of Q_A^2 have the same origin [12, 30], and thus need to be renormalized in the same way, and (b) the quantity $1 - \exp\left\{-\frac{1}{4} r_\perp^2 Q_A^2 \ln \frac{4}{r_\perp^2 \Lambda^2}\right\}$ in the numerator of Eq. (2.4) can be recognized as the scattering amplitude for a color dipole of size r_\perp which scatters off the nucleus. More precisely, this is the dipole made of the two primary gluons radiated by the valence quarks (the gluons which define the distribution), and the scattering amplitude describes the color precession of these primary gluons when propagating through the color field of the nucleus (see [12] for details). As well known, a small dipole couples predominantly to gluons with momenta $k_\perp^2 \lesssim 1/r_\perp^2$, so it is indeed natural to choose the size of the dipole as the argument for the running of the corresponding coupling constant; this is also the choice made in other studies of the evolution of the dipole scattering amplitude with increasing energy [39, 40, 46, 50, 51].

There is one more subtle point about our choice in Eq. (2.5) : as a density of color charge, the quantity μ_A involves itself a factor of α_s , that we have implicitly treated as a constant in our arguments above. Specifically, for $A \times N_c$ valence quarks which are homogeneously distributed within the nuclear disk with radius R_A , one obtains [12]

$$\mu_A = \frac{2\alpha_s A}{R_A^2}. \quad (2.6)$$

Treating α_s in Eq. (2.6) as a constant amounts to neglecting quantum corrections to the distribution of the valence quarks, which is in the spirit of the MV model. One sees that, in writing Eq. (2.5), we have treated differently the vertices describing the radiation of classical color fields from the valence quarks, and those describing the scattering of the color dipole off these classical fields. This is justified for the present purposes because these vertices play different roles in the subsequent evolution with increasing y : Whereas the valence quarks act simply as sources for the primary gluons at $y = 0$, and as such they can be viewed as classical colored particles, the quantum evolution proceeds via gluon radiation from the primary gluons, and the vertices describing this radiation are of the same type as those describing the scattering of the color dipole in Eq. (2.4). Thus dressing just these vertices is the minimal way to render Eq. (2.4) consistent with the quantum evolution which includes running coupling effects.

The emergence of the dipole scattering amplitude in Eqs. (2.4) and (2.5) illustrates the deep connection between **unitarization** effects in scattering processes at high energy and **saturation** effects in the nuclear gluon distribution: Both types of effects arise from non-linearities associated with strong gluon fields, which here are encoded in the exponential

terms² in the integrands of Eqs. (2.4) and (2.5). The transition from the linear regime to the non-linear one takes place when the exponent is of order one. More precisely, we shall define the **saturation momentum** $Q_s(A)$ such that the exponent is equal to one when $r = 2/Q_s(A)$. For running coupling, Eq. (2.5) immediately implies $Q_s^2(A) = Q_A^2 \sim A^{1/3}$. For fixed coupling, the saturation scale turns out to be larger than the scale Q_A introduced by the color sources

$$Q_s^2(A) = Q_A^2 \ln \frac{Q_s^2(A)}{\Lambda^2} \sim A^{1/3} \ln A^{1/3}, \quad (2.7)$$

and this difference will be seen to have important consequences. Loosely speaking, the ratio

$$\rho_A \equiv \frac{Q_s^2(A)}{Q_A^2} = \ln \frac{Q_s^2(A)}{\Lambda^2} \sim \ln A^{1/3}, \quad (2.8)$$

will play the same role in the fixed coupling case as the inverse of the coupling constant in the case of a running coupling. In fact, for a running coupling, we shall define similarly $\rho_A \equiv \ln(Q_s^2/\Lambda^2)$, and then it is clear that $1/\rho_A$ is essentially the same as the coupling evaluated at the saturation momentum : $\alpha_s(Q_s^2) = b_0/\rho_A$. Since the MV model makes sense only for weak coupling, it is justified to treat ρ_A as a large parameter, $\rho_A \gg 1$, which we shall do in what follows. It is interesting to note in this context that, for a gold nucleus at typical RHIC energies one expects $Q_s^2(A) \simeq 2 \text{ GeV}^2$, which together with $\Lambda \simeq 200 \text{ MeV}$, yields $\rho_A \simeq \ln 50 \simeq 4$.

It is straightforward to compute the dominant behavior of the gluon distribution at asymptotically large ($k_\perp \gg Q_s(A)$) or small ($k_\perp \ll Q_s(A)$, with $k_\perp \gg \Lambda$ though) momenta. One finds :

(a) Fixed coupling:

$$\varphi_A(k_\perp) \approx \begin{cases} \frac{1}{\alpha_s N_c} \frac{Q_A^2}{k_\perp^2}, & \text{for } k_\perp \gg Q_s(A) \\ \frac{1}{\alpha_s N_c} \ln \frac{Q_s^2(A)}{k_\perp^2}, & \text{for } k_\perp \ll Q_s(A) \end{cases} \quad (2.9)$$

(a) Running coupling:

² Physically, these exponentials represent the S -matrix for dipole-nucleus scattering.

$$\varphi_A(k_\perp) \approx \begin{cases} \frac{1}{b_0 N_c} \frac{Q_A^2}{k_\perp^2}, & \text{for } k_\perp \gg Q_A \\ \frac{1}{N_c} \left\langle \frac{1}{\alpha_s} \right\rangle \ln \frac{Q_A^2}{k_\perp^2}, & \text{for } k_\perp \ll Q_A \end{cases} \quad (2.10)$$

The average inverse coupling constant which enters the last equation is defined as

$$\left\langle \frac{1}{\alpha_s} \right\rangle \equiv \frac{1}{2b_0} \left(\ln \frac{Q_A^2}{\Lambda^2} + \ln \frac{k_\perp^2}{\Lambda^2} \right) = \frac{1}{b_0} \ln \frac{k_\perp Q_A}{\Lambda^2}. \quad (2.11)$$

The high-momentum behavior in these equations, which is obtained after linearizing the exponential terms Eqs. (2.4) and (2.5), is recognized as the bremsstrahlung spectrum due to radiation from independent color sources. This would be the spectrum at any k_\perp in the absence of non-linear effects in the dynamics of the radiated gluons. But already at high- k_\perp , this spectrum receives non-linear corrections which are suppressed by powers of $Q_s^2(A)/k_\perp^2$ ('higher-twist' effects; see below). The dominant behavior at low momenta is obtained after neglecting the exponential terms Eqs. (2.4) and (2.5), and is correct to leading logarithmic accuracy; that is, the first corrective term would be a constant term under the logarithm.

As we shall see in Sect. 2.3, the asymptotic expressions above are already sufficient to demonstrate the existence of a peak in the ratio \mathcal{R}_{pA} . But in order to study the properties of this peak, we also need the gluon occupation factor at generic (intermediate) momenta, which given the simplicity of the MV model can be computed analytically.

In fact, in the case of a running coupling, we have been able to evaluate the integral in Eq. (2.5) in analytic form, with a result which is displayed in the Appendix, and which will be also discussed below. For fixed coupling, we do not have such an exact result, but we have found a convenient series representation of the integral in Eq. (2.4), which converges very fast, and renders the physical interpretation of the result transparent.

Let us consider the fixed coupling case first. After rewriting the exponent in the integrand of Eq. (2.4) as (cf. Eq. (2.7) and (2.8))

$$\frac{1}{4} r_\perp^2 Q_A^2 \ln \frac{4}{r_\perp^2 \Lambda^2} = t \left(1 + \frac{\ln 1/t}{\rho_A} \right), \quad t \equiv \frac{r_\perp^2 Q_s^2(A)}{4}, \quad (2.12)$$

one can decompose the integral into two pieces as

$$\begin{aligned}\varphi_A(k_\perp) &= \int d^2 r_\perp e^{-ik_\perp \cdot r_\perp} \left\{ \frac{1 - e^{-\frac{1}{4} r_\perp^2 Q_s^2(A)}}{\pi \alpha_s N_c r_\perp^2} + \frac{e^{-\frac{1}{4} r_\perp^2 Q_s^2(A)}}{\pi \alpha_s N_c r_\perp^2} \left[1 - \exp\left(-t \frac{\ln 1/t}{\rho_A}\right) \right] \right\} \\ &= \varphi_A^{\text{sat}}(k_\perp) + \varphi_A^{\text{twist}}(k_\perp),\end{aligned}\tag{2.13}$$

where the first, ‘saturating’, piece can be explicitly evaluated, and reads

$$\varphi_A^{\text{sat}}(k_\perp) = \frac{1}{\alpha_s N_c} \Gamma(0, z),\tag{2.14}$$

while the second piece — the sum of all-‘twist’ contributions (see below) — can be evaluated as a series expansion, obtained by expanding the exponential within the square brackets in powers of $(t \ln 1/t)/\rho_A$ as

$$\varphi_A^{\text{twist}}(k_\perp) = -\frac{1}{\alpha_s N_c \rho_A} \int dt J_0(\sqrt{4zt}) e^{-t} \sum_{n=1}^{n_{\text{max}}} \left(\frac{t}{\rho_A}\right)^{n-1} \frac{\ln^n t}{n!}.\tag{2.15}$$

In these equations, $z \equiv k_\perp^2/Q_s^2(A)$, $\Gamma(0, z)$ is the incomplete Gamma function:

$$\Gamma(0, z) = \int_z^\infty \frac{e^{-t}}{t} dt,\tag{2.16}$$

$n_{\text{max}} \sim e^{\rho_A} = Q_s^2(A)/\Lambda^2 \gg 1$, and the truncation of the series in Eq. (2.15) at $n \leq n_{\text{max}}$ reflects the upper cutoff $r_{\text{max}} = 2/\Lambda$ which is implicit in the integral over r_\perp in the first line of Eq. (2.13). (The corresponding integral giving φ_A^{sat} , Eq. (2.14), has been extended up to infinity, since rapidly convergent.) Without a truncation, the series would be asymptotically divergent, but the divergent behavior would start to manifest itself only at very large orders, beyond n_{max} . On the other hand, when $\rho_A \gg 1$ the truncated series is rapidly convergent for any z , and therefore $\varphi_A(k_\perp)$ can be computed even analytically with high accuracy (see the Appendix for details).

The first important observation about the decomposition in Eq. (2.13) is that the second piece, φ_A^{twist} , is multiplied by an overall factor $1/\rho_A$ (this is manifest on Eq. (2.15)), and thus is parametrically suppressed at large A . This implies that, in the saturation region at $z \lesssim 1$, the gluon distribution is dominated by the first piece, φ_A^{sat} . In particular, φ_A^{sat} captures the leading behavior at low momenta $k_\perp \ll Q_s(A)$, cf. Eq. (2.9): indeed, $\Gamma(0, z) \approx \ln 1/z$ for $z \ll 1$, whereas φ_A^{twist} is analytic near $z = 0$. In fact, if one remembers that $1/\rho_A$ can be effectively identified with α_s (cf. the discussion after Eq. (2.8)), it becomes clear that the $1/\alpha_s$ -enhancement of the gluon distribution, which is the hallmark of saturation, is associated solely with φ_A^{sat} : For $z \lesssim 1$, the latter provides a plateau with a height of $\mathcal{O}(1/\alpha_s)$, whereas φ_A^{twist} brings only a small correction, of $\mathcal{O}(1)$.

The second important observation is that the saturating piece φ_A^{sat} is **compact**, in the sense that it vanishes exponentially at momenta outside the saturation region (since $\Gamma(0, z) \approx e^{-z}/z$ for $z \gg 1$). By contrast, it can be checked that, for $z \gg 1$, the function φ_A^{twist} can be expanded in powers of $1/z$ (up to logarithmic corrections), thus generating the ‘twist expansion’ of the MV model. It should be stressed that each of the terms in the truncated series in Eq. (2.15) contains terms to all orders in the twist expansion: the first term ($n = 1$) includes the bremsstrahlung spectrum $\propto 1/z$, together with an infinite series of ‘higher-twist’ terms (i.e., terms of order $1/z^2$, or higher), the second term ($n = 2$) starts at order $1/z^2$, etc. The first few terms in the twist expansion are exhibited in the Appendix.

We see that the gluon distribution of a large nucleus in the MV model naturally decouples into two pieces, one which controls the spectrum at saturation, and another one which controls the tail of the distribution at high momenta. It is natural to interpret the first piece, φ_A^{sat} , as the **occupation factor in the color glass condensate**. The fact that this distribution appears to be compact is probably just specific to the MV model, since, as we shall see, this feature is washed out by the quantum evolution (cf. Sect. 5.3). The previous considerations also suggest that the twist terms contribute only little to the physics of the Cronin peak in the MV model. This will be confirmed by the analysis in the next subsection.

The corresponding discussion in the case of a running coupling is even simpler, since the corresponding ‘twist’ piece involves only one term, instead of a series of terms. Also, some arguments become more transparent since, with a running coupling, $1/\alpha_s(Q_s^2(A))$ and ρ_A/b_0 are explicitly identified. Specifically, Eq. (2.5) can be decomposed as:

$$\begin{aligned} \varphi_A(k_\perp) &= \varphi_A^{\text{sat}}(k_\perp) + \varphi_A^{\text{twist}}(k_\perp), \\ \varphi_A^{\text{sat}}(z) &= \frac{1}{b_0 N_c} \rho_A \Gamma(0, z), \quad \varphi_A^{\text{twist}}(z) = \int dt J_0(\sqrt{4zt}) \frac{1 - e^{-t}}{b_0 N_c t} \ln \frac{1}{t}, \end{aligned} \quad (2.17)$$

where the saturating piece is explicitly enhanced by the factor ρ_A (that is, it is of $\mathcal{O}(1/\alpha_s)$), while φ_A^{twist} is of $\mathcal{O}(1)$ for $z \sim 1$, and can be expanded in powers of $1/z$ for $z \gg 1$ (thus generating the twist expansion). The only noticeable difference with respect to the fixed coupling case is that, now, $\varphi_A^{\text{twist}}(z)$ is not analytic near $z \rightarrow 0$, but rather yields a large **negative** contribution $-(1/2b_0 N_c) \ln^2 z$ in that limit, which contributes to the dominant low-momentum behavior exhibited in Eq. (2.10). Since, however, the overall contribution remains **positive** for any $k_\perp \geq \Lambda$, it is clear that $\varphi_A^{\text{sat}}(k_\perp)$ is still the dominant contribution at any $\Lambda \leq k_\perp \leq Q_A$. The integral giving φ_A^{twist} is explicitly evaluated in the Appendix, where its twist expansion will be also considered.

The previous considerations are illustrated in Figs. 2 and 3, which exhibit the gluon occupation factor $\varphi_A(k_\perp)$, and its various contributions $\varphi_A^{\text{sat}}(k_\perp)$ and $\varphi_A^{\text{twist}}(k_\perp)$, in the MV model with fixed and running coupling, in either linear scale (Fig. 2), or log-log scale

in a wider range of momenta (Fig. 3).

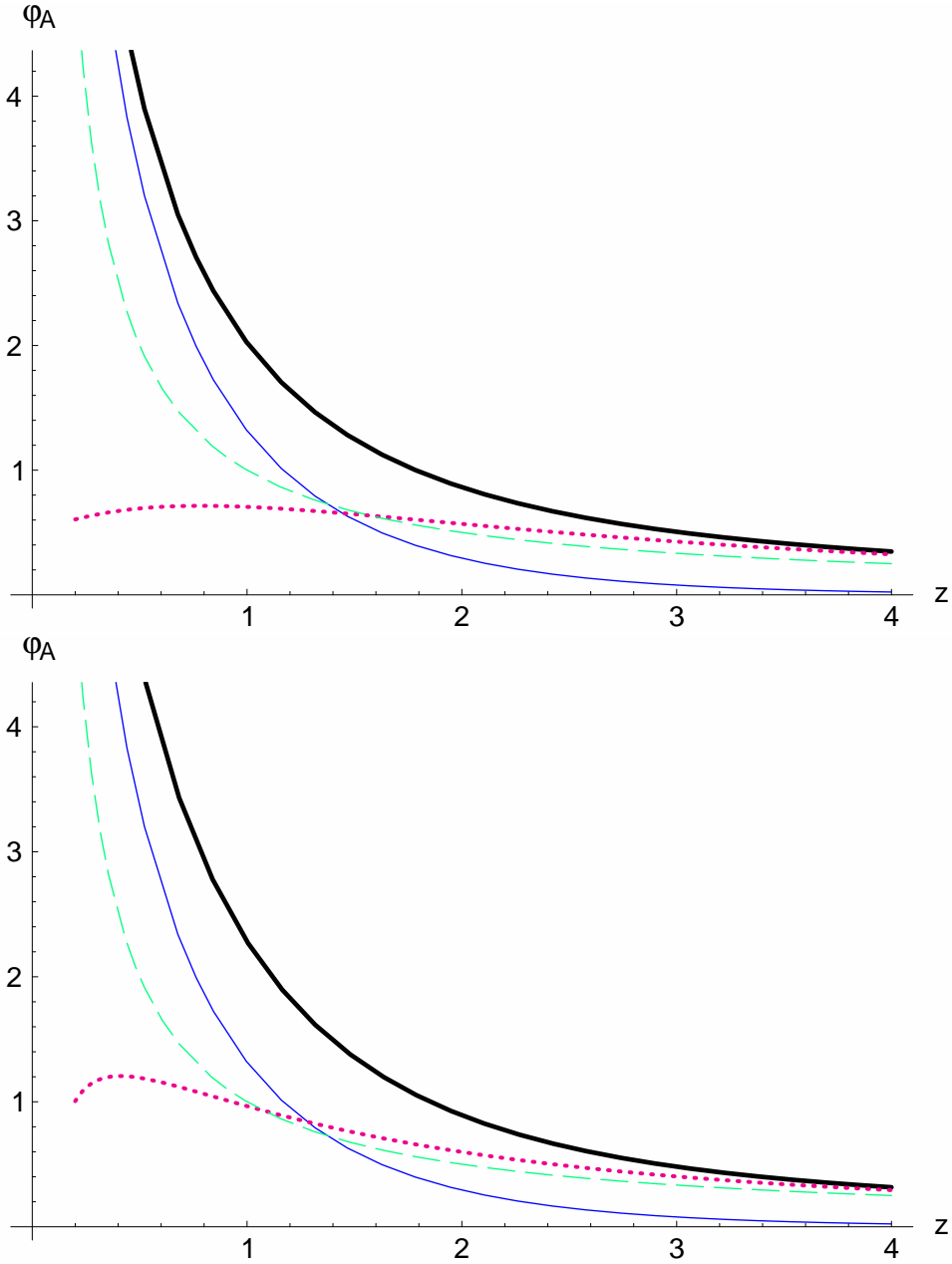


Fig. 2. The gluon occupation factor $\varphi_A(z)$ as a function of the scaled momentum variable $z = k^2/Q_s^2(A)$ in the MV model with either fixed (figure above) or running (below) coupling and $\rho_A = 6$. With respect to the text definitions, we plot the quantities $\rho_A \alpha_s N_c \times \varphi_A$ for fixed coupling, and $b_0 N_c \times \varphi_A$ for running coupling. The black (thick) line corresponds to $\varphi_A(z)$; the blue (solid) line shows the saturation contribution $\varphi_A^{\text{sat}}(z)$; the magenta (dotted) line shows the twist contribution $\varphi_A^{\text{twist}}(z)$; the green (dashed) line represents the bremsstrahlung spectrum.

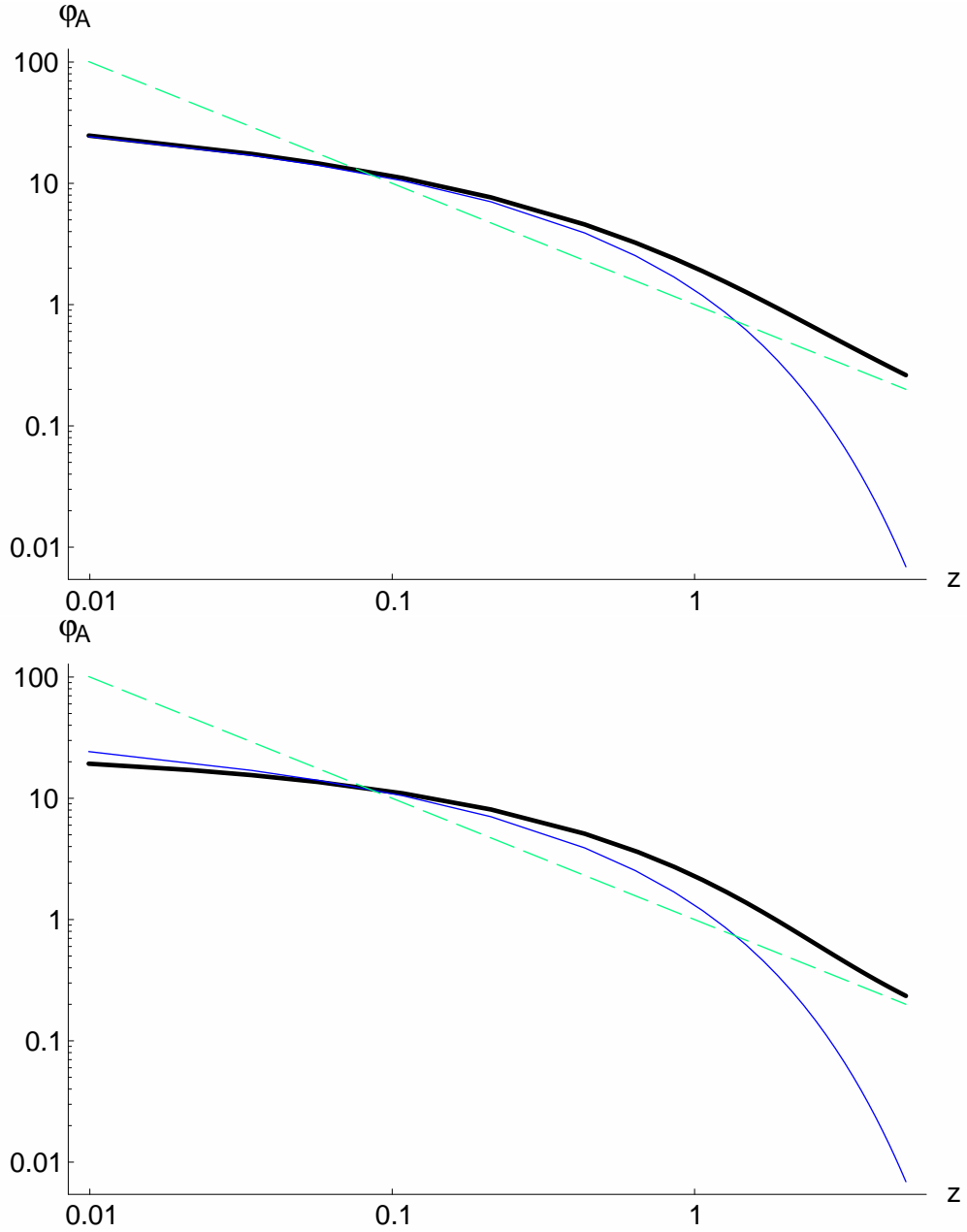


Fig. 3. Logarithmic plot of the gluon occupation factor $\varphi_A(z)$ as a function of the scaled momentum variable $z = k^2/Q_s^2(A)$ in the MV model with either fixed (figure above) or running (below) coupling and $\rho_A = 6$. The plotted quantities are rescaled as explained in the caption to Fig. 2. The black (thick) line corresponds to the gluon occupation factor $\varphi_A(z)$; the blue (solid) line shows the saturation contribution $\varphi_A^{\text{sat}}(z)$; the green (dashed) line represents the bremsstrahlung spectrum.

2.3 Cronin effect in the McLerran–Venugopalan model

To form the ratio \mathcal{R}_{pA} , Eq. (1.1), one also needs the gluon distribution in the proton, $\varphi_p(k_\perp, y)$. For $y = 0$ and $k_\perp \gg \Lambda$, the proton is in the perturbative (i.e., linear) region, and will be described by the bremsstrahlung spectrum in Eqs. (2.9) or (2.10) (for fixed and running coupling, respectively) with $Q_A^2 \rightarrow Q_p^2$, and $Q_p = \mathcal{O}(\Lambda)$. For instance,

$$\varphi_p(k_\perp) = \frac{1}{\alpha_s N_c} \frac{Q_p^2}{k_\perp^2} \Theta(k_\perp - Q_p) \quad (\text{fixed coupling}). \quad (2.18)$$

We shall assume the following relation between the two scales:

$$Q_A^2 = A^{1/3} Q_p^2, \quad (2.19)$$

which holds formally if one extrapolates the MV model (a priori valid for a large nucleus) down to $A = 1$.

Note that the quantity in the denominator of Eq. (1.1), namely $A^{1/3} \varphi_p(k_\perp)$, coincides with the nuclear gluon distribution in the high momentum limit (i.e., the bremsstrahlung spectrum in Eqs. (2.9) or (2.10)). Thus, within the MV model at least, the ratio $\mathcal{R}_{pA}(k_\perp)$ is also a measure of the deviation of the actual nuclear gluon distribution from the corresponding prediction of linear perturbation theory. As already discussed, this deviation is associated with non-linear effects in the gluon dynamics, in particular with saturation. We immediately conclude that $\mathcal{R}_{pA}(k_\perp)$ must approach one at high k_\perp :

$$\mathcal{R}_{pA}(k_\perp) \simeq 1 \quad \text{for} \quad k_\perp \gg Q_s(A). \quad (2.20)$$

By using this condition together with very general properties of saturation³, we can deduce the existence of a Cronin peak without any detailed calculation:

Consider the fixed coupling case, for definiteness. The basic consequence of saturation is that, for momenta $k_\perp \lesssim Q_s(A)$, the nuclear occupation factor develops a plateau with the height of $\mathcal{O}(1/\alpha_s)$; that is, $\varphi_A(k_\perp) \approx (1/\alpha_s N_c) \bar{\varphi}(z)$, where $z \equiv k_\perp^2/Q_s^2(A)$, and the function $\bar{\varphi}(z)$ is slowly varying when $z < 1$, and is of $\mathcal{O}(1)$ when $z \sim 1$. This function depends upon k_\perp and A only through z because it is dimensionless, and $Q_s(A)$ is the only

³ Of course, all the properties to be discussed below are manifest on the expressions (2.14) and (2.17) for $\varphi_A^{\text{sat}}(k_\perp)$, but here we would like to construct our argument without relying on the explicit formulae for φ_A that we have obtained previously, in order to emphasize the general conditions required by the existence of the peak.

scale in the problem other than k_\perp (since at saturation the spectrum cannot be sensitive to the non-perturbative scale Λ). We deduce that:

$$\mathcal{R}_{pA}(k_\perp) \approx \frac{k_\perp^2}{Q_A^2} \bar{\varphi}(z) = \rho_A z \bar{\varphi}(z), \quad \text{for} \quad k_\perp \lesssim Q_s(A). \quad (2.21)$$

Since $\bar{\varphi}(z)$ is only logarithmically divergent as $z \rightarrow 0$, it is clear that the ratio $\mathcal{R}_{pA}(k_\perp)$ is much smaller than one for k_\perp small enough (e.g., it is of $\mathcal{O}(A^{-1/3})$ when $k_\perp \sim Q_p$), but it is of $\mathcal{O}(\rho_A)$ — and thus strictly larger than one — for $k_\perp = Q_s(A)$. This behavior at small k_\perp , together with the asymptotic behavior (2.20) at large k_\perp , immediately imply that the ratio \mathcal{R}_{pA} must have a maximum at some intermediate value of k_\perp .

This general argument does not tell us where is the maximum actually located, and not even whether there is a single maximum, or several. But it is highly probable, and will be confirmed by the explicit calculations below, that there is indeed only one maximum, which is located near $Q_s(A)$ and thus has a height of $\mathcal{O}(\rho_A)$: Indeed, there is no intrinsic scale larger than $Q_s(A)$ in the problem, and for $k_\perp < Q_s(A)$ the ratio is still increasing with k_\perp , as manifest on Eq. (2.21).

Note the specific way how the large factor ρ_A has entered the calculation in Eq. (2.21): this is due to the mismatch (2.7) between the scale Q_A^2 associated with the color sources and the saturation scale $Q_s^2(A)$ generated by the non-linear gluon dynamics. It is easy to check that a similar enhancement occurs also for a running coupling, although in that case the argument is more direct: the factor ρ_A is introduced by the inverse coupling in the saturation condition $\varphi_A(k_\perp = Q_A) \approx \kappa/\alpha_s(Q_A^2)N_c$, with $\kappa \sim \mathcal{O}(1)$.

We conclude that the existence of the Cronin peak is a consequence of the fact that the gluon distribution at saturation is larger, by a factor of $\rho_A \sim \ln A^{1/3}$, than the naïve extrapolation of the bremsstrahlung spectrum down to $k_\perp \sim Q_s(A)$. This logarithmic enhancement is due to non-linear effects which cause the gluon occupation factor to increase faster with $1/k_\perp^2$ than predicted by linear perturbation theory, before eventually saturating to a value of order $1/\alpha_s$ at $k_\perp \lesssim Q_s(A)$.

We now rely on the explicit formulae for φ_A established in the previous subsection to give a complete description of the peak. For more clarity, we start with the large- A limit, in which the gluon occupation factor for momenta around $Q_s(A)$ is given by the saturating piece φ_A^{sat} , up to corrections of $\mathcal{O}(1/\rho_A)$. Using $\varphi_A^{\text{sat}}(k_\perp)$ from either Eq. (2.14) or Eq. (2.17), one finds the same expression for the ratio \mathcal{R}_{pA} with both fixed and running coupling, namely:

$$\mathcal{R}_{pA}(k_\perp) \approx z \Gamma(0, z) \rho_A \quad \text{for} \quad k_\perp \sim Q_s(A). \quad (2.22)$$

This is of the form anticipated in Eq. (2.21), and thus is of order ρ_A when $z \sim 1$ ($\Gamma(0, 1) = 0.219\dots$). It can be checked that the function $f(z) \equiv z\Gamma(0, z)$ has a maximum at $z_0 \approx 0.435$, with the peak value $f(z_0) \approx 0.281$. Moreover, this peak is very pronounced, since $f(z)$ is almost linearly increasing below the peak, but exponentially decreasing above it.

It is then straightforward to add the contribution of the twist terms in Eq. (2.15) or (2.17), and compute their effect on the location and the magnitude of the peak in an expansion in powers of $1/\rho_A$. One finds (with $\mathcal{R}_{\max}(A) \equiv \mathcal{R}_{pA}(z_0)$) :

$$\begin{aligned} z_0 &= 0.435 + \frac{0.882}{\rho_A} + \frac{2.122}{\rho_A^2} + \mathcal{O}(\rho_A^{-3}), \\ \mathcal{R}_{\max}(A) &= 0.281 \rho_A + 0.300 + \frac{0.294}{\rho_A} + \mathcal{O}(\rho_A^{-2}), \end{aligned} \tag{2.23}$$

in fixed coupling case, and respectively

$$\begin{aligned} z_0 &= 0.435 + \frac{1.382}{\rho_A} + \frac{2.038}{\rho_A^2} + \mathcal{O}(\rho_A^{-3}), \\ \mathcal{R}_{\max}(A) &= 0.281 \rho_A + 0.524 + \frac{0.804}{\rho_A} + \mathcal{O}(\rho_A^{-2}), \end{aligned} \tag{2.24}$$

in the running coupling case.

Finally, for both fixed and running coupling one can compare the results obtained above in the $1/\rho_A$ expansion to the corresponding exact results, and the agreement is good even for $\rho_A = 4$ (which, we recall, is a realistic value at RHIC). For example, with running coupling and $\rho_A = 4$, the exact calculation yields $z_0 = 0.89$ and $\mathcal{R}_{\max} = 1.85$, while Eq. (2.24) predicts $z_0 = 0.91$ and $\mathcal{R}_{\max} = 1.85$.

In Fig. 4, where we show the Cronin ratio in the MV model with both fixed and running coupling, we also represent the individual contributions separated in the r.h.s. of Eq. (2.13) (or (2.17)), to better emphasize that the ‘twist’ effects give only a small contribution in the region of the peak. As obvious on this figure, the effect of the twist corrections is to flatten the peak a little bit, and also to move it towards larger momenta. Still, a well pronounced peak emerges because, even for ρ_A as small as 4, the dominant contribution to $\varphi_A(k_\perp)$ for k_\perp around $Q_s(A)$ is still given by the compact, ‘saturating’, piece φ_A^{sat} . Accordingly, the nuclear occupation factor shows an exponential fall-off for momenta just above $Q_s(A)$. It can be easily checked that the behavior changes from an exponential to a power law around $z \sim \ln \rho_A$.

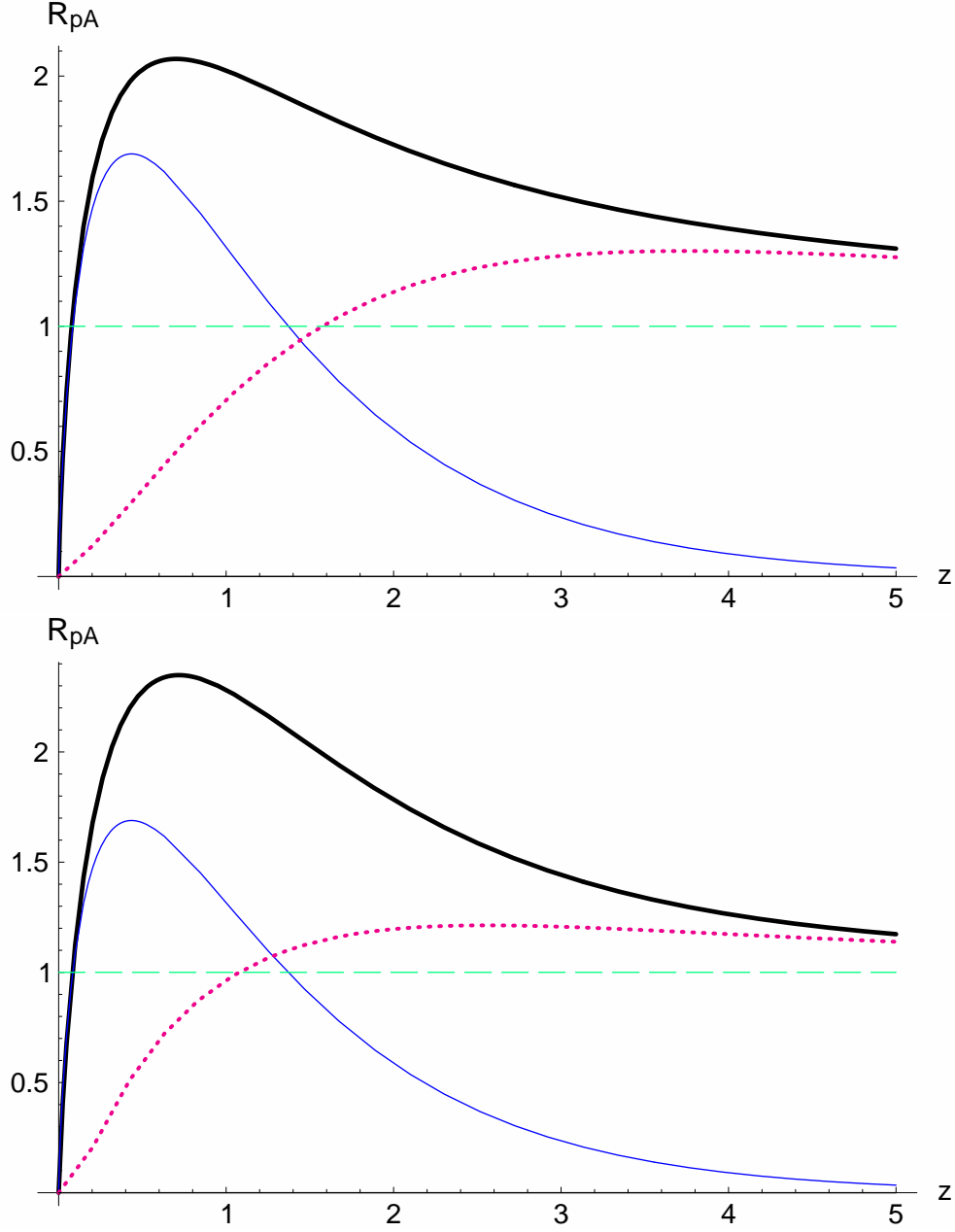


Fig. 4. The Cronin ratio $\mathcal{R}_{pA}(z)$ as a function of the scaled momentum variable $z = k^2/Q_s^2(A)$ in the fixed (above) and running (below) coupling McLerran-Venugopalan model for $\rho_A = 6$. The black (thick) line corresponds the ratio $\mathcal{R}_{pA}(z)$; the blue (solid) line shows the saturation contribution $\mathcal{R}_{pA}^{\text{sat}}(z)$; the magenta (dotted) line shows the twist contribution $\mathcal{R}_{pA}^{\text{twist}}(z)$.

2.4 A sum rule and its consequences

In this subsection we shall discuss an alternative, global, argument in favor of the existence of the Cronin peak in the MV model, which sheds more light on the role of non-linear effects in the nuclear gluon distribution. This argument, due to Kharzeev, Kovchegov, and Tuchin [24], is specific to the MV model — it is based on a sum-rule which reflects the basic property of this model that color sources are uncorrelated —, and cannot be extended to $y > 0$ (since the quantum evolution introduces correlations among the color sources; see below). But even within the MV model, the use of this argument is quite subtle, because of possible complications with ultraviolet divergences. In fact, as we shall explain below, the original formulation of the relevant sum-rule in Ref. [24] is not mathematically rigorous, which may have given rise to confusion (especially, in relation with the generalization of this sum-rule to $y > 0$; see the discussion in Ref. [25]). In what follows, we shall properly restate the argument, and then present a stronger version of it, based on partial sum-rules, which provides a more detailed information on the distribution of gluon at saturation.

Specifically, the argument in Ref. [24] is based on the following ‘sum-rule’ (the IR cutoff Λ is strictly needed only for the proton) :

$$\int_{\Lambda^2} \frac{d^2 k_{\perp}}{\pi} \left\{ \varphi_A(k_{\perp}) - A^{1/3} \varphi_p(k_{\perp}) \right\} = 0, \quad (2.25)$$

which holds indeed within the MV model, for both fixed and running coupling, as we shall demonstrate shortly. From this relation, one can infer the existence of a Cronin peak through the following reasoning: Since at low momenta $k_{\perp} \ll Q_s(A)$ we have $\varphi_A(k_{\perp}) < A^{1/3} \varphi_p(k_{\perp})$ due to gluon saturation in the nucleus, whereas at large momenta $k_{\perp} \gg Q_s(A)$ the two functions approach the same limit, one concludes that $\varphi_A(k_{\perp})$ must be larger than $A^{1/3} \varphi_p(k_{\perp})$ at some intermediate momenta, in order to give rise to the same integrated distribution. One reason for the debate around this argument in the literature [25] is that in Ref. [24] the sum-rule has been abusively written as:

$$\int_{\Lambda^2} \frac{d^2 k_{\perp}}{\pi} \varphi_A(k_{\perp}) = A^{1/3} \int_{\Lambda^2} \frac{d^2 k_{\perp}}{\pi} \varphi_p(k_{\perp}). \quad (2.26)$$

At a first sight, this might look identical to Eq. (2.25), but in reality Eq. (2.26) is meaningless, since the expressions on both sides are logarithmically divergent in the ultraviolet. If, moreover, one introduces an upper cutoff Q^2 to eliminate these divergences, then the ensuing, finite, expressions do not coincide with each other for any finite Q^2 (see below). The would-be divergent pieces (i.e., the contributions proportional to $\ln Q^2$) are indeed the same for both integrals — because $\varphi_A(k_{\perp}) \simeq A^{1/3} \varphi_p(k_{\perp})$ for large $k_{\perp} \gg Q_s(A)$ —, but by itself this property only tells us that the integral in the left hand side of Eq. (2.25)

is well defined, but not also that the value of this integral is actually zero. In other terms, the equality of the divergent pieces in Eq. (2.26) carries no information about the behavior of the integrands at intermediate momenta, and thus cannot guarantee the existence of the Cronin peak [25].

Still, as we shall prove below, the difference $\mathcal{G}_A(Q^2) - A^{1/3}\mathcal{G}_p(Q^2)$ vanishes like $1/Q^2$ when $Q^2 \rightarrow \infty$, so the sum-rule (2.25) holds indeed as written. We have defined here:

$$\mathcal{G}_A(Q^2) \equiv \int_{\Lambda^2}^{Q^2} \frac{d^2 k_{\perp}}{\pi} \varphi_A(k_{\perp}), \quad (2.27)$$

(together with a similar expression for the proton) which, up to a global factor $\pi R_A^2 \times (N_c^2 - 1)/(2\pi)^2$ (cf. Eq. (2.1)), is the integrated gluon distribution in the MV model, i.e., the total number of gluons localized within a transverse area $1/Q^2$.

Our proof of Eq. (2.25) is very similar to the original one in Ref. [24], namely it uses the Fourier representation of the integrand (cf. Eqs. (2.4)–(2.5)) to easily perform the integral over k_{\perp} , and thus produce a δ -function $\delta^{(2)}(r_{\perp})$. Then, the sum-rule immediately follows because the integrand vanishes when $r_{\perp} \rightarrow 0$. For instance, in the case of a running coupling, Eq. (2.5), we write (we omit unnecessary constant factors) :

$$\begin{aligned} & \int \frac{d^2 k_{\perp}}{\pi} \int d^2 r_{\perp} e^{-ik_{\perp} \cdot r_{\perp}} \left\{ \frac{1 - e^{-\frac{1}{4} r_{\perp}^2 Q_A^2}}{r_{\perp}^2} - \frac{Q_A^2}{4} \right\} \ln \frac{4}{r_{\perp}^2 \Lambda^2} \\ & \propto \lim_{r_{\perp} \rightarrow 0} \left\{ \frac{1 - e^{-\frac{1}{4} r_{\perp}^2 Q_A^2}}{r_{\perp}^2} - \frac{Q_A^2}{4} \right\} \ln \frac{4}{r_{\perp}^2 \Lambda^2} = 0, \end{aligned} \quad (2.28)$$

which vanishes as $r_{\perp}^2 \ln r_{\perp}^2$ when $r_{\perp} \rightarrow 0$.

If the above integral over k_{\perp} is restricted to some finite, but large Q^2 , with $Q^2 \gg Q_A^2$, then instead of the δ -function $\delta^{(2)}(r_{\perp})$ one generates a smooth distribution in r_{\perp} which is peaked at $r_{\perp} = 0$, with the peak height proportional to Q^2 , and the width of the peak of order $1/Q^2$. When integrated over such a distribution, the ‘higher-twist’ terms in Eq. (2.28) (i.e., the higher order terms in the expansion of the exponential) give contributions which vanish as powers of $1/Q^2$ when $Q^2 \rightarrow \infty$. The dominant higher-twist contribution, of order $1/Q^2$, turns out to be **negative** (this is explicitly computed in the Appendix). Thus, for a finite, but large, Q^2 , the total number of gluons with transverse area $1/Q^2$ is **smaller** in the MV spectrum of a nucleus than in the corresponding bremsstrahlung spectrum (i.e., than it would be in the absence of non-linear effects). Specifically, one can use the results in the Appendix to deduce that

$$\mathcal{G}_A(Q^2) - \mathcal{G}_{BS}(Q^2) \simeq -\frac{1}{b_0 N_c} \frac{Q_s^4(A)}{2Q^2} \quad \text{for} \quad Q^2 \gg Q_s^2(A), \quad (2.29)$$

with $\mathcal{G}_{BS}(Q^2) \equiv A^{1/3} \mathcal{G}_p(Q^2)$. This is illustrated in Fig. 5.

The sum–rule (2.25) can be understood as the consequence of two basic properties, out of which one is generic — the fact that the non–linear effects fall off as inverse powers of k_\perp^2 in the high–momentum limit —, and the other one is specific to the MV model: the fact that the color sources (the valence quarks) are **uncorrelated**. Specifically, the second property implies that, at high momenta $k_\perp \gg Q_s(A)$, the gluon distributions produced by the 3A valence quarks sum up incoherently, so that the leading–twist terms cancel exactly in the difference $\varphi_A(k_\perp) - A^{1/3} \varphi_p(k_\perp)$. Moreover, by the first property, the remaining terms in this difference involve higher powers of $1/k_\perp^2$, which explains Eq. (2.29), and thus the sum–rule (2.25).

The above considerations also help us to understand why the sum rule is bound to fail after taking the quantum evolution with y into account: At $y > 0$, the color sources are predominantly gluons which are themselves products of radiation, and thus are correlated with each other (unlike the valence quarks) even in the leading–twist approximation. Because of that, the gluon occupation factors in the nucleus and in the proton are not simply proportional to each other, not even at high k_\perp . This can be easily verified on Eqs. (3.15) and (3.26), which give the dominant behavior at large momenta for $y > 0$. For instance, for fixed coupling, Eq. (3.15) implies (we omit the trivial factor $1/\alpha_s N_c$):

$$\begin{aligned} \varphi_A(k_\perp, y) - A^{1/3} \varphi_p(k_\perp, y) &\approx \frac{Q_A^2}{k_\perp^2} \left\{ e^{\sqrt{4\bar{\alpha}_s y \rho(A, k_\perp)}} - e^{\sqrt{4\bar{\alpha}_s y \rho(p, k_\perp)}} \right\} \\ &\approx -\rho_A \frac{Q_A^2}{k_\perp^2} \sqrt{\frac{\bar{\alpha}_s y}{\rho(A, k_\perp)}} e^{\sqrt{4\bar{\alpha}_s y \rho(A, k_\perp)}} \quad \text{for} \quad k_\perp \gg Q_s(A, y), \end{aligned} \quad (2.30)$$

where $\rho(A, k_\perp) \equiv \ln k_\perp^2 / Q_s^2(A)$, $\rho(p, k_\perp) \equiv \ln k_\perp^2 / Q_p^2 = \rho(A, k_\perp) + \rho_A$, and in writing the second line we have kept only the leading term at large $\rho(A, k_\perp)$. Although the expression above does vanish as $k_\perp \rightarrow \infty$, it is clear that it is not integrable in the sense of Eq. (2.25). The very fact that the sum–rule fails to apply at $y > 0$ does not preclude the existence of the Cronin peak: The sum–rule is only a **sufficient** condition for the existence of the peak, but not also a **necessary** one. And indeed the peak does persist (although its height is rapidly decreasing) in the early stages of the evolution, as we shall show in Sect. 5. This is also seen in the numerical results in Ref. [25].

Returning to the MV model, where the sum–rule (2.25) is valid, it is instructive to understand its physical implications in more detail: Eq. (2.25) tells us that the net result of the non–linear effects in the gluon dynamics is merely a **redistribution** of the gluons in the transverse momentum space. As it should be clear from the previous arguments, and

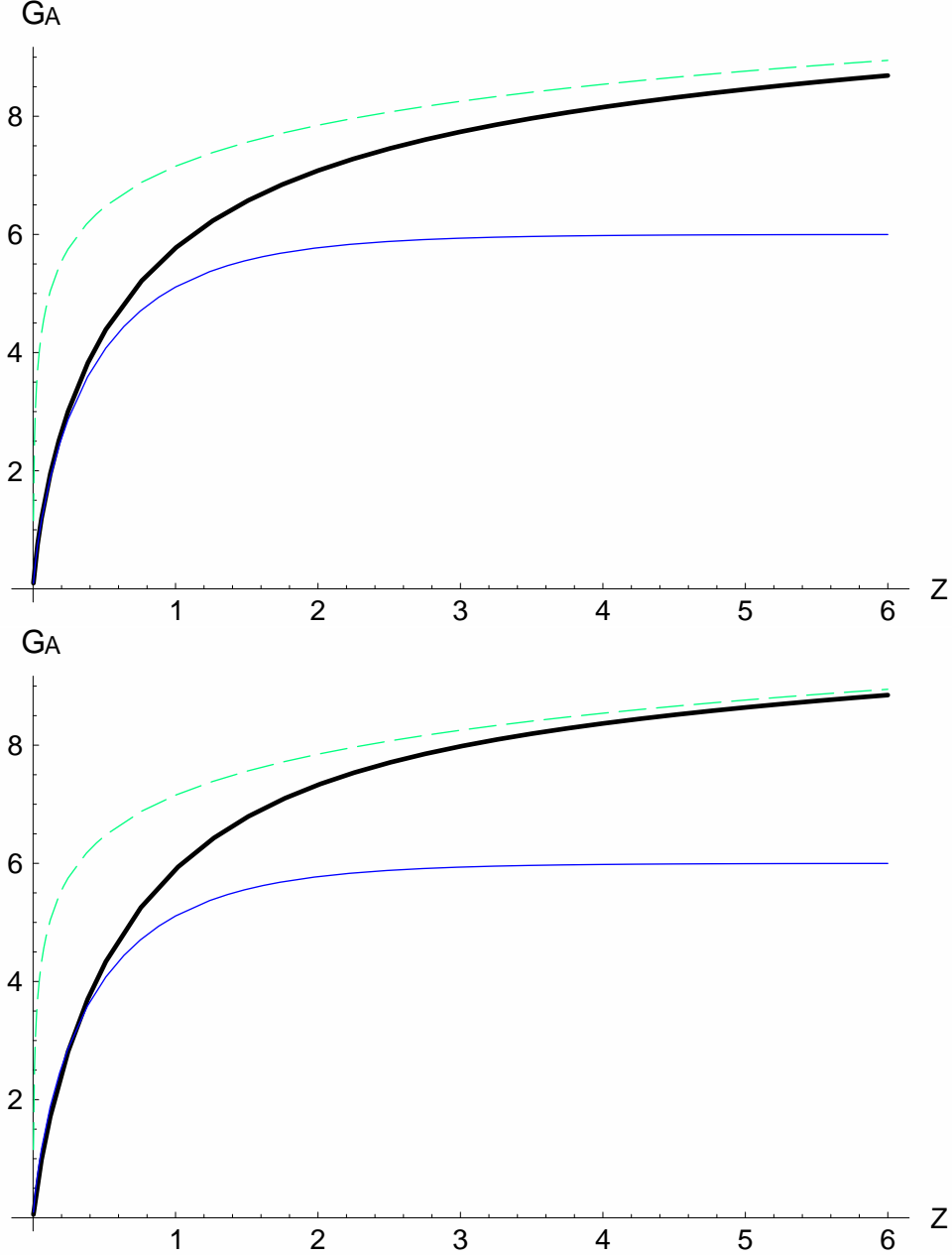


Fig. 5. The integrated gluon distribution function $\mathcal{G}_A(Z)$ as a function of the scaled momentum variable $Z = Q^2/Q_s^2(A)$ in fixed (above) and running (below) coupling McLerran-Venugopalan model for $\rho_A = 6$. With respect to the text definitions, we plot the quantities $[\rho_A \alpha_s N_c / Q_s^2(A)] \times \mathcal{G}_A$ for fixed coupling, and $[b_0 N_c / Q_s^2(A)] \times \mathcal{G}_A$ for running coupling. The black (thick) line corresponds to the integrated gluon distribution function $\mathcal{G}_A(Z)$; the blue (solid) line shows the saturation contribution $\mathcal{G}_A^{\text{sat}}(Z)$; the green (dashed) line represents the bremsstrahlung distribution function.

also from the plot in Fig. 3, this redistribution is associated with repulsive interactions which push the gluons towards the modes with larger momenta. In Fig. 3 one can see that, whereas at low momenta $k_\perp < Q_c(A)$ the gluon occupation factor is larger for the bremsstrahlung spectrum than for the MV spectrum, at higher momenta $k_\perp > Q_c(A)$ the opposite situation occurs. Here, $Q_c(A)$ is defined by⁴ (see Eq. (2.9)):

$$\frac{Q_A^2}{k_\perp^2} \sim \ln \frac{Q_s^2(A)}{k_\perp^2} \quad \text{for} \quad k_\perp \sim Q_c(A), \quad (2.31)$$

which implies :

$$Q_c^2(A) \simeq \frac{Q_A^2}{\ln \frac{Q_s^2(A)}{Q_c^2(A)}} \simeq \frac{Q_A^2}{\ln \frac{Q_s^2(A)}{Q_A^2}} \simeq \frac{Q_s^2(A)}{\rho_A \ln \rho_A}, \quad (2.32)$$

where we have also used $Q_s^2(A) = Q_A^2 \rho_A$, cf. Eq. (2.7). It is easily checked that $\Lambda^2 \ll Q_c^2(A) \ll Q_s^2(A)$ (since $\rho_A \gg 1$).

Thus, the effect of the interactions is to move the gluons up in transverse momentum, from below $Q_c(A)$ to above it. This explains, in particular, why when counting the gluons up to a finite (large) Q^2 , one necessarily finds a smaller number for the MV spectrum than for the bremsstrahlung one, cf. Eq. (2.29). But as we shall explain now, at large $k_\perp \gg Q_s(A)$ the effects of this redistribution are only tiny: **Most of the gluons which are in excess in the bremsstrahlung spectrum at $k_\perp < Q_c(A)$ are found in the MV spectrum in the saturation region at $k_\perp \lesssim Q_s(A)$.** In particular, the enhancement factor $1/\alpha_s \sim \rho_A$ characteristic of saturation finds its origin in the phase-space for bremsstrahlung radiation at momenta $\Lambda < k_\perp < Q_c(A)$. This factor is large because of the infrared sensitivity of the bremsstrahlung spectrum.

A simple way to see this is to notice that the total number of gluons in the region $\Lambda < k_\perp < Q_s(A)$ is essentially the same for the bremsstrahlung spectrum and for the MV spectrum. Indeed, we have first :

$$\mathcal{G}_{BS}(Q_s^2(A)) = \int_{\Lambda^2}^{Q_s^2(A)} \frac{d^2 k_\perp}{\pi} \frac{1}{\alpha_s N_c} \frac{Q_A^2}{k_\perp^2} = \frac{Q_A^2}{\alpha_s N_c} \ln \frac{Q_s^2(A)}{\Lambda^2} = \frac{Q_s^2(A)}{\alpha_s N_c}, \quad (2.33)$$

where the saturation momentum $Q_s(A)$ has been reconstructed as $Q_s^2(A) = Q_A^2 \rho_A$, cf. Eq. (2.7). Note that the large factor $\rho_A = \ln Q_s^2(A)/\Lambda^2$ has been generated from the

⁴ The subsequent formulae in this subsection are written for the case of a fixed coupling, for definiteness. It can be easily checked that analog formulae, leading to similar conclusions, apply also for the MV model with a running coupling.

phase-space for the bremsstrahlung gluons at $\Lambda < k_\perp < Q_s(A)$. For the MV spectrum, we shall define $\mathcal{G}_A(Q_s^2(A))$ as the total number of gluons contained in the saturating component of the spectrum $\varphi_A^{\text{sat}}(k_\perp)$. This is appropriate since $\varphi_A(k_\perp) \approx \varphi_A^{\text{sat}}(k_\perp)$ for any $k_\perp < Q_s(A)$, whereas at larger momenta $\varphi_A^{\text{sat}}(k_\perp)$ falls off exponentially. One then obtains:

$$\mathcal{G}_A(Q_s^2(A)) = \int \frac{d^2k_\perp}{\pi} \frac{1}{\alpha_s N_c} \Gamma(0, k_\perp^2/Q_s^2(A)) = \frac{Q_s^2(A)}{\alpha_s N_c}. \quad (2.34)$$

(The simplest way to obtain this result is to notice that the unrestricted integral of $\varphi_A^{\text{sat}}(k_\perp)$ is tantamount to letting $r_\perp \rightarrow 0$ in the integral representation of $\varphi_A^{\text{sat}}(k_\perp)$ in Eq. (2.13).) As anticipated, the final expressions in Eqs. (2.33) and (2.34) are identical. But, of course, the way how these gluons are distributed in k_\perp is very different in the two cases: For the bremsstrahlung spectrum, which is infrared divergent, most of these gluons are located at low momenta $k_\perp < Q_c(A)$, while for the MV spectrum they are rather uniformly distributed at all momenta up to $Q_s(A)$. For instance (see Eq. (2.32)):

$$\mathcal{G}_{BS}(Q_c^2(A)) = \int_{\Lambda^2}^{Q_c^2(A)} \frac{d^2k_\perp}{\pi} \frac{1}{\alpha_s N_c} \frac{Q_A^2}{k_\perp^2} = \frac{Q_A^2}{\alpha_s N_c} \ln \frac{Q_c^2(A)}{\Lambda^2} \approx \frac{Q_A^2}{\alpha_s N_c} (\rho_A - \ln \rho_A), \quad (2.35)$$

is almost the same as the result in Eq. (2.33) (in particular, it includes already the enhancement factor ρ_A due to the logarithmic phase-space⁵). This confirms the fact that the color glass condensate in the MV model is formed by redistributing the ‘infrared’ gluons at $k_\perp < Q_c(A)$ in the bremsstrahlung spectrum.

3 Non-linear gluon evolution in the Color Glass Condensate

Within the effective theory for the CGC [26], the evolution of the gluon distribution with y is not described by a single, closed, equation, but rather by an infinite hierarchy of coupled equations, which relate n -point functions with arbitrary $n \geq 2$ (by itself, $\varphi(k_\perp, y)$ corresponds to a 2-point function), and are compactly summarized in a *functional* evolution equation, the JIMWLK equation. Fortunately, this complicated evolution simplifies considerably in interesting limiting cases, which are tractable through analytic approximations [35, 36].

At low momenta $k_\perp \lesssim Q_s(A, y)$, the gluons form a condensate with occupation factors of order $1/\alpha_s$, and the dynamics is highly non-linear. Still, one can rely on mean field

⁵ Although $Q_c^2(A) \approx Q_s^2(A)/\rho_A \ll Q_s^2(A)$, the logarithmic phase-space at $\Lambda < k_\perp < Q_c(A)$ (namely $\rho_A - \ln \rho_A$) is almost the same as that for the whole interval $\Lambda < k_\perp < Q_s(A)$ (which is equal to ρ_A).

approximations to deduce a formula for $\varphi(k_\perp, y)$ valid in the low momentum limit $k_\perp \ll Q_s(A, y)$ [35–37, 55, 58], which will be presented in Sect. 3.1 below.

At high momenta $k_\perp \gg Q_s(A, y)$, the gluon density is low, and non-linear effects in the evolution become negligible. Then, the general equations for the evolution of the gluon distribution boil down to a single, linear, equation: the BFKL equation [43]. The latter controls also the approach towards saturation from the above (at least, approximately), and thus determines the saturation momentum $Q_s(A, y)$ [7, 38–41].

For a fixed coupling, we shall discuss in Sect. 3.2 the solution to the BFKL equation in the saddle point approximation and with saturation boundary conditions [38–41] (see also [48]). Our derivation of this solution will be quite schematic, and only intended to emphasize a subtle point — namely, the fact that it is the saturation scale in the initial conditions, $Q_s(A)$, which sets the infrared cutoff for the transverse phase-space available for evolution [42] —, and to prepare the ground for a general discussion of high- k_\perp suppression through quantum evolution, to be presented in Sect. 4.

For a running coupling, with the scale for running set by the gluon transverse momentum k_\perp , we shall follow the analysis in Refs. [39–41], from which we shall simply quote here the relevant results, and discuss their range of validity.

3.1 *Non-linear evolution at low k_\perp : Saturation and universality*

In the high density regime deeply at saturation ($k_\perp \ll Q_s(A, y)$), the color fields are strong ($A^i \sim 1/g$) and the dynamics is fully non-linear, which makes it difficult to use standard perturbative techniques. On the other hand, these conditions are favorable to the use of mean field approximations [35, 36], which enable us to determine the y - and k_\perp -dependencies of the gluon occupation factor. Similar results are also obtained from studies of the unitarization effects in dipole-hadron scattering [37, 55, 58].

Remarkably, it turns out that the functional form of the gluon occupation factor at saturation is **universal** [35]: For $k_\perp \ll Q_s(A, y)$, $\varphi_A(k_\perp, y)$ is independent of either the initial condition at $y = 0$, or the details of the evolution leading to saturation, except for the corresponding dependencies of the saturation scale itself. Moreover, this universal form happens to be the same as in the MV model (cf. the expressions in the second lines of Eqs. (2.9) and (2.10)), which is quite non-trivial, and to some extent surprising, since the physical conditions leading to this functional form are very different in the two cases: Whereas in the MV model the color sources are uncorrelated, and the logarithmic behavior at low k_\perp is merely the result of non-linear effects in the classical equations of motions for the color fields [12, 30], in the effective theory at small x the color sources are strongly correlated, in such a way to ensure color neutrality over a transverse size $\sim 1/Q_s(A, y)$

[35, 36, 58], and the logarithmic behavior at low k_\perp is already encoded in the correlations of the color sources (i.e., it holds independently of the presence of non-linear terms in the classical field equations; the latter affect only the overall normalization of the gluon distribution, which in this non-linear regime is anyway not under control).

Specifically, for fixed coupling, one finds [35–37] :

$$\varphi_A(k_\perp, y) \approx \frac{a_0}{\alpha_s N_c} \ln \frac{Q_s^2(A, y)}{k_\perp^2}, \quad (\text{fixed coupling}), \quad (3.1)$$

whereas for running coupling (with the scale for running set by the gluon momentum k_\perp) one obtains [12, 58].

$$\varphi_A(k_\perp, y) \approx \frac{a_0}{N_c} \left\langle \frac{1}{\alpha_s} \right\rangle \ln \frac{Q_s^2(A, y)}{k_\perp^2}, \quad (\text{running coupling}), \quad (3.2)$$

with (compare to Eq. (2.11)) :

$$\left\langle \frac{1}{\alpha_s} \right\rangle \equiv \frac{1}{2b_0} \left\{ \ln \frac{Q_s^2(A, y)}{\Lambda^2} + \ln \frac{k_\perp^2}{\Lambda^2} \right\}. \quad (3.3)$$

The overall factor a_0 in these equations is a number of order one which cannot be computed analytically (and which needs not be the same for fixed and running coupling).

Note that, in the fixed coupling case, the gluon distribution at saturation depends upon the two kinematical variables k_\perp and y only via the ratio $z \equiv k_\perp^2/Q_s^2(A, y)$. This property, known as **geometric scaling** [56], reflects the fact that the saturation momentum is the only intrinsic scale at saturation. As manifest on Eq. (3.2), the running of the coupling introduces a second intrinsic scale, namely Λ , and this is a source of geometric scaling violations, which are however under control.

3.2 Linear evolution at high k_\perp : Fixed coupling

In the low density regime at high momenta $k_\perp \gg Q_s(A, y)$, the dynamics is linear, and the nuclear gluon occupation factor can be obtained (to the present accuracy) by solving the BFKL equation [43] with initial conditions at $y = 0$ provided by the MV model (cf. Eq. (2.4)–(2.5)) and with an ‘absorptive’ boundary condition at $k_\perp \sim Q_s(A, y)$ [39, 40] which mimics the non-linear effects in the approach towards saturation. (Similar results

have been recently obtained [41] through direct studies of the non-linear Kovchegov equation [32, 33].) In particular, the saturation scale itself is obtained by requiring $\varphi_A(k_\perp, y)$ to become of order $1/\alpha_s$ at saturation (up to subleading terms of $\mathcal{O}(1)$) :

$$\varphi_A(k_\perp, y) \simeq \frac{\kappa}{\alpha_s(Q_s^2(A, y))N_c} \quad \text{for} \quad k_\perp \sim Q_s(A, y). \quad (3.4)$$

(κ is a number of order one.)

When y and/or k_\perp are relatively large (see below), an approximate analytic solution can be obtained, via a saddle point approximation. Here we shall outline only a few steps in the construction of this solution (see Refs. [38, 39] for details).

For fixed coupling, the solution to the BFKL equation for $\varphi_A(k_\perp, y)$ can be written in Mellin form as:

$$\varphi_A(k_\perp, y) = \int_C \frac{d\gamma}{2\pi i} \left(\frac{Q_0^2}{k_\perp^2} \right)^\gamma e^{\bar{\alpha}_s y \chi(\gamma)} \widetilde{\varphi}_A(\gamma; Q_0), \quad (3.5)$$

where $\bar{\alpha}_s = \alpha_s N_c / \pi$, $\chi(\gamma) = 2\psi(1) - \psi(\gamma) - \psi(1 - \gamma)$ with $\psi(\gamma) \equiv d \ln \Gamma(\gamma) / d\gamma$ and complex γ is the eigenvalue of the BFKL kernel, $\widetilde{\varphi}_A(\gamma; Q_0)$ is the Mellin transform of the initial condition $\varphi_A(k_\perp)$, Eq. (2.4):

$$\widetilde{\varphi}_A(\gamma; Q_0) = \int_0^\infty \frac{dk_\perp^2}{k_\perp^2} \left(\frac{k_\perp^2}{Q_0^2} \right)^\gamma \varphi_A(k_\perp), \quad (3.6)$$

and Q_0 is an arbitrary reference scale introduced for dimensional reasons, and which drops out in the complete result, as obvious on the above equations. Given the behavior of the initial distribution $\varphi_A(k_\perp)$ in various limits, cf. Eq. (2.9), it can be checked that the integral over k_\perp^2 in Eq. (3.6) is absolutely convergent for $0 < \text{Re } \gamma < 1$. Thus the contour for the complex integration in Eq. (3.5) can be chosen as $C = \{\gamma = \gamma_1 + i\gamma_2; -\infty < \gamma_2 < \infty\}$, with a fixed γ_1 in the range $0 < \gamma_1 < 1$.

The same study of the convergence properties of the integral in Eq. (3.6) tells us that **this integral is dominated by momenta of the order of the initial saturation momentum $Q_s(A)$** : Indeed, for large $k_\perp \gg Q_s(A)$, $\varphi_A(k_\perp) \propto 1/k_\perp^2$, and the integral is saturated by momenta of the order of the lower cutoff $Q_s(A)$. Furthermore, for low momenta $k_\perp \ll Q_s(A)$, the initial distribution saturates: $\varphi_A(k_\perp) \propto \ln(Q_s^2/k_\perp^2)$, so the integral is now dominated by momenta near the upper cutoff, i.e., by $k_\perp \sim Q_s(A)$ once again. Thus, after performing the integral over k_\perp , $Q_s(A)$ replaces Q_0 as the **natural** reference scale in the Mellin representation of the solution $\varphi_A(k_\perp, y)$. Then, Eq. (3.5) can be rewritten as:

$$\varphi_A(k_\perp, y) = \frac{1}{\alpha_s N_c} \int_C \frac{d\gamma}{2\pi i} \left(\frac{Q_s^2(A)}{k_\perp^2} \right)^\gamma e^{\bar{\alpha}_s y \chi(\gamma)} \widetilde{\varphi}_A(\gamma; \rho_A), \quad (3.7)$$

where any reference to the arbitrary scale Q_0 has disappeared. Note that, for more clarity, we have extracted a factor $1/\alpha_s N_c$ out of the (Mellin transform of) the initial condition $\widetilde{\varphi}_A(\gamma; \rho_A)$. The latter still depends upon $Q_s(A)$, but only logarithmically, via $\rho_A \equiv \ln(Q_s^2(A)/\Lambda^2)$. The precise form of the function $\widetilde{\varphi}_A(\gamma; \rho_A)$ will not be needed in what follows. Rather, we shall use its approximate form which is obtained when $\varphi_A(k_\perp)$ in Eq. (3.6) is replaced by the simplest interpolation between the asymptotic behaviors shown in Eq. (2.9). This reads :

$$\widetilde{\varphi}_A(\gamma; \rho_A) = -\frac{\Gamma(\gamma)\psi(1-\gamma)}{\rho_A} + \frac{\Gamma(\gamma)}{\gamma} + \dots \approx \frac{1}{\rho_A} \frac{1}{1-\gamma} + \frac{1}{\gamma^2}. \quad (3.8)$$

The first term in the last (approximate) equality, which has a pole at $\gamma = 1$ and is suppressed as $1/\rho_A$, comes from the high- k_\perp behavior (the bremsstrahlung spectrum in Eqs. (2.9)), while the second term, with a double pole at $\gamma = 0$, comes from the saturating behavior at low k_\perp .

3.2.1 The saddle point approximation

At this stage, it becomes natural to introduce the logarithmic momentum variable $\rho \equiv \ln(k_\perp^2/Q_s^2(A)) = \rho(A, k_\perp)$, and notice that, when either $\bar{\alpha}_s y$, or ρ , or both, are large, the integral in Eq. (3.7) can be evaluated via a **saddle point approximation**. Specifically, if one writes:

$$\varphi_A(k_\perp, y) = \frac{1}{\alpha_s N_c} \int_C \frac{d\gamma}{2\pi i} e^{\bar{\alpha}_s y F(\gamma, r)} \widetilde{\varphi}_A(\gamma; \rho_A), \quad (3.9)$$

where:

$$r \equiv \frac{\rho}{\bar{\alpha}_s y}, \quad F(\gamma, r) = -\gamma r + \chi(\gamma), \quad (3.10)$$

then the saddle point $\gamma_0 \equiv \gamma_0(r)$ satisfies the condition:

$$\left. \frac{\partial F}{\partial \gamma}(\gamma, r) \right|_{\gamma=\gamma_0(r)} = -r + \chi'(\gamma_0(r)) = 0, \quad (3.11)$$

which shows that $\gamma_0(r)$ is a real number, in between 0 and 1. The behavior of the function $\chi(\gamma)$ in this range is illustrated in Fig. 6.

After expanding around the saddle point and performing the Gaussian integral over the small fluctuations, one obtains :

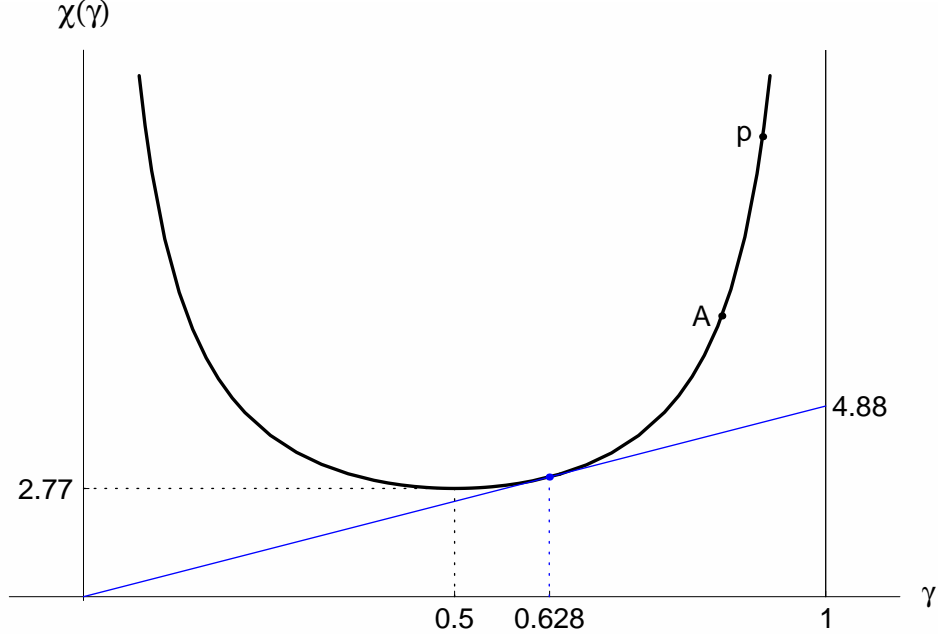


Fig. 6. *The BFKL eigenvalue $\chi(\gamma)$ and the graphical solution to the saturation problem* The value $\gamma_s = 0.628$ corresponds to the saturation saddle point and the value $\chi(\gamma_s)/\gamma_s = 4.88$ determines the asymptotic energy dependence of the saturation momentum (for comparison, the “hard pomeron” saddle point $\gamma_P = 1/2$ and its intercept $\omega_P = 4 \ln 2 = 2.77$ are shown). The points **p** and **A** correspond to the proton and the nucleus respectively, for the same transverse momentum and rapidity, when they are far above the saturation scale.

$$\varphi_A(k_\perp, y) \approx \frac{1}{\alpha_s N_c} \frac{e^{\bar{\alpha}_s y F(\gamma_0, r)}}{\sqrt{2\pi \bar{\alpha}_s y \chi''(\gamma_0)}} \widetilde{\varphi}_A(\gamma_0; \rho_A). \quad (3.12)$$

This is a reasonable approximation to Eq. (3.7) provided $\bar{\alpha}_s y \gtrsim 1$, $\rho \gtrsim 1$, and at least one of these quantities is much larger than one.

When r varies from 0 to ∞ , the function $\gamma_0(r)$ is monotonously increasing, and spans the range from $\gamma_0(0) = 1/2$ to $\gamma_0(\infty) = 1$. Note, however, that physically the ratio r cannot be smaller than the value $r_s \equiv \rho_s(y)/\bar{\alpha}_s y$ (with $\rho_s(y) \equiv \ln[Q_s^2(A, y)/Q_s^2(A)]$) which corresponds to the saturation momentum. Indeed, the linear approximation is justified only as long as $k_\perp \gg Q_s(A, y)$, or $\rho > \rho_s(y)$.

To compute the saturation momentum, and the corresponding saddle point $\gamma_s \equiv \gamma_0(r_s)$, we shall use the saturation boundary condition (3.4), together with the approximation (3.12) for $\varphi_A(k_\perp, y)$, which for this purpose is extrapolated down to $k_\perp \sim Q_s(A, y)$. It can be justified that this is a legitimate procedure for the calculation of the energy dependence of $Q_s(A, y)$, although not necessarily also for its absolute normalization [38, 39]. To the accuracy of interest here, Eqs. (3.12) and (3.4) imply just that the exponent in Eq. (3.12)

must vanish on the saturation line:

$$F(\gamma_0(r), r) \Big|_{r=r_s} \equiv -\gamma_s r_s + \chi(\gamma_s) = 0, \quad (3.13)$$

which shows that r_s is a pure number, to be denoted as c in what follows. This number together with γ_s are determined by Eqs. (3.11) and (3.13) as: $\gamma_s = \chi(\gamma_s)/\chi'(\gamma_s) = 0.627\dots$ and $c \equiv r_s = \chi'(\gamma_s) = 4.883\dots$ [7, 37–39].

Note that in writing the saturation condition in the form (3.13) we have neglected the effect of the Gaussian fluctuations around the saddle point. The reason is that this effect is modified by the absorptive boundary condition at saturation [39] (that we neglect here), and thus cannot be correctly computed in the present approximations. In what follows, we shall often ignore such slowly varying prefactors, but only include the dominant behavior at high energy. To the same accuracy, the nuclear saturation momentum reads:

$$Q_s^2(A, y) \simeq Q_s^2(A) e^{c\bar{\alpha}_s y}, \quad c = 4.883\dots \quad (3.14)$$

This expression appears to satisfy the initial condition $Q_s^2(A, y=0) = Q_s^2(A)$, but this is only formal, since the calculation above is valid only for relatively large y , with $\alpha_s y > 1$, so the extrapolation to $y \rightarrow 0$ is not justified. In fact, the energy dependence of $Q_s^2(A, y)$ displayed in Eq. (3.14) is only the first term in an asymptotic expansion at large y , out of which also the second term [39, 40] and the third one [41] are presently known.

For practical purposes, the saddle point approximation (3.12) is still quite involved, since the function $\gamma_0(r)$ is known only implicitly, as the solution to Eq. (3.11). However, important simplifications leading to fully explicit formulae can be performed either for very large momenta, $\rho \gg \bar{\alpha}_s y$ — this corresponds to the so-called “double-logarithmic accuracy”, or DLA, regime —, or for momenta above, but relatively close to the saturation scale, where one can expand Eq. (3.12) around the saturation saddle point. Below, we shall refer to the latter regime as the “BFKL regime”⁶.

Let us briefly describe here the modifications which should be brought into the previous formulae in order to adapt them to the case of a proton. Recall that there is no saturation scale (i.e., no analog of the nuclear scale $Q_s(A)$) in the proton at $y = 0$. The infrared cutoff is rather set by the scale Q_p which is soft and reflects non-perturbative physics (cf. Eq. (2.18)). This is therefore also the scale which enters the formulae for the linear evolution of $\varphi_p(k_\perp, y)$ with increasing y . E.g., the proton analog of Eq. (3.7) is obtained

⁶ Note that this is not the usual BFKL regime associated with the saddle point $\gamma_{\mathbb{P}} = 1/2$ and corresponding to the high energy limit $\alpha_s y \gg \rho$. Whereas $\gamma_{\mathbb{P}} = 1/2$ describes the evolution with y at fixed (and relatively low) k_\perp , $\gamma_s = 0.63$ corresponds rather to an evolution where, when increasing y , k_\perp is correspondingly increased, in such a way that the condition $k_\perp^2 > Q_s^2(A, Y)$ (or $\rho > \rho_s(Y)$) remains satisfied.

by replacing $Q_s(A) \rightarrow Q_p$ and taking an initial condition $\widetilde{\varphi}_p(\gamma) = 1/(1 - \gamma)$ (compare to Eq. (3.8)). In particular, the variable ρ for the proton is defined as $\rho(p, k_\perp) \equiv \ln(k_\perp^2/Q_p^2)$. Of course, for sufficiently large y , the gluon density in the proton will become large, and a (hard) saturation scale $Q_s(p, y)$ will be eventually generated. The dominant y -dependence of this scale at large y is described again by Eq. (3.14), but with $Q_s(A) \rightarrow Q_p$. More generally, all the formulae to be obtained below in this section can be translated to the case of a proton by replacing everywhere $Q_s(A) \rightarrow Q_p$.

3.2.2 DLA regime

If $\rho \gg \alpha_s y$, the saddle point is close to one, and only the first term (the one having a pole at $\gamma = 1$) must be retained in the initial condition (3.8). A straightforward calculation yields $\gamma_0(r) \approx 1 - 1/\sqrt{r}$, and :

$$\varphi_A(k_\perp, y) \simeq \frac{1}{\alpha_s N_c} \frac{Q_A^2}{k_\perp^2} \frac{e^{\sqrt{4\bar{\alpha}_s y \rho}}}{\sqrt{2\pi\sqrt{4\bar{\alpha}_s y \rho}}}, \quad (3.15)$$

where the factor Q_A^2 has been reconstructed as $Q_s^2(A)/\rho_A$. This approximation is valid for $\bar{\alpha}_s y \rho \gg 1$, and as long as this condition is satisfied, Eq. (3.15) can be even used for relatively small y , with $\bar{\alpha}_s y \ll 1$. Indeed, in this regime Eq. (3.15) can be obtained from the DGLAP equation [57], which provides a resummation based on the assumptions that $\alpha_s \rho \geq 1$, but $\alpha_s y \ll 1$.

3.2.3 BFKL regime: weak universality and approximate scaling

When ρ is larger than $\rho_s(y) \equiv \ln(Q_s^2(A, y)/Q_s^2(A)) = c\bar{\alpha}_s y$, but not much larger, one can obtain an explicit form for $\varphi_A(k_\perp, y)$ by expanding the general saddle point approximation, Eq. (3.12), in powers of $r - r_s$ (or, equivalently, in powers of $(\rho - \rho_s)/\rho_s$). To second order in this expansion, one obtains [38–41]

$$\varphi_A(k_\perp, y) \approx \frac{\kappa_0}{\alpha_s N_c} \{\rho - \rho_s + \Delta\} e^{-\gamma_s(\rho - \rho_s)} \exp\left\{-\frac{(\rho - \rho_s)^2}{2\beta\bar{\alpha}_s y}\right\}, \quad (3.16)$$

or, more explicitly [recall that $\rho - \rho_s = \ln(k_\perp^2/Q_s^2(A, y))$] :

$$\varphi_A(k_\perp, y) \approx \frac{\kappa_0}{\alpha_s N_c} \left\{ \ln \frac{k_\perp^2}{Q_s^2(A, y)} + \Delta \right\} \left(\frac{Q_s^2(A, y)}{k_\perp^2} \right)^{\gamma_s} \exp\left\{-\frac{1}{2\beta\bar{\alpha}_s y} \ln^2 \frac{k_\perp^2}{Q_s^2(A, y)}\right\} \quad (3.17)$$

In these equations, $\gamma_s \simeq 0.63$ appears as an “anomalous dimension” (recall that, at very high k_\perp , the actual power of $1/k_\perp^2$ was one, both in the initial condition at $y = 0$, and in the DLA approximation (3.15) at $y > 0$). Furthermore, $\beta \equiv \chi''(\gamma_s) = 48.518\dots$ plays the role of a diffusion coefficient for the diffusion in $\ln(k_\perp^2/Q_s^2)$.

The constant numbers κ_0 and Δ in Eq. (3.17) are not known⁷, as they depend upon the detailed matching onto the (unknown) solution in the transition region towards saturation. In particular, Eqs. (3.17) and (3.4) need not match with each other, since there is no reason why Eq. (3.17) should remain correct down to $Q_s(A, y)$. But in writing Eq. (3.17) we have nevertheless assumed that, when extrapolated to $k_\perp \sim Q_s(A, y)$, the BFKL solution becomes parametrically of the same order as the actual solution in the transition region (namely, they are both of order $1/\alpha_s$). This may look surprising in view of the previous experience with the MV model where we have seen that, when extrapolated down to $Q_s(A)$, the twist piece φ_A^{twist} remains parametrically smaller (by a factor ρ_A) than the actual distribution at saturation φ_A^{sat} . The two functions match with each other only at the (parametrically larger) momenta $k_\perp^2 \sim (\ln \rho_A) Q_s^2(A)$. Still, as we shall see through a more detailed analysis in Sect. 5.3, the evolution with y is such that a power-law, ‘twist’, tail develops in the gluon distribution at momenta just above $Q_s(A, y)$, and this tail is predominantly generated via radiation from those gluons which were originally at saturation (i.e., which at $y = 0$ were included in φ_A^{sat}). Thus, for $\alpha_s y \gtrsim 1$, the twist contributions generated by the evolution are **not** parametrically suppressed with respect to the saturating distribution anymore.

An important property of Eq. (3.17), that we shall refer to as **weak universality** (as opposed to the **strong universality** that has been found at saturation [35]) is the fact that the functional form of this expression, seen as a function of $z \equiv k_\perp^2/Q_s^2(A, y)$ and y , is independent of the initial condition at $y = 0$ (and, in particular, of A), but rather is fully determined by the quantum (BFKL) evolution together with the saturation boundary condition: $\varphi_A(k_\perp, y) = \varphi(z, y)$, with φ an universal function. The initial condition affects only the value of the saturation momentum, cf. Eq. (3.14) [42].

The factor linear in $\rho - \rho_s$ in the right hand side of Eq. (3.16), or (3.17), does not come from the expansion of Eq. (3.12), but rather from the absorptive boundary condition at saturation [39, 41], that we have ignored so far. The reason why this factor cannot be neglected (in contrast, e.g., with the prefactor in the expression (3.14) for the saturation scale) is that this factor introduces a dependence upon ρ which is not suppressed at large y . The other factors in Eq. (3.16), which involve $\rho - \rho_s$ in the exponent, do come from the expansion of Eq. (3.12). A priori, one would expect this expansion to be valid so long as $(\rho - \rho_s)/\rho_s \ll 1$, since this is the “small parameter”. However, since β is a relatively large number, the second order term in the expansion, quadratic in $\rho - \rho_s$, remains small

⁷ But it seems natural to impose $\Delta \geq 1/\gamma$, to avoid that Eq. (3.17) become a decreasing function of $1/k_\perp^2$ when approaching $Q_s(A, y)$ from the above.

as compared to the linear term even for $\rho - \rho_s \sim \rho_s$. We conclude that Eq. (3.16) (or (3.17)) is a good approximation for any ρ within the following range [38] :

$$0 < \rho - \rho_s(y) \lesssim \rho_s(y), \quad (3.18)$$

often referred to as the “extended scaling window”, since within this range the BFKL solution approximately preserves the geometric scaling property characteristic of saturation [38, 39]: More precisely, Eq. (3.16) shows scaling so long as $\rho - \rho_s(y) \ll \sqrt{2\beta\bar{\alpha}_s y}$, whereas for larger ρ , the scaling is violated by the diffusion term. Both the scaling property, and its violation, seem to be necessary to understand the small- x data at HERA [56, 59, 60].

Note finally that the existence of a relatively large window for geometric scaling **above** the saturation momentum is a consequence of the evolution⁸, so it takes some finite amount of rapidity (typically, $\bar{\alpha}_s y \sim 1$) until this behavior is actually reached.

3.2.4 The geometric scaling line : Approximately matching BFKL and DLA

The approximate solutions that we have found so far apply in different kinematical regions — $\rho \gg \alpha_s y$ for the DLA formula (3.15), and $\rho - \rho_s \lesssim \rho_s$ for the BFKL expression (3.16) —, which have no overlap with each other. So, a priori, there seems to be no reason why these expressions could be matched onto each other. Still, if one chooses $\rho = 2\rho_s(y) = 2c\bar{\alpha}_s y$, and one estimates both the DLA and the BFKL expressions along this line, then one finds that the dominant (exponential) behavior in y is very similar, although not exactly the same, for both approximations. This is in agreement with an observation [38] that the **geometric scaling line** $\rho = 2\rho_s(y)$ is approximately the borderline between the regions dominated by the saturation saddle point and, respectively, by the DLA saddle point in the $y - \ln k_\perp^2$ plane.

This opens the possibility to achieve at least an **approximate matching** between the two limiting expressions, by appropriately tuning the borderline between these two regime. Of course, there is no fundamental reason in favor of this matching, but this will be convenient in practice, as it will allow us to avoid exponentially large discontinuities when studying the ratio \mathcal{R}_{pA} in different regimes. Specifically, we shall tune the upper limit in the window (3.18) in such a way that the leading, exponential, behavior along that line be exactly the same for the DLA and BFKL approximations with fixed coupling. A straightforward calculation shows that Eq. (3.18) must be replaced by

⁸ For instance, there is no such a window in the initial conditions at $y = 0$, where the property of geometric scaling can be defined with respect to the dependencies upon k_\perp and A . As manifest on Eq. (2.13)–(2.15), it is only the saturating distribution which is just function of $z = k_\perp^2/Q_s^2(A)$; the twist terms have additional, explicit, dependencies upon A (and Λ), through factors of $1/\rho_A$.

$$0 < \rho - \rho_s(y) \leq \nu \rho_s(y), \quad (3.19)$$

or, equivalently,

$$Q_s^2(A, y) \ll k_\perp^2 < Q_g^2(A, y) \equiv Q_s^2(A, y) \left(\frac{Q_s^2(A, y)}{Q_s^2(A)} \right)^\nu, \quad (3.20)$$

with $\nu \approx 1.708$ determined by solving the following equation:

$$c[(1 - \gamma_s)\nu + 1] - \sqrt{4c(\nu + 1)} - \frac{(\nu c)^2}{2\beta} = 0. \quad (3.21)$$

As anticipated, ν is a number of order one.

3.3 Linear evolution at high k_\perp : Running coupling

Since the (leading-order) BFKL equation corresponds to a fixed-coupling approximation, the inclusion of the running is a priori ambiguous. Physical arguments, together with recent experience [40, 45] with the next-to-leading order BFKL equation [44], suggest that it should be appropriate to use a coupling which is running with the transverse momentum k_\perp of the gluon [i.e., $\alpha_s \equiv \alpha_s(k_\perp^2)$]. This running has been already used in obtaining Eq. (3.2), valid in the saturation region. With such a running, the BFKL equation becomes difficult to solve in general, even formally, so it is interesting to keep in mind that, in order to study the high-energy limit⁹, one can also use the running with the saturation momentum [i.e., $\alpha_s \equiv \alpha_s(Q_s^2(A, y))$]. Indeed, with increasing y , the relative separation from the saturation line $(\rho - \rho_s(y))/\rho_s(y)$ becomes smaller and smaller, and we can approximate, e.g. (with $b \equiv b_0 N_c/\pi = 12N_c/(11N_c - 2N_f)$),

$$\bar{\alpha}_s(k_\perp^2) \equiv \frac{b}{\ln(k_\perp^2/\Lambda^2)} \approx \bar{\alpha}_s(Q_s^2(A, y)) \left(1 - \frac{\rho - \rho_s(y)}{\tau_A(y)} \right). \quad (3.22)$$

In this equation $\tau_A(y) = \ln(Q_s^2(A, y)/\Lambda^2) = \rho_s(y) + \rho_A$ (see Eq. (3.23) below for a more precise definition). By using just the first term in this expansion, i.e., $\bar{\alpha}_s(Q_s^2(A, y))$, one obtains the correct dominant behavior at high energy for both the saturation momentum and the gluon distribution [38–41]. However, interesting subleading effects at high energy (like the “diffusion term” in the gluon distribution) are not correctly given by

⁹ In the present context, this is the limit in which, with increasing y , ρ is increased as well, in such a way to remain in the linear regime at $\rho > \rho_s(y)$.

this approximation, whose applicability at finite y is restricted to a rather narrow strip $(\rho - \rho_s)/\rho_s \ll 1$ above the saturation line. To keep control on such subleading effects, we shall follow Refs. [39–41] and use the whole expression in the r.h.s. of Eq. (3.22) when studying the “BFKL regime” precursory of saturation. Of course, the resulting approximation will be still limited to $(\rho - \rho_s)/\rho_s \ll 1$ — because of the expansion performed in Eq. (3.22), and also of the other approximations needed when solving the (corresponding version of) BFKL equation [39, 40] —, but as we shall see, the accessible window is considerably wider with this improved running.

On the other hand, for much larger momenta, such that $\rho - \rho_s \gtrsim \rho_s$, the running effects cannot be expanded anymore, and the actual running coupling $\bar{\alpha}_s(k_\perp^2)$ has to be used. But in this regime, the BFKL equation itself boils down to the DLA equation, which is much simpler, and whose exact solution is known also with running coupling.

As it should be clear from the previous considerations, the strategy for performing approximations is now different from the fixed coupling case: Rather than solving first the general BFKL equation and then simplifying the result, it is more convenient to perform the approximations on the equation itself, and then solve a simpler equation. Since the approximations that we shall consider are different for the BFKL and the DLA regimes, our analysis will not cover the whole linear regime at $\rho > \rho_s(y)$: the intermediate region between the BFKL and DLA regimes remains out of control.

But before we present the general results, let us use the simplified running $\bar{\alpha}_s(Q_s^2(A, y))$ to give a rapid derivation of the leading energy dependence of the saturation momentum at large y . With this running, the only modification in the previous, fixed-coupling, analysis refers to the replacement $\bar{\alpha}_s y \rightarrow h_A(y)$ in the exponent of the integrand in Eq. (3.5) (and the subsequent formulae). Here, $h_A(y)$ is defined as the solution to $dh_A/dy = \alpha_s(Q_s^2(A, y))$ with $h_A(0) = 0$. Then calculations entirely similar to those described in the previous subsection lead to the condition $r_s \equiv \rho_s(y)/h_A(y) = c$, where $c = 4.883\dots$ and $\rho_s(y) \equiv \ln(Q_s^2(A, y)/Q_A^2)$, as before. This condition together with the equation defining $h_A(y)$ form a coupled system of equations for the functions $h_A(y)$ and $Q_s^2(A, y)$, whose solution is conveniently written as [38, 39, 42]:

$$Q_s^2(A, y) \simeq \Lambda^2 e^{\tau_A(y)}, \quad \tau_A(y) \equiv \sqrt{2cby + \rho_A^2}. \quad (3.23)$$

For completeness, we note that $ch_A(y) = \tau_A(y) - \rho_A$.

For relatively small y , such that $2cby \ll \rho_A^2$, one can expand $\tau_A(y) \simeq \rho_A + (bcy/\rho_A)$. Then, Eq. (3.23) reduces to the same expression as for fixed coupling, cf. Eq. (3.14), but with $\bar{\alpha}_s$ evaluated at the initial saturation scale (i.e., $\bar{\alpha}_s \equiv \bar{\alpha}_s(Q_A^2) = b/\rho_A$) [40].

But with increasing y , the dependence on A becomes weaker and weaker¹⁰ [42] :

$$Q_s^2(A, y) \simeq \Lambda^2 e^{\sqrt{2cby}} \exp \left\{ \frac{\rho_A^2}{2\sqrt{2cby}} \right\} \quad \text{for} \quad 2cby \gg \rho_A^2. \quad (3.24)$$

By using similar formulae (with $\rho_A \rightarrow \rho_p \sim 1$) also for the proton, it becomes clear that, unlike in the fixed coupling case, where the ratio $Q_s^2(A, y)/Q_s^2(p, y) = Q_s^2(A)/Q_s^2(p)$ is independent of y and thus fixed by the initial conditions, in the case of a running coupling, this ratio decreases with y , and converges to one at large y [42] :

$$\frac{Q_s^2(A, y)}{Q_s^2(p, y)} \simeq \exp \left\{ \frac{\rho_A^2 - \rho_p^2}{2\sqrt{2cby}} \right\} \simeq 1 \quad \text{for} \quad 2cby \gtrsim \rho_A^4. \quad (3.25)$$

Thus, due to running coupling effects in the evolution, the initial difference between the proton and the nucleus is washed out after a rapidity evolution $cby \sim \rho_A^4$.

3.3.1 DLA regime

With a running coupling $\bar{\alpha}_s(k_\perp^2)$, the solution to the DLA equation — the simplified equation valid at high k_\perp^2 , which is a common limit of the BFKL and DGLAP equations — is well known, even exactly. For consistency with the other approximations that we have considered so far, we shall only use the corresponding saddle point approximation, valid when $4by\eta \gg 1$, with $\eta \sim \ln \rho$ (see below for a precise definition). This reads:

$$\varphi_A(k_\perp, y) \simeq \frac{1}{b_0 N_c} \frac{Q_A^2}{k_\perp^2} \frac{e^{\sqrt{4by\eta}}}{\sqrt{2\pi\sqrt{4by\eta}}}, \quad \eta \equiv \ln \left[\frac{\ln \frac{k_\perp^2}{\Lambda^2}}{\ln \frac{Q_A^2}{\Lambda^2}} \right]. \quad (3.26)$$

We expect this to be a good approximation so long as $\rho - \rho_s > \rho_s$, a condition that in practice we shall use under the stronger form $\rho - \rho_s > \tau_A$.

3.3.2 BFKL regime

The solution to the BFKL equation with the running coupling expanded as in Eq. (3.22) has been obtained in [39] (see also Refs. [40, 41]) for the case of the dipole scattering amplitude. In what follows we shall adapt this solution to the case of the gluon distribution,

¹⁰ Choosing $\rho_A = 4$ (a reasonable value for the RHIC phenomenology) and using $2cby \sim 10y$, one finds that the running effects become important — in the sense that the two terms under the square root in Eq. (3.23) become comparable — already for y of order one.

explain its properties, and carefully establish its validity limits (thus going beyond the original discussion in Refs. [39–41]).

When applied to the gluon occupation factor, the solution in Refs. [39–41]) reads

$$\varphi_A(k_\perp, y) = \frac{\kappa_0}{\alpha_s(k_\perp^2)N_c} \tau_A^{1/3} z^{-\gamma_s} \text{Ai} \left(\xi_1 + \frac{\ln z + \Delta}{D \tau_A^{1/3}} \right) \exp \left(-\frac{2}{3\beta} \frac{\ln^2 z}{\tau_A} \right), \quad (3.27)$$

with the following notations: κ_0 is a pure constant of $\mathcal{O}(1)$, $\tau_A(y)$ has been defined in Eq. (3.23), $\gamma_s = 0.628$ is the saturation saddle point, $z \equiv k_\perp^2/Q_s^2(A, y)$, and therefore $\ln z = \ln(k_\perp^2/Q_s^2) = \rho - \rho_s$. Furthermore, $\text{Ai}(x)$ is the Airy function, $\xi_1 = -2.33\dots$ is its first (rightmost) zero, Δ is a constant that we are not able to determine,

$$D = [\chi''(\gamma_s)/(2\chi(\gamma_s))]^{1/3} = 1.99\dots, \quad (3.28)$$

is the “anomalous” diffusion coefficient, and $\beta = \chi''(\gamma_s) = 48.5\dots$ is the “standard” one (however, notice the $3/2$ factor in the Gaussian in Eq. (3.27), instead of a 2 in Eq. (3.16)). Note that, in the present context, we find it more natural to measure the transverse momenta with respect to Λ , rather than with respect to the original saturation scale (as we did for fixed coupling).

To the same approximation, the saturation momentum is given by

$$Q_s^2(A, y) = \Lambda^2 \exp \left(\tau_A - \frac{3|\xi_1|}{4D} \tau_A^{1/3} + \Delta \right). \quad (3.29)$$

Since obtained after high energy approximations, Eqs. (3.27) and (3.29) apply only for y large enough, such that $by/\rho_A \gtrsim 1$. (This is the usual condition $\bar{\alpha}_s y \gtrsim 1$ for the validity of the BFKL approximation, where $\bar{\alpha}_s$ is now evaluated at the original saturation momentum Q_A .) As expected, Eqs. (3.29) and (3.23) show the same dominant behavior at large y .

The validity range of Eq. (3.27) in z is determined by the various approximations performed in deriving this result [39]: First, there is the condition $\ln z \ll \tau_A$, which has two sources: (i) the expansion of the BFKL χ function around the saturation saddle–point¹¹ (the analog of the saddle–point approximation in the fixed coupling case), and (ii) the expansion of the running coupling around the saturation line, cf. Eq. (3.22). Second, there is a more restrictive condition, related to the further approximations performed when solving the “diffusion equation” (Eq. (74) in Ref. [39]) obtained after expanding the χ

¹¹ By itself, this expansion could be justified up to $\ln z \sim \tau_A$, because of the relative large value of the coefficient β .

function. This condition leads to the following window for the applicability of Eq. (3.27) :

$$0 < \ln z \equiv \rho - \rho_s \ll \frac{3\gamma_s D^2}{\sqrt{5}} \tau_A^{2/3}, \quad (3.30)$$

to be referred as the ‘BFKL regime’ in the presence of a running coupling. This window includes several interesting kinematical regimes, as we discuss now:

Using the expansion of the Airy function around its zero,

$$\text{Ai}(\xi_1 + x) = \text{Ai}'(\xi_1) \left(x + \frac{\xi_1}{6} x^3 + \dots \right) \quad \text{for } x \ll 1, \quad (3.31)$$

one can deduce an approximation for φ valid near to the saturation line, namely,

$$\varphi_A(k_\perp, y) \approx \frac{\kappa_0}{\alpha_s(k_\perp^2) N_c} z^{-\gamma_s} (\ln z + \Delta), \quad (3.32)$$

where trivial constants have been absorbed in the unknown multiplicative factor κ_0 . Except for the mild scaling violations brought by the factor $1/\alpha_s(k_\perp)$, this expression is a scaling function, i.e., a function of $z = k_\perp^2/Q_s^2(A, y)$. Eq.(3.32) is valid so long as the cubic term in (3.31) is smaller than the linear one; this condition implies $k_\perp \ll Q_g(A, y)$ where:

$$Q_g^2(A, y) \approx Q_s^2(A, y) \exp\left(\sqrt{\frac{6}{|\xi_1|}} D \tau_A^{1/3}\right). \quad (3.33)$$

Thus, it is natural to choose $Q_g(A, y)$ as the upper boundary for the region of geometric scaling in the present case. Note that, with running coupling, this region is only a small part of the BFKL regime defined by Eq. (3.30). Since $\tau_A(y)$ is monotonously increasing with A and y , and approaches an A -independent value when $y \rightarrow \infty$, it is clear that

$$Q_g^2(A_1, y) > Q_g^2(A_2, y) \quad \text{for } A_1 > A_2, \quad (3.34)$$

and the two scales will approach each other at very large y . Note also that the expression in Eq.(3.32) is a universal function, in the sense of Sect. 3.2.3.

Consider also the region outside the scaling domain, at $\ln z \gtrsim \tau_A^{1/3}$. Using the asymptotic form of the Airy function,

$$\text{Ai}(x) \approx \frac{1}{2\sqrt{\pi}} \frac{1}{x^{1/4}} \exp\left(-\frac{2}{3} x^{3/2}\right) \quad \text{for } x \gg 1, \quad (3.35)$$

one immediately finds

$$\varphi_A(k_\perp, y) \approx \frac{\kappa_0}{\alpha_s(k_\perp^2) N_c} \frac{\tau_A^{5/12}}{\ln^{1/4} z} \exp\left(-\gamma_s \ln z - \frac{2}{3D^{3/2}} \frac{\ln^{3/2} z}{\tau_A^{1/2}} - \frac{2}{3\beta} \frac{\ln^2 z}{\tau_A}\right), \quad (3.36)$$

where κ_0 has been redefined in order to absorb some trivial constants, and Δ has been dropped since it is small compared to $\ln z$ in the region of interest. Note the appearance of diffusion terms of two types — from the Gaussian Eq. (3.27), and from the asymptotic expansion of the Airy function —, which both lead to **scaling violations**. There is also a mild violation from the prefactors.

Moreover, at variance with the fixed coupling case (cf. Eq. (3.16)), the scaling violations in Eq. (3.36) are synonymous of **universality violations**: indeed, the “diffusion time” $\tau_A(y)$ (which replaces the $\bar{\alpha}_s y$ of the fixed coupling case) is now explicitly dependent on A . But for sufficiently large y , the A -dependence of $\tau_A(y)$ becomes very weak, as we have seen, and universality gets restored when $2cby \gg \rho_A^2$. For even larger y , such that $2cby \gg \rho_A^4$, the saturation momentum becomes independent of A , cf. Eq. (3.25), so the gluon occupation factor — which in this regime is a universal function of z and y — is then the same in the proton and in the nucleus for any k_\perp in the BFKL regime.

4 High- k_\perp suppression from quantum evolution: The general argument

Before we embark ourselves in a systematic analysis of the ratio $\mathcal{R}_{pA}(k_\perp, y)$, let us present here a general argument explaining why the quantum evolution leads to a suppression in this ratio at generic momenta. The argument can be succinctly formulated as follows¹²: The suppression of the ratio $\mathcal{R}_{pA}(k_\perp, y)$ with increasing y is due to the different evolution rates for the gluon distribution in the nucleus and in the proton: the proton distribution evolves faster because (a) the corresponding saturation momentum in the initial conditions is much smaller ($Q_p \ll Q_s(A)$), and (b) the convexity of the function $\chi(\gamma)$ (the eigenvalue of the BFKL kernel) accelerates the evolution with increasing ρ . In particular, the difference between the proton and the nuclear evolution rates is particularly pronounced at small y (when the proton is in the DLA regime for the interesting values of k_\perp), which explains the rapid suppression seen in the early stages of the evolution [25].

Moreover, similar arguments will allow us to conclude that, after some initial evolution $\bar{\alpha}_s y \gtrsim 1$, and for transverse momenta in the proton perturbative region ($k_\perp \gg Q_s(p, y)$), the ratio $\mathcal{R}_{pA}(k_\perp, y)$ is monotonously increasing with k_\perp , and a decreasing function of A . The monotonic behavior with k_\perp shows that the Cronin peak has already disappeared for such values of y . As for the A -dependence, this can be related to the experimental observation that the central-to-peripheral ratio R_{CP} for (pseudo)rapidity $\eta > 1$ is smaller for central collisions than for more peripheral ones [4–6]. (Peripheral collisions involve less nucleons than the central ones, thus effectively corresponding to smaller values of A .) This tendency is opposite to that identified at $y = 0$ in our theoretical calculations (cf.

¹² We would like to thank Al Mueller for helping us clarifying this general argument.

Eqs. (2.23)–(2.24)), and also at $\eta = 0$ in the experimental results at RHIC [4–6], where the amplitude of the Cronin peak appears to be increasing with A .

In this context, it is interesting to notice that the quantity α (the logarithmic slope in the parametrization $R_{CP} \sim e^{\alpha\eta}$) which has been measured at BRAHMS [4] corresponds in our approach to the right hand side of either Eq. (4.6), or Eq. (4.13), for the nucleus in the linear regime, or in the saturation regime, respectively. With this interpretation, α is dominated by the linear evolution of the proton, and is not the same as the saturation exponent (in contrast to a suggestion in Ref. [4]).

The general arguments to be presented in this section apply for the case of fixed coupling alone: for a running coupling, we have used different approximations in the BFKL and DLA regimes, so, based on these approximations, one cannot construct a general argument valid in the whole perturbative region. But in Sect. 6 we shall check through explicit calculations that all the conclusions about the general behavior of the ratio $\mathcal{R}_{pA}(k_\perp, y)$ to be established below in this section remain true for a running coupling.

4.1 A general argument on the y -dependence

The y -dependence of the ratio in Eq. (1.1) is encoded in:

$$\frac{d \ln \mathcal{R}_{pA}}{dy} = \frac{d \ln \varphi_A}{dy} - \frac{d \ln \varphi_p}{dy}. \quad (4.1)$$

We shall study separately the linear and the saturation regimes for the nucleus. The proton will be always in the linear regime, as described by the BFKL solution in the saddle point approximation, Eq. (3.12).

4.1.1 Nucleus in the linear regime ($k_\perp \gg Q_s(A, y)$)

In this regime, both the proton and the nucleus are described by Eq. (3.12), which implies:

$$\ln \varphi_A(k_\perp, y) \approx \bar{\alpha}_s y F(\gamma_0(r_A), r_A), \quad (4.2)$$

where we have neglected the slowly varying prefactors. Here, we have introduced the more specific notation:

$$r_A(k_\perp, y) \equiv \frac{\rho(A, k_\perp)}{\bar{\alpha}_s y} = \frac{\ln k_\perp^2 / Q_s^2(A)}{\bar{\alpha}_s y}, \quad (4.3)$$

(with $Q_s(A) \rightarrow Q_p$ for the proton) to emphasize that quantities like $\rho \equiv \rho(A, k_\perp)$ and r_A are different for the proton and the nucleus, even when considered for the same values of the kinematical variables k_\perp and y . Since $Q_s(A) \gg Q_p$ then, clearly,

$$\rho(A, k_\perp) < \rho(p, k_\perp), \quad \text{and} \quad r_A(k_\perp, y) < r_p(k_\perp, y). \quad (4.4)$$

After taking a total derivative w.r.t. y in Eq. (4.2), and using the saddle point condition, Eq. (3.11), together with the definition (3.10) of the function F , one finds :

$$\frac{d \ln \varphi_A}{dy} \approx \bar{\alpha}_s \chi(\gamma_A), \quad (4.5)$$

(with the simplified notation $\gamma_A \equiv \gamma_0(r_A)$) and therefore:

$$\frac{1}{\bar{\alpha}_s} \frac{d \ln \mathcal{R}_{pA}}{dy} \approx \chi(\gamma_A) - \chi(\gamma_p), \quad (4.6)$$

which is always **negative** (for k_\perp and y within its range of validity), as we show now: Since $\chi(\gamma)$ is a convex function ($\chi''(\gamma) > 0$ for $0 < \gamma < 1$), the function $\gamma_0(r)$ which gives the saddle point is monotonously increasing:

$$\frac{d\gamma_0(r)}{dr} = \frac{1}{\chi''(\gamma_0(r))} > 0, \quad (4.7)$$

(this follows by differentiating the saddle point condition (3.11) w.r.t. r), which together with Eq. (4.4) implies that $\gamma_A < \gamma_p$, from which Eq. (4.6) finally follows because $\chi(\gamma)$ is monotonously increasing for any $\gamma > 1/2$ (recall that $\gamma_A \geq \gamma_s \approx 0.63$). Some of these properties are manifest on Fig. 6.

Moreover, the suppression rate (4.6) is largest in the early stages of the evolution, but decreases with y , and approaches zero (through negative values) when $y \rightarrow \infty$. Indeed, the difference:

$$r_p(k_\perp, y) - r_A(k_\perp, y) = \frac{\rho(p, k_\perp) - \rho(A, k_\perp)}{\bar{\alpha}_s y} = \frac{\ln(Q_s^2(A)/Q_p^2)}{\bar{\alpha}_s y} \approx \frac{\rho_A}{\bar{\alpha}_s y}, \quad (4.8)$$

is independent of k_\perp and largest at small y , but it decreases with y , and vanishes asymptotically at very large y . Therefore, when $y \rightarrow \infty$, we have $\gamma_A - \gamma_p \rightarrow 0$, and thus also $\chi(\gamma_A) - \chi(\gamma_p) \rightarrow 0$.

To be more specific, consider two interesting physical regimes:

a) For very large $k_\perp \gg Q_g(A, y)$, both the proton and the nucleus are in the DLA regime, where $r \gg 1$, $\gamma_0(r) \approx 1 - 1/\sqrt{r}$, $\chi(\gamma_0) \approx \sqrt{r}$, and therefore:

$$\frac{1}{\bar{\alpha}_s} \frac{d \ln \mathcal{R}_{pA}}{dy} \approx \sqrt{\frac{\rho(A, k_\perp)}{\bar{\alpha}_s y}} - \sqrt{\frac{\rho(p, k_\perp)}{\bar{\alpha}_s y}}, \quad (4.9)$$

which confirms that the rate of variation is largest in the early stages of the evolution (although Eq. (4.9) cannot be trusted, strictly speaking, when $y \rightarrow 0$).

b) For k_\perp and y such that both the nucleus and the proton are in the BFKL regime (which becomes possible when y is large enough for $Q_g(p, y) > Q_s(A, y)$; see Fig. 1), then one can expand both $\chi(\gamma_A)$ and $\chi(\gamma_p)$ around $\gamma_s \approx 0.63$. This is entirely similar to the expansion leading from Eq. (3.12) to Eq. (3.16), and gives:

$$\frac{1}{\bar{\alpha}_s} \frac{d \ln \mathcal{R}_{pA}}{dy} \approx -\frac{c\rho_A}{\beta\bar{\alpha}_s y} \left\{ 1 + \frac{1}{c\bar{\alpha}_s y} \left(\ln \frac{k_\perp^2}{Q_s^2(A, y)} + \frac{\rho_A}{2} \right) \right\}, \quad (4.10)$$

which shows that, when increasing y and k_\perp in such a way that $\ln(k_\perp^2/Q_s^2(A, y)) \sim \text{const.}$, the rate eventually becomes independent of k_\perp , and vanishes as $1/y$.

4.1.2 Nucleus in the saturation regime ($k_\perp \leq Q_s(A, y)$)

All we need to know about this regime for the present purposes is that the nuclear gluon distribution at saturation is only a function of $z \equiv k_\perp^2/Q_s^2(A, y)$. To remain in the saturation region when increasing y , one must simultaneously increase k_\perp along a line parallel to the saturation line, such that z remains fixed. Proceeding as before, we have:

$$\ln \mathcal{R}_{pA}(z, y) \approx \ln \varphi_A(z) - \bar{\alpha}_s y \chi(\gamma_p) + \gamma_p \ln \frac{z Q_s^2(A, y)}{Q_p^2}, \quad (4.11)$$

where the proton saddle point γ_p is now determined by (cf. Eq. (3.11)) :

$$\chi'(\gamma_p) = \frac{\ln[z Q_s^2(A, y)/Q_p^2]}{\bar{\alpha}_s y} = \frac{\ln[z Q_s^2(A)/Q_p^2]}{\bar{\alpha}_s y} + \chi'(\gamma_s). \quad (4.12)$$

In the above equation, the second equality follows after using Eq. (3.14) for the saturation momentum and recalling that $c = \chi'(\gamma_s) \approx 4.88$ with $\gamma_s \approx 0.63$. Taking a derivative w.r.t. y in Eq. (4.11) and using Eq. (4.12) yields:

$$\left. \frac{1}{\bar{\alpha}_s} \frac{d \ln \mathcal{R}_{pA}}{dy} \right|_z \approx \gamma_p \chi'(\gamma_s) - \chi(\gamma_p), \quad (4.13)$$

which is negative for any y , as is quite obvious by inspection of Fig. 6 : The straightline $f(\gamma_p) \equiv \gamma_p \chi'(\gamma_s)$ is the line which is tangent to $\chi(\gamma_p)$ at $\gamma_p = \gamma_s$; but $\chi(\gamma_p)$ is a convex function, and thus it lies above its tangent for any $\gamma_p \neq \gamma_s$. Moreover, the suppression rate is very large at small y (since $\chi(\gamma_p) \rightarrow \infty$ as $\gamma_p \rightarrow 1$), but it decreases to zero when $y \rightarrow \infty$ (recall that $\gamma_s \chi'(\gamma_s) = \chi(\gamma_s)$). We conclude that the ratio $\mathcal{R}_{pA}(z, y)$ is rapidly decreasing with y in the early stages of the evolution, and approaches a constant value for very large y .

4.2 A general argument on the k_\perp -dependence

We now present a mathematically similar argument which allows us to characterize the k_\perp dependence of the ratio $\mathcal{R}_{pA}(k_\perp, y)$. We would like to show that, for a fixed rapidity y with $\bar{\alpha}_s y \gtrsim 1$ (such that the saddle point approximation (3.12) applies), and for all momenta $k_\perp \gg Q_s(p, y)$ (where the proton is in a linear regime), the function $\mathcal{R}_{pA}(k_\perp, y)$ is monotonously increasing with k_\perp .

Consider first the linear regime for the nucleus, at $k_\perp \gg Q_s(A, y)$. Using Eq. (4.2) and the saddle point condition, Eq. (3.11), one obtains (e.g., for the proton),

$$\frac{d \ln \varphi_p}{d \ln(k_\perp^2/\Lambda^2)} \approx -\gamma_p, \quad (4.14)$$

together with a similar formula for the nucleus, and therefore:

$$\frac{d \ln \mathcal{R}_{pA}}{d \ln(k_\perp^2/\Lambda^2)} \approx \gamma_p - \gamma_A, \quad (4.15)$$

which by the previous arguments is strictly positive and vanishes asymptotically when $k_\perp \rightarrow \infty$. Thus, in this regime, the function $\mathcal{R}_{pA}(k_\perp, y)$ is strictly increasing with k_\perp for any fixed y , and saturates to a constant value when $k_\perp \rightarrow \infty$. As it will be checked in Sect. 6, this limiting value is one.

Consider also the case where the nucleus is deeply at saturation ($k_\perp \ll Q_s(A, y)$). Then, φ_A is only logarithmically decreasing with $z \equiv k_\perp^2/Q_s^2(A, y)$ (see Eq. (3.1)), while φ_p has a faster, power-like, decrease, with ‘‘anomalous dimension’’ $\gamma_p \geq \gamma_s \simeq 0.63$ (cf. Eq. (4.14)). Therefore, in this range too, the function $\mathcal{R}_{pA}(k_\perp, y)$ is increasing with k_\perp .

The previous analysis does not cover the nuclear transition region at $k_\perp \sim Q_s(A, y)$. But the discussion following Eq. (3.17) shows that, when $\bar{\alpha}_s y \gtrsim 1$, there is no large (i.e., parametrically enhanced) mismatch between the value of φ_A at $k_\perp \sim Q_s(A, y)$, Eq. (3.4), and the corresponding extrapolation of the BFKL solution (3.17): the original mismatch between φ_A^{sat} and φ_A^{twist} at $k_\perp \sim Q_s(A)$ (cf. Sect. 2.2) has been washed out by the evolution. This property, together with the above finding that φ_A is monotonously increasing with k_\perp on both sides of the saturation line, precludes the existence of a (parametrically enhanced) peak at $k_\perp \sim Q_s(A, y)$. That is, the peak must have already disappeared when $\bar{\alpha}_s y \gtrsim 1$. The mechanism for this disappearance will be clarified in Sect. 5.3.

4.3 A general argument on the A -dependence

Finally, let us use similar arguments to study the dependence of the ratio \mathcal{R}_{pA} upon the atomic number A . We shall find that, after an evolution¹³ $\bar{\alpha}_s y \gtrsim 1$, the ratio becomes a decreasing function of A . We shall consider the A -dependence for two cases: (a) with fixed k_\perp and y (this corresponds to the real experimental situation for the measurement of R_{CP} at RHIC) and (b) with fixed $z \equiv k_\perp^2/Q_s^2(A, y)$ and y (as relevant, e.g., for the A -dependence of the Cronin peak).

Notice first that the dominant A -dependence enters the gluon occupation factor through the ratio between k_\perp^2 and the saturation momentum (see, e.g., Eqs. (3.1) and (3.12)); the factor $\widetilde{\varphi}_A$ in the latter brings only a subleading, logarithmic, dependence on A , whose contribution to the derivative in Eq. (4.16) below is suppressed by a factor $1/\rho_A$.

(a) With fixed k_\perp and y , $\varphi_p(k_\perp, y)$ is clearly independent of A , and one can rely on Eq. (3.12) (nucleus in the linear regime) to write:

$$\begin{aligned} \left. \frac{\partial}{\partial A} \ln \mathcal{R}_{pA} \right|_{k_\perp, y} &= \frac{\partial \ln \varphi_A}{\partial A} - \frac{\partial \ln A^{1/3}}{\partial A} = \frac{\partial \rho}{\partial A} \frac{\partial \ln \varphi_A}{\partial \rho} - \frac{\partial \ln A^{1/3}}{\partial A} \\ &\simeq -\frac{\partial \rho_A}{\partial A} (-\gamma_A) - \frac{\partial \rho_A}{\partial A} = -\frac{\partial \rho_A}{\partial A} (1 - \gamma_A) < 0, \end{aligned} \quad (4.16)$$

where we have also used $\rho(A, k_\perp) \equiv \ln k_\perp^2/Q_s^2(A) = \ln k_\perp^2/\Lambda^2 - \rho_A$ and the relation (4.14) written for the nucleus. The same conclusion holds when the nucleus is deeply at saturation, since there φ_A is only logarithmically varying with $k_\perp^2/Q_s^2(A, y)$ (and thus with A). Finally, for k_\perp around $Q_s(A, y)$ one can rely on the same matching argument as in

¹³ This is a conservative estimate, necessary for the validity of the general arguments in this section. But the explicit calculations in Sect. 5.1 will reveal that, for $k_\perp \sim Q_s(A, y)$ at least, \mathcal{R}_{pA} starts to be a decreasing function of A already after the shorter evolution $\bar{\alpha}_s y \sim 1/\rho_A$.

the previous discussion of the k_\perp -dependence to conclude that the ratio \mathcal{R}_{pA} preserves a monotonic, decreasing, behavior with A .

(b) Consider now the situation in which A and k_\perp are increased simultaneously, in such a way that $z \equiv k_\perp^2/Q_s^2(A, y)$ stays fixed. Then $\rho(A, k_\perp) \equiv \ln k_\perp^2/Q_s^2(A)$ is fixed as well, and the gluon distributions of the nucleus (seen now as a function of z and y) has no extra dependence on A . On the other hand, the distribution of the proton becomes now dependent on A , through k_\perp : Writing the proton ρ -variable as

$$\rho(p, k_\perp) \equiv \ln \frac{k_\perp^2}{Q_p^2} = \ln z + \ln \frac{Q_s^2(A, y)}{Q_p^2} \simeq \ln z + c\bar{\alpha}_s y + \rho_A, \quad (4.17)$$

where the last term carries the dependence on A , and using Eq. (4.14), one deduces that

$$\left. \frac{\partial \ln \varphi_p}{\partial A} \right|_{z, y} = -\gamma_p \frac{\partial \rho_A}{\partial A}. \quad (4.18)$$

This yields the expected conclusion that \mathcal{R}_{pA} is decreasing with A :

$$\left. \frac{\partial}{\partial A} \ln \mathcal{R}_{pA} \right|_{z, y} = -\frac{\partial \rho_A}{\partial A} (1 - \gamma_p) < 0. \quad (4.19)$$

Note also that the rate of decrease in \mathcal{R}_{pA} is faster when measured with k_\perp and y fixed than with z and y fixed (because $1 - \gamma_A > 1 - \gamma_p$).

5 The evolution of the Cronin peak with increasing y

The problem of the evolution of the Cronin peak with increasing y is a delicate one, as it involves the nuclear transition region towards saturation, on which we have little analytic control at $y > 0$. Moreover, the experience with the MV model suggests that the existence of the peak and its properties are tributary to the actual behavior of the nuclear gluon distribution $\varphi_A(k_\perp, y)$ at momenta just above the saturation scale: If the distribution is rapidly decreasing with k_\perp (say, according to an exponential law), then a pronounced peak exists; but if its decrease is only power-like, then there is at most a very flat peak, if any. In the MV model, the gluon distribution above $Q_s(A)$ has been found to be the superposition between an exponential and a power-law tail, with the exponential being the dominant contribution though, since parametrically enhanced at large A . As we shall see below in this section, the effect of the evolution is to enhance the power-law contributions, which for $\alpha_s y \sim 1$ become as large as the exponential one (for momenta just above $Q_s(A)$). When this happens, the Cronin peak has completely flattened out.

In order to study this flattening, one needs a more accurate calculation which follows the non-linear evolution of the nucleus in the saturation region. To achieve the necessary accuracy while still preserving an analytic control, we shall perform just one step in the evolution of the MV model according to the non-linear Kovchegov equation [33]. Strictly speaking, this calculation applies only for rapidities $\alpha_s y \ll 1$, but as we shall see in Sect. 5.3, this is enough to reveal the mechanism responsible for the flattening of the peak. By extrapolation, we shall then conclude that the peak disappears after an evolution $\alpha_s y \sim 1$.

Whereas the flattening of the peak is a rather subtle effect which has to do with the nuclear evolution, the rapid decrease in the height of the peak, on the other hand, is a more robust phenomenon, and also easier to calculate, since this is due solely to the perturbative evolution of the proton. Because of that, we shall begin our analysis in this section with a study of the evolution of the magnitude of the peak with increasing y . Since we expect the peak to follow the nuclear saturation momentum, we shall consider the evolution of the ratio $\mathcal{R}_{pA}(k_\perp, y)$ along the nuclear saturation line $k_\perp = Q_s(A, y)$. This is possible within the present approximation because, along this particular line, the nuclear gluon distribution is known, cf. Eq. (3.4). By itself, this calculation cannot tell us whether a peak actually exists or not; but so long as the peak exists, it provides us with a correct estimate for the magnitude of the peak and its parametric dependencies upon A and y . Although, as we shall argue later, the peak disappears already when $\alpha_s y \sim 1$, in Sects. 5.1 and 5.2 we shall follow the evolution along the nuclear saturation line up to very large y . This will reveal the basic features of the high- k_\perp suppression, to be more systematically analyzed in Sect. 6.

5.1 The suppression of the peak: Fixed coupling

In this subsection and the following one, we shall need only the (proton and nuclear) gluon distributions along the nuclear saturation line $k_\perp = Q_s(A, y)$. For the nucleus, this is simply a constant times $1/\alpha_s$, cf. Eq. (3.4). For the proton, the corresponding distribution is in a linear regime, which can be either DLA, or BFKL, depending upon the value of y : With increasing y , the proton geometric scale $Q_g(p, y_c)$ rises faster than the nuclear saturation momentum, so the corresponding evolution lines in the plane $y - \ln k_\perp^2$ cross each other at some rapidity y_c (see Fig. 1), where the proton changes from the DLA to the BFKL regime. The condition $Q_s(A, y_c) = Q_g(p, y_c)$ together with Eqs. (3.14) and (3.20) imply :

$$c\bar{\alpha}_s y_c \simeq \frac{1}{\nu} \ln \frac{Q_s^2(A)}{Q_p^2} \simeq \frac{\rho_A}{\nu}. \quad (5.1)$$

5.1.1 $y < y_c$: Proton in the DLA regime

For $y < y_c$, but such that $\bar{\alpha}_s y \rho > 1$, one can use Eq. (3.15) with $Q_s(A) \rightarrow Q_p$ to deduce :

$$\begin{aligned} \mathcal{R}_{\text{sat}}(A, y) &\equiv \mathcal{R}_{pA}(k_{\perp} = Q_s(A, y), y) \sim \frac{Q_s^2(A, y)}{A^{1/3} Q_p^2} e^{-\sqrt{4\bar{\alpha}_s y \rho}} \\ &\sim \rho_A \exp\left\{c\bar{\alpha}_s y - \sqrt{4\bar{\alpha}_s y(\rho_A + c\bar{\alpha}_s y)}\right\}, \end{aligned} \quad (5.2)$$

where we have used Eqs. (2.7), (2.19) and (3.14) to write:

$$\frac{Q_s^2(A, y)}{A^{1/3} Q_p^2} = \frac{Q_s^2(A, y)}{Q_A^2} = e^{c\bar{\alpha}_s y} \frac{Q_s^2(A)}{Q_A^2} = e^{c\bar{\alpha}_s y} \rho_A, \quad (5.3)$$

and also (recall that $Q_p^2 \sim \Lambda^2$) :

$$\rho \equiv \ln \frac{Q_s^2(A, y)}{Q_p^2} = c\bar{\alpha}_s y + \ln \frac{Q_s^2(A)}{Q_p^2} \simeq c\bar{\alpha}_s y + \rho_A. \quad (5.4)$$

Note that, in writing Eq. (5.2), we have ignored the slowly varying prefactor in Eq. (3.15), since presently we are only interested in the dominant parametric dependencies upon A and y . When $y \rightarrow 0$, Eq. (5.2) is formally consistent with the corresponding result in the MV model, Eq. (2.22), but one should keep in mind that the results obtained here cannot be used for very small values of y .

Eq. (5.2) offers, in particular, an estimate for the magnitude of the Cronin peak; indeed, for as long as it survives, the peak should be located in the vicinity of $Q_s(A, y)$. Note that, for any $0 < y \leq y_c$, the expression within the exponent in Eq. (5.2) is negative, showing that the magnitude of the peak is rapidly decreasing with y . Since the initial maximum at $y = 0$ was relatively large ($\mathcal{R}_{\text{max}}(A) \sim \rho_A$, cf. Eq. (2.23)), it is interesting to check how fast is the height of the peak decreasing to a value which is parametrically of order one. The condition $\mathcal{R}_{\text{sat}}(A, y) \sim 1$ for $y \sim y_0$ implies:

$$\bar{\alpha}_s y_0 \sim \frac{\ln^2 \rho_A}{4\rho_A} \sim \frac{(\ln \ln A^{1/3})^2}{\ln A^{1/3}} \ll \bar{\alpha}_s y_c. \quad (5.5)$$

This is a small rapidity interval, but is still within the reach of the saddle point approximation (3.15), since $\rho_A \bar{\alpha}_s y_0 \sim \ln^2 \rho_A > 1$. In fact, for such a short evolution in y , one can ignore the evolution of the nucleus in the vicinity of the peak, i.e., one can neglect

$c\bar{\alpha}_s y \ll 1$ next to ρ_A within Eq. (5.2). This is reassuring since, when $\alpha_s y \ll 1$, one cannot really trust the BFKL approximation (3.14) for the saturation scale of the nucleus.

In view of this, it is possible to obtain a more accurate estimate for the rapidity y_0 by using the MV model for the gluon distribution of the nucleus together with the complete DLA expression (3.15) for the proton distribution, including the prefactor. This yields:

$$\bar{\alpha}_s y_0 = \frac{1}{4\rho_A} \ln^2 \left[a\rho_A \sqrt{\ln(a\rho_A)} \right], \quad a \equiv \sqrt{2\pi} z_0 \Gamma(0, z_0) \simeq 0.706. \quad (5.6)$$

The corrections to this result (coming either from the evolution of the nucleus, cf. Sect. 5.3, or from the twist terms in the MV model, that we have neglected here) are of $\mathcal{O}(\rho_A^{-2})$.

Eq. (5.2) also shows that, after a short rapidity evolution $\bar{\alpha}_s y \sim 1/\rho_A$, the magnitude of the Cronin peak becomes a **decreasing** function of ρ_A (and thus of A), in sharp contrast with the corresponding behavior at $y = 0$, cf. Eq. (2.23). This behavior is in agreement with the general arguments about A -dependence given in Sect. 4.

As anticipated, the rapid decrease in the height of the Cronin peak during the early stages of the evolution is to be attributed solely to the fast evolution of the proton. For larger rapidities, $y \gg y_0$, the evolution of the nucleus starts to matter as well (and Eq. (3.14) can be trusted), but as long as $y \leq y_c$ the proton evolution is still faster, so \mathcal{R}_{sat} keeps decreasing with y , as manifest on Eq. (5.2). In particular, for $y = y_c$ one has:

$$\mathcal{R}_{\text{sat}}(A, y_c) \sim \rho_A e^{-\kappa\rho_A} \sim \frac{\ln A^{1/3}}{A^{\kappa/3}} \ll 1, \quad \kappa = \frac{1}{\nu} \left(\sqrt{4(1+\nu)/c} - 1 \right) \approx 0.29. \quad (5.7)$$

For even larger y , Eq. (5.2) would predict an **increase** of the peak with y , but this is incorrect, since for $y > y_c$ this equation does not apply any longer.

5.1.2 $y > y_c$: Proton in the BFKL regime

For $y > y_c$, the proton enters the scaling window (3.20), where Eq. (3.17) becomes appropriate. We shall shortly argue that, when this happens, the Cronin peak has already disappeared; but it is still interesting to follow the ratio $\mathcal{R}_{pA}(k_\perp, y)$ further up along the nuclear saturation line. By using Eq. (3.17) with $Q_s(A, y) \rightarrow Q_s(p, y)$, together with the relations:

$$\frac{Q_s^2(A, y)}{Q_s^2(p, y)} = \frac{Q_s^2(A)}{Q_p^2} = A^{1/3} \rho_A, \quad \ln(A^{1/3} \rho_A) \simeq \rho_A, \quad (5.8)$$

one finds (with the simpler notation $\gamma \equiv \gamma_s$) :

$$\mathcal{R}_{\text{sat}}(A, y) \sim \frac{1}{A^{\frac{1-\gamma}{3}}} \frac{1}{\rho_A^{1-\gamma}} \exp \left\{ \frac{\rho_A^2}{2\beta\bar{\alpha}_s y} \right\} \ll 1. \quad (5.9)$$

Note the emergence of the power of A in the denominator, which provides a strong suppression factor which is independent of y . This power was missing in the DLA (compare to Eq. (5.2)), but appears here as a consequence of the ‘anomalous dimension’ $\gamma < 1$ characteristic of the BFKL solution in the vicinity of the saturation line [38, 39].

Note furthermore that Eq. (5.9) shows only a weak dependence on y , coming from the “diffusion term” in Eq. (3.17): the dominant dependencies, which are exponential, have cancelled in the ratio between the nuclear and the proton saturation momenta, cf. Eq. (5.8). Thus, as compared to the DLA regime at $y < y_c$, where $\mathcal{R}_{\text{sat}}(A, y)$ is rapidly decreasing with y , in the BFKL regime at $y > y_c$ this ratio almost stabilizes at a very small value, proportional to an inverse power of A .

In particular, when approaching y_c from the above, one finds:

$$\mathcal{R}_{\text{sat}}(A, y_c) \sim \frac{1}{(A^{1/3}\rho_A)^\kappa} \sim \frac{1}{(A^{1/3} \ln A^{1/3})^\kappa}, \quad (5.10)$$

where κ has now been generated as $\kappa = 1 - \gamma - \nu c/2\beta$, but this is the same power as in Eq. (5.7), by construction (because of our matching between the DLA and BFKL approximations along the geometric scaling line). The subleading dependencies on A , which are logarithmic, are different in Eqs. (5.7) and (5.10), but this difference merely reflects our imperfect matching.

Furthermore, for very large y , such that $2\beta\bar{\alpha}_s y \gg \rho_A^2$ (in practice, this limit is approached very fast, since $2\beta \approx 97$ is a large number), the ratio becomes independent of y :

$$\mathcal{R}_{\text{sat}}(A, y) \sim \frac{1}{(A^{1/3}\rho_A)^{1-\gamma}} \sim \frac{1}{(A^{1/3} \ln A^{1/3})^{1-\gamma}} \quad \text{for} \quad 2\beta\bar{\alpha}_s y \gg \rho_A^2. \quad (5.11)$$

To summarize, the inverse power of A which characterizes the suppression increases from $\kappa \approx 0.29$ at the end of the DLA regime to $1 - \gamma \approx 0.37$ at asymptotically large y , which shows that a large fraction of the suppression is actually built during the DLA phase of the evolution.

5.2 The suppression of the peak: Running coupling

With running coupling, the kinematical domains in which our ‘DLA’ and ‘BFKL’ approximations apply are well separated from each other, and the intermediate region between the two regimes is not under control. From Sect. 3.3, we recall that for very large k_\perp , such that $\ln z > \tau_p(y)$ (with $z \equiv k_\perp^2/Q_s^2(p, y)$), the proton is described by the DLA approximation (3.26), while for intermediate k_\perp , within the range $0 < \ln z < \text{const} \times \tau_p^{2/3}(y)$ (cf. Eq. (3.30)), the BFKL approximation (3.27) applies. Thus, when the momentum is taken along the nuclear saturation line ($k_\perp = Q_s(A, y)$, or $\ln z \simeq \tau_A(y) - \tau_p(y)$), the proton is in the DLA regime for $y < y_c$, and in the BFKL regime for $y \gtrsim y'_c$. Here, $2cby_c \approx \rho_A^2$, and y'_c is determined from the condition $\tau_A(y) - \tau_p(y) \approx \text{const} \times \tau_p^{2/3}(y)$ as:

$$2cby'_c \approx \left(\frac{\sqrt{5}}{6\gamma_s D^2} \right)^{6/5} \rho_A^{12/5}, \quad (5.12)$$

where the constant factor in the r.h.s. has been obtained according to Eq. (3.30). For even larger $y \geq y''_c$, the proton enters its geometrical scaling region, where the simpler expression (3.32) applies; y''_c is clearly determined by the condition $Q_s^2(A, y''_c) = Q_g^2(p, y''_c)$, which together with Eq. (3.33) implies:

$$2cby''_c \approx \left(\frac{|\xi_1|}{24D^2} \right)^{3/4} \rho_A^3. \quad (5.13)$$

Finally, for y so large that $2cby \gtrsim \rho_A^4$, the proton saturation momentum catches up with that of nucleus, cf. Eq. (3.25), and then the proton too enters a non-linear regime. The constant factors appearing in the above equations for y_c , y'_c and y''_c are not really under control, but their parametric dependencies on ρ_A are correct as written.

At this level, several differences with respect to the fixed coupling case are already manifest: First, there is an interval in rapidity that remains out of control, namely

$$\rho_A^2 \lesssim 2cby \lesssim \rho_A^{12/5}. \quad (5.14)$$

Second, the characteristic rapidities y'_c and y''_c , at which the proton enters the BFKL and scaling regimes respectively, are parametrically larger than the (unique) corresponding scale for fixed coupling, namely y_c in Eq. (5.1). This shows that the evolution is **slower** in the presence of a running coupling. Third, with a running coupling, the linear (BFKL) approximation for the proton does not apply up to arbitrarily large y , but only so long as $2cby \lesssim \rho_A^4$. But for larger y , and $k_\perp = Q_s(A, y)$, the proton and nuclear distributions coincide with each other, so the ratio \mathcal{R}_{sat} reduces to the trivial factor $1/A^{1/3}$.

Other differences between the fixed and running coupling scenarios will be revealed by the subsequent analysis.

5.2.1 $y < y_c$: Proton in the DLA regime

In this regime, the proton is described by Eq. (3.26) where, for $k_{\perp}^2 = Q_s^2(A, y)$, the variable η can be evaluated as (see also Eq. (3.23)):

$$\eta = \ln \ln \frac{Q_s^2(A, y)}{\Lambda^2} - \ln \ln \frac{Q_p^2}{\Lambda^2} \simeq \ln \tau_A(y). \quad (5.15)$$

By also using Eq. (3.4) for the nucleus, one finds :

$$\mathcal{R}_{\text{sat}}(A, y) \sim \tau_A(y) \exp \left\{ \tau_A(y) - \rho_A - \sqrt{4by \ln \tau_A(y)} \right\}, \quad (5.16)$$

which for $y \rightarrow 0$ is of $\mathcal{O}(\rho_A)$, but it decreases rapidly with y , and it becomes of order one already after a small rapidity evolution y_0 , with:

$$y_0 \simeq \frac{1}{4b} \ln \rho_A \sim \ln A^{1/3}. \quad (5.17)$$

The saddle point approximation for $\varphi_p(k_{\perp}, y)$, Eq. (3.26), is justified for $y \sim y_0$ since $\sqrt{4by_0\eta} \simeq \sqrt{4by_0 \ln \rho_A} = \ln \rho_A > 1$. We find a situation similar to the fixed coupling case (cf. Eq. (5.5)), namely, y_0 is so small that the corresponding evolution of the nucleus can be neglected: $\tau_A(y_0) - \rho_A \sim \ln \rho_A / \rho_A \ll 1$, and therefore $Q_s^2(A, y) \simeq Q_A^2$ for $y \leq y_0$. In particular, one can use the MV model for the nucleus in order to obtain a more accurate estimate for y_0 , valid up to corrections of $\mathcal{O}(\rho_A^{-2})$ (the analog of Eq. (5.6)) :

$$y_0 = \frac{1}{4b \ln \rho_A} \ln^2 \left[a \rho_A \sqrt{\ln(a \rho_A)} \right], \quad a \equiv \sqrt{2\pi} z_0 \Gamma(0, z_0) \simeq 0.706. \quad (5.18)$$

When comparing Eqs. (5.5) and (5.17), it appears that the running coupling estimate for y_0 is parametrically larger than the fixed coupling one in the limit where A is large. This confirms the fact that the running effects slow down the evolution. However, one should keep in mind that the rapidity is naturally measured in units of $1/\alpha_s$, and whereas $\alpha_s y_0 \sim \ln^2 \rho_A / \rho_A$ for fixed coupling, we also have $\alpha_s(Q_A^2) y_0 \sim \ln \rho_A / \rho_A$ for running coupling. Thus, when expressed in natural units, the two values are rather close to each other, and the fixed coupling estimate could be even slightly larger.

5.2.2 $y > y'_c$: Proton in the BFKL regime

So long as $2cb y \ll \rho_A^4$ (with $y > y'_c$ though), the proton saturation momentum remains considerably smaller than that of the nucleus, so the proton with $k_{\perp} \sim Q_s(A, y)$ is in the

BFKL regime (3.30), where Eq. (3.27) applies. Therefore, the ratio $\mathcal{R}_{\text{sat}}(A, y)$ is known analytically within this whole range, up to an overall constant factor. In order to simplify the discussion, we shall study this ratio in particular intervals of rapidity, so that Eq. (3.27) reduces to either Eq. (3.36) or Eq. (3.32).

- The interval $\rho_A^{12/5} \lesssim 2cby \lesssim \rho_A^3$.

In this region, φ_p is described by Eq. (3.36) with $\ln z = \ln(Q_s^2(A, y)/Q_s^2(p, y)) \approx \tau_A(y) - \tau_p(y)$. Since we are in a regime where $2cby \gg \rho_A^2$ we can expand $\tau_A(y) = \sqrt{2cby + \rho_A^2}$, to obtain

$$\ln z = \frac{1}{2} \frac{\rho_A^2}{\sqrt{2cby}} + \dots \quad (5.19)$$

(Subleading terms in this expansion, including those arising from the $y^{1/6}$ contributions to the saturation momentum, cf. Eq. (3.29), result in multiplicative factors in $\mathcal{R}_{\text{sat}}(A, y)$ that go to 1 when $\rho_A \gg 1$.) Then it is straightforward to show that

$$\mathcal{R}_{\text{sat}}(A, y) \approx \frac{1}{A^{1/3}} \frac{\sqrt{\rho_A}}{(2cby)^{1/3}} \exp \left[\frac{\gamma_s}{2} \frac{\rho_A^2}{(2cby)^{1/2}} + \frac{2}{3(2D)^{3/2}} \frac{\rho_A^3}{2cby} + \frac{1}{6\beta} \frac{\rho_A^4}{(2cby)^{3/2}} \right]. \quad (5.20)$$

Notice that with increasing y , the ratio is decreasing. The main difference with respect to the corresponding result for fixed coupling, Eq. (5.9), is that for running coupling the dominant y -dependencies do not compensate in the ratio $Q_s^2(A, y)/Q_s^2(p, y)$. Thus, at least for not too large y , Eq. (5.20) preserves a relatively fast decrease with y , which is dominated by the first term in the exponent, proportional to the ‘‘anomalous dimension’’. The other terms in the exponent, due to diffusion effects, are parametrically smaller than the first term. However, since these terms are exponentiated, their contribution to \mathcal{R}_{sat} cannot be neglected in general.

At the low end of our interval, i.e. when $2cby \simeq \rho_A^{12/5}$, the ratio becomes

$$\mathcal{R}_{\text{sat}}(A) \approx \frac{\rho_A^{-3/10}}{A^{1/3}} \exp \left[\frac{\gamma_s}{2} \rho_A^{4/5} + \frac{2}{3(2D)^{3/2}} \rho_A^{3/5} + \frac{1}{6\beta} \rho_A^{2/5} \right] \quad \text{for } 2cby \approx \rho_A^{12/5}. \quad (5.21)$$

Notice that the very leading behavior $A^{-1/3} \sim \exp(-\rho_A)$, has settled in already at this rapidity, and what remains in the exponent is fractional powers of ρ_A . These powers (4/5, 3/5 and 2/5) are smaller than 1, so that $\mathcal{R}_{\text{sat}}(A)$ is (much) smaller than 1, but the whole exponent is positive so that $\mathcal{R}_{\text{sat}}(A)$ is (much) larger than $A^{-1/3}$. This behavior is not unexpected though; one would really need to go back to lower rapidities such that $2cby \sim \rho_A^2$, in order to see the power of A deviate from $-1/3$ (cf. Eq. (5.20)).

At the upper end of our interval, i.e. when $2cby \simeq \rho_A^3$, the expression becomes considerably

simpler since one can keep only the first term in the exponent of Eq. (5.20). One has

$$\mathcal{R}_{\text{sat}}(A) \approx \frac{1}{A^{1/3}} \frac{1}{\sqrt{\rho_A}} \exp \left[\frac{\gamma_s}{2} \sqrt{\rho_A} \right] \quad \text{for } 2cby \approx \rho_A^3, \quad (5.22)$$

which clearly shows more suppression than Eq. (5.21).

- The interval $\rho_A^3 \lesssim 2cby \lesssim \rho_A^4$.

In this region the proton is in the perturbative geometric scaling region and its gluon occupation factor is given by Eq. (3.32). The Cronin ratio becomes

$$\mathcal{R}_{\text{sat}}(A, y) \approx \frac{1}{A^{1/3}} \left[\Delta + \frac{1}{2} \frac{\rho_A^2}{\sqrt{2cby}} \right]^{-1} \exp \left[\frac{\gamma_s}{2} \frac{\rho_A^2}{\sqrt{2cby}} \right]. \quad (5.23)$$

It is again clear that $\mathcal{R}_{\text{sat}}(A, y)$ is a decreasing function of y . At the low end of the interval, i.e. when $2cby \simeq \rho_A^3$, we obtain again Eq. (5.22). On the other hand when we approach the upper end ρ_A^4 , we have

$$\mathcal{R}_{\text{sat}}(A) \propto \frac{1}{A^{1/3}} \quad \text{for } 2cby \approx \rho_A^4, \quad (5.24)$$

where the constant of proportionality in the last equation cannot be determined (since the proton approaches a non-linear regime), but it is a number greater than 1.

5.2.3 $2cby > \rho_A^4$: Proton at saturation

Even though this region is not analytically under control, since the proton distribution becomes non-linear, it is clear that, when further increasing y , the ratio will be (slowly) decreasing until it stabilizes, for $2cby \gg \rho_A^4$, at the very small value:

$$\mathcal{R}_{\text{sat}}(A, y) \simeq \frac{1}{A^{1/3}} \quad \text{for } 2cby \gg \rho_A^4, \quad (5.25)$$

which is simply the factor introduced by hand in the definition (1.1) of \mathcal{R}_{pA} . Note that also the overall normalization is now under control. This reflects the fact that, in this limit, the nuclear and proton saturation scales coincide with each other, cf. Eq. (3.25), so the corresponding occupation factors at $k_\perp \sim Q_s(A, y)$ coincide as well.

Moreover, by the same argument, it is clear that for $2cby \gg \rho_A^4$, the limiting value $\mathcal{R}_{pA} = 1/A^{1/3}$ is reached for **any** $k_\perp \leq Q_g(A, y)$ — this includes the saturation region, and also the window (3.30) for the BFKL regime — since in this whole range of momenta the

gluon distribution is **universal** (for sufficiently large y), i.e., it depends upon the specific properties of the hadron at hand only via its saturation momentum (cf. Sect. 3.3). This will be further discussed in Sect. 6.

Let us finally compare the asymptotic regimes for fixed and running coupling: By inspection of Eqs. (5.11) and (5.25), it becomes clear that the ultimate value of \mathcal{R}_{sat} is much smaller for running coupling, and it is reached after a much longer evolution. Note, however, that if one measures the rapidity in units of $1/\alpha_s$, with α_s evaluated at the nuclear saturation scale $Q_s(A, y)$ as natural, then for large y :

$$\bar{\alpha}_s(Q_s^2(A, y)) \equiv \frac{b}{\ln(Q_s^2(A, y)/\Lambda^2)} \simeq \frac{b}{\sqrt{2cby}} \quad \text{for} \quad 2cby \gg \rho_A^2, \quad (5.26)$$

and the asymptotic regime in Eq. (5.25) corresponds to $\bar{\alpha}_s y \gg \rho_A^2$. This is parametrically of the same order in A as the evolution required to reach the limit (5.11) in the fixed coupling case. Still, the presence of the large factor $\beta \approx 48$ in the fixed coupling condition $\beta \bar{\alpha}_s y \gg \rho_A^2$ makes that, in practice, the lowest value of \mathcal{R}_{sat} is reached considerably faster with fixed coupling evolution than with the running coupling one. In view of this, the running coupling evolution is indeed slower.

5.3 The flattening of the Cronin peak

Since restricted to momenta along the saturation line $k_\perp = Q_s(A, y)$, the previous analysis could not tell us whether a maximum actually exists or not, neither describe its detailed properties, like the position of the peak and its actual shape. To study this, we need the nuclear gluon distribution for $y > 0$ and generic momenta around $Q_s(A, y)$, that we shall compute in this section to lowest non-trivial order in $\bar{\alpha}_s y$, that is, after a single step in the quantum evolution. Since, as we shall see, the quantum evolution and the twist expansion interfere with each other, it is convenient to choose the same “small parameter”, namely $1/\rho_A \ll 1$, to control both of them. If $\Delta Y \equiv \bar{\alpha}_s y$ denotes the rapidity increment that we shall consider (this satisfies $\Delta Y \ll 1$), then our objective in what follows will be to construct the nuclear gluon distribution $\varphi_A(k_\perp, \Delta Y)$ in such a way that, for $\Delta Y \sim 1/\rho_A$ and $k_\perp \lesssim Q_s(A, y)$, all the terms to order $1/\rho_A$ are correctly included. This means that when we use this result to construct the \mathcal{R}_{pA} -ratio (and therefore we multiply by ρ_A ; see e.g. Eq. (2.22)), we just lose contributions that vanish when $\rho_A \gg 1$.

This implies, in particular, that only the terms of $\mathcal{O}(1)$ and of $\mathcal{O}(1/\rho_A)$ need to be kept in the initial condition $\varphi_{\text{in}} \equiv \varphi_A(k_\perp, Y = 0)$. (Throughout this subsection, we shall often omit the subscript A on the various formulae, to simplify writing.) We thus write:

$$\varphi_{\text{in}} = \varphi_0 + \frac{1}{\rho_A} \varphi_1 + \mathcal{O}(\rho_A^{-2}), \quad (5.27)$$

where φ_0 is the same as the saturating piece in Eq. (2.13) (i.e., the piece involving the function $\Gamma(0, z)$), which is of $\mathcal{O}(1)$, while φ_1 is the term with $n = 1$ in the twist expansion shown in Eq. (2.15) (which, we recall, includes the bremsstrahlung spectrum together with higher twist effects to all orders in $1/z$) and is of $\mathcal{O}(1/\rho_A)$.

To study the non-linear evolution with y , it is convenient to use the Kovchegov equation [33], since this is a closed equation. This can be written both in momentum space, i.e., as an equation for $\varphi(k_\perp, Y)$, and in coordinate space, as an equation for the dipole scattering amplitude which appears in Eq. (2.2). In what follows, both forms of this equation will be used, for convenience. We start by rewriting Eq. (2.2) as:

$$\varphi(k_\perp, Y) = \frac{1}{\alpha_s N_c} \int \frac{d^2 r_\perp}{\pi r_\perp^2} e^{-ik_\perp \cdot r_\perp} \mathcal{N}(r_\perp, Y) = \frac{2}{\alpha_s N_c} \int \frac{dr}{r} J_0(kr) \mathcal{N}(r, Y). \quad (5.28)$$

In the following we shall omit the overall factor $1/\alpha_s N_c$, which we can restore at the end. In terms of $\mathcal{N}(r, Y) \equiv \mathcal{N}_{xy}(Y)$ (with $r_\perp = x_\perp - y_\perp$), the Kovchegov equation reads:

$$\frac{\partial \mathcal{N}_{xy}}{\partial Y} = \int \frac{d^2 z_\perp}{2\pi} \mathcal{K}_{xyz} (\mathcal{N}_{xz} + \mathcal{N}_{zy} - \mathcal{N}_{xy} - \mathcal{N}_{xz} \mathcal{N}_{zy}), \quad (5.29)$$

where \mathcal{K}_{xyz} is the dipole emission kernel :

$$\mathcal{K}_{xyz} \equiv \frac{(x_\perp - y_\perp)^2}{(x_\perp - z_\perp)^2 (z_\perp - y_\perp)^2}. \quad (5.30)$$

One can transform the above integration over z_\perp into an integration over the sizes of the emitted dipoles r_1 and r_2 :

$$\begin{aligned} \frac{\partial \mathcal{N}(r)}{\partial Y} &= \int \frac{dr_1}{r_1} \frac{dr_2}{r_2} r^2 \ell d\ell J_0(\ell r_1) J_0(\ell r_2) J_0(\ell r) \\ &\times [\mathcal{N}(r_1) + \mathcal{N}(r_2) - \mathcal{N}(r) - \mathcal{N}(r_1) \mathcal{N}(r_2)]. \end{aligned} \quad (5.31)$$

Through Eq. (5.28), this gives a non-linear equation for $\varphi(k_\perp, Y)$, in which the structure of the non-linear term is actually simpler [33, 38] :

$$\frac{\partial \varphi}{\partial Y} = \mathcal{K} \otimes \varphi - \frac{1}{2} \varphi^2, \quad (5.32)$$

where now \mathcal{K} is an operator with the BFKL eigenvalue spectrum, but for our current purposes we prefer to view it as a multiple integration determined from Eqs. (5.28) and

(5.31), that is :

$$\begin{aligned} \mathcal{K} \otimes \varphi = & 2 \int \frac{dr_1}{r_1} \frac{dr_2}{r_2} r dr \ell d\ell J_0(\ell r_1) J_0(\ell r_2) J_0(\ell r) J_0(kr) \\ & \times [\mathcal{N}(r_1) + \mathcal{N}(r_2) - \mathcal{N}(r)]. \end{aligned} \quad (5.33)$$

To obtain the change $\Delta\varphi$ in φ after a small step in rapidity $\Delta Y \ll 1$, it is enough to iterate the evolution equation only once. This gives:

$$\Delta\varphi = \Delta Y \left(\mathcal{K} \otimes \varphi_{\text{in}} - \frac{\varphi_{\text{in}}^2}{2} \right) + \mathcal{O}((\Delta Y)^2), \quad (5.34)$$

with φ_{in} the initial condition. To keep the discussion simple, we shall imagine that $\Delta Y \sim 1/\rho_A$, which is the amount of rapidity (up to $\ln \rho_A$ factors) that gives a suppression of the Cronin peak to a value of order $\mathcal{O}(1)$, due to the fast evolution of the proton (cf. Eq. (5.5)). Then we have:

$$\Delta\varphi = \Delta Y \left(\mathcal{K} \otimes \varphi_0 - \frac{1}{2} \varphi_0^2 \right) + \mathcal{O}\left(\frac{\Delta Y}{\rho_A}, (\Delta Y)^2\right), \quad (5.35)$$

and therefore the evolved gluon distribution is finally written as

$$\varphi = \varphi_0 + \frac{1}{\rho_A} \varphi_1 + \Delta Y \tilde{\varphi}_0 + \mathcal{O}\left(\frac{1}{\rho_A^2}, \frac{\Delta Y}{\rho_A}, (\Delta Y)^2\right), \quad (5.36)$$

where we have introduced the shorthand notation

$$\tilde{\varphi}_0 = \mathcal{K} \otimes \varphi_0 - \frac{1}{2} \varphi_0^2. \quad (5.37)$$

Eq. (5.36) fulfills our objective in that all the neglected terms there become of order $1/\rho_A^2$ when $\Delta Y \sim 1/\rho_A$ (for generic momenta $k_\perp \sim Q_s(A, y)$).

To compute the action of the BFKL operator on φ_0 we shall use Eq. (5.33) in which $\mathcal{N} \rightarrow \mathcal{N}_0 \equiv 1 - \exp(-r^2 Q_s^2/4)$. Since the three separate integrations (corresponding to the three terms in the square bracket) in (5.33) are individually ultraviolet divergent (the divergences only cancel in their sum), we shall regulate the $r_{1,2}$ integrations by letting

$$\int \frac{dr_1}{r_1} \frac{dr_2}{r_2} \rightarrow \lim_{\epsilon \rightarrow 0^+} \int \frac{dr_1}{r_1^{1-2\epsilon}} \frac{dr_2}{r_2^{1-2\epsilon}}, \quad (5.38)$$

with the limit to be taken at the end of the calculation. After performing each of the three

(multiple) integrations separately, and adding the respective results, we obtain :

$$\mathcal{K} \otimes \varphi_0 = \lim_{\epsilon \rightarrow 0^+} \frac{1}{2} \frac{\Gamma^2(\epsilon)}{\Gamma^2(1-\epsilon)} \left(\frac{z}{4}\right)^{-2\epsilon} \times \left[1 - 2z^\epsilon \Gamma(1-\epsilon) \Phi(\epsilon, 1, -z) + z^{2\epsilon} \Gamma(1-2\epsilon) \Phi(2\epsilon, 1, -z)\right], \quad (5.39)$$

where, as usual, we have used the scaled momentum variable $z = k^2/Q_s^2(A)$. Here, $\Phi(\epsilon, 1, -z) \equiv_1 F_1(\epsilon, 1, -z)$ is the confluent hypergeometric function, whose properties will be reviewed in the Appendix. The $\epsilon \rightarrow 0$ limit in this last expression is finite. After also combining this with the non-linear contribution, which simply reads $-(1/2)\Gamma^2(0, z)$, we finally find :

$$\tilde{\varphi}_0 = \frac{\pi^2}{12} - \frac{1}{2} [\gamma_E + \ln z + \Gamma(0, z)]^2 + \frac{1}{2} \Phi^{200}(0, 1, -z), \quad (5.40)$$

where $\gamma_E = 0.577$ is the Euler–Mascheroni constant, and $\Phi^{200}(0, 1, -z)$ is a particular derivative of the confluent hypergeometric function, to be defined in the Appendix. It is illuminating to study the small- and large- z limits of $\tilde{\varphi}_0$, which are given by

$$\tilde{\varphi}_0 = \begin{cases} \frac{\pi^2}{12} - \frac{z^2}{4} + \dots & \text{if } z \ll 1 \\ \frac{1}{z} + \frac{1}{2z^2} + \dots & \text{if } z \gg 1. \end{cases} \quad (5.41)$$

When z is small, we simply obtain a constant correction. This is consistent with the fact that the low- k_\perp limit of φ is not affected by the evolution — this is rather fixed by Eq. (5.28) as $\varphi(k, Y) \rightarrow \ln k_\perp^2$ when $k_\perp \rightarrow 0$ —, but it is only the scale in this logarithm which changes with y : this is the saturation momentum $Q_s(A, y)$, since this is the scale at which the dipole starts to be completely absorbed: $\mathcal{N}(r, Y) \simeq 1$ for $r \gtrsim 1/Q_s(A, y)$. This discussion suggests that the term $(\pi^2/12) \Delta Y$ coming from the one-step evolution could be interpreted as the first contribution to the evolution of the saturation scale.

The crucial point about the correction induced by evolution, as displayed in Eqs. (5.40)–(5.41), is that this contains **power-law** tails at large z , despite the fact that it has been generated by evolving the **compact** (saturating) part of the initial distribution alone. This is due to the fact that the (perturbative) gluon interactions — as encoded in the BFKL kernel — are long-ranged, in both the momentum and the coordinate space (see Eq. (5.30)). A similar phenomenon is the generation of power-law tails in impact parameter space when solving the Kovchegov equation (5.29), as found in Ref. [52].

Thus, in addition to the original “twist” contributions encoded in the function φ_1 , which are parametrically suppressed at large A , the evolved gluon distribution in Eq. (5.36) contains other power-law contributions which are not parametrically suppressed, because

they are generated by the evolution of the gluons which were originally at saturation: φ_0 and $\tilde{\varphi}_0$ are parametrically of the same order, and the induced piece $\Delta\varphi = \Delta Y \tilde{\varphi}_0$ is small only as long as ΔY itself is small. But although we cannot rely on the previous approximations to go up to larger values of $Y = \bar{\alpha}_s y$, it is clear that, for $\bar{\alpha}_s y \sim 1$ and momenta $k_\perp \sim Q_s(A, y)$, the twist terms induced by the evolution become as large as the saturating distribution. (Incidentally, this justifies the fact that, for $\bar{\alpha}_s y \gtrsim 1$, we can rely on the linear, BFKL, evolution to approach the saturation region from the above; see also the discussion after Eq. (3.17))

We are now in a position to explain the rapid flattening of the Cronin peak, as seen in the numerical simulations in Ref. [25]. We have already noticed, in the analysis of the Cronin peak in the MV model in Sect. 2.3, that the presence of long-range tails has the effect to flatten the peak, and to push it towards larger values of k_\perp . At $y = 0$ and for a large value of A , a well pronounced peak exists just because of the compact contribution to the gluon distribution due to the saturated gluons (i.e., $\varphi_0 \equiv \varphi^{\text{sat}}$) is the dominant contribution at $k_\perp \lesssim Q_s(A)$ (see Figs. 2 and Figs. 4). However, with increasing y , the power-law tails are enhanced, and the effect of this enhancement is particularly pronounced in the early stages of the evolution ($\bar{\alpha}_s y \ll 1$), when the modes at high k_\perp receive large contributions from the evolution of the gluons which were originally at saturation. In this way, the exponential tail which was present in the saturating distribution at $y = 0$ is rapidly washed out, and replaced by a power law tail which starts already at $k_\perp \sim Q_s(A, y)$. When this happens, the peak in the ratio \mathcal{R}_{pA} flattens out completely and disappears. In view of the previous estimates, we expect a complete flattening for $\bar{\alpha}_s y \sim 1$. But the effect shows up already for smaller rapidities, where our one-step evolution is a good approximation.

To illustrate this, we have represented in Fig. 7 the ratio \mathcal{R}_{pA} (for $\rho_A = 6$) obtained by using the result in Eq. (5.36) for the nuclear gluon distribution together with the DLA approximation for the proton distribution¹⁴. For comparison, we have also represented on the same plot the ratio which is obtained when the non-evolved, MV model, distribution is used for the nucleus. The rapid suppression of the peak, due to the fast rise in the proton distribution, is clearly seen in both cases. But in the absence of nuclear evolution the peak is always there; just its amplitude gets smaller and smaller. By contrast, when using the evolved nucleus distribution from Eq. (5.36) the flattening of the peak is manifest, and in fact the maximum has almost disappeared after an evolution $\Delta Y = 2/\rho_A \approx 0.3$.

It is also visible on Fig. 7 that with increasing y , the position of the peak moves towards larger momenta — in agreement with our expectation that the peak should follow the

¹⁴ To be able to perform this calculation also for very small values of Y , where the saddle point approximation is not appropriate anymore, we have used the exact solution to the DLA equation, which is well known to read (compare to Eq. (3.15)) : $\varphi_p(k_\perp, y) = \frac{1}{\alpha_s N_c} \frac{Q_p^2}{k_\perp^2} I_0(\sqrt{4\bar{\alpha}_s y \rho})$, with $\rho = \ln(k_\perp^2/Q_p^2)$ and $I_0(z)$ the modified Bessel function of the first kind.

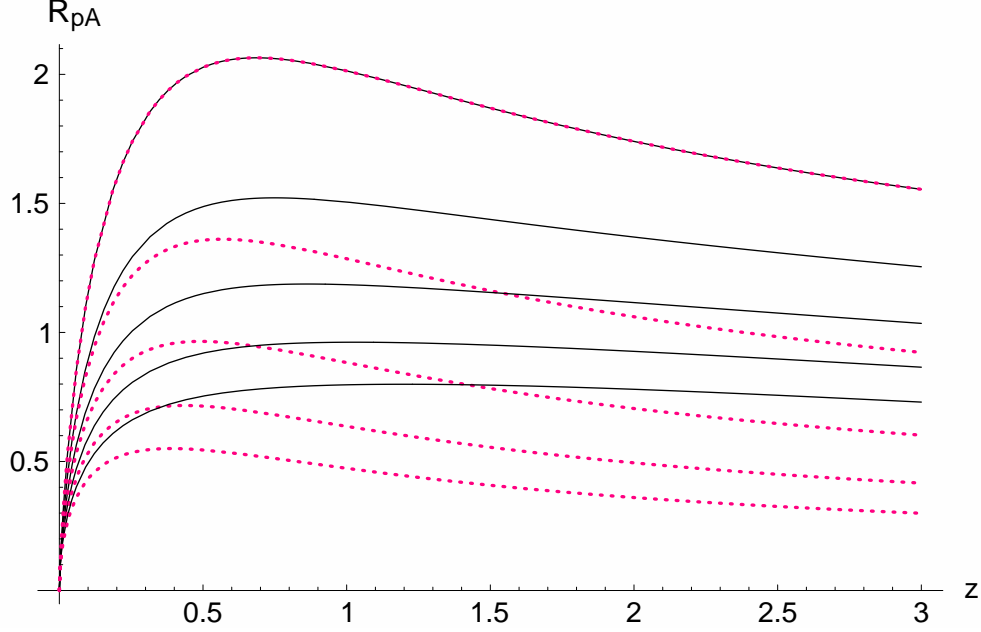


Fig. 7. The Cronin ratio $\mathcal{R}_{pA}(z)$ below and near the saturation scale for $\rho_A = 6$. The black (solid) lines correspond to an evolved nuclear wavefunction by $\Delta Y \ll 1$. The red (dotted) lines correspond to an unevolved one (MV). The proton wavefunction is always given by the full DLA solution. The curves, from top to bottom, correspond to $\Delta Y = n/(2\rho_A)$ with $n = 0, 1, \dots, 4$.

nuclear saturation momentum —, but it does that only *very slowly*. This is so slow because, first, the nucleus evolves only little for such a small rapidity increment, and, second, there is an opposite effect due to the DLA evolution of the proton, which for the small values of Y of interest here is almost compensating the evolution towards larger k_\perp due to the nucleus. Using Eq. (5.36) for the nuclear distribution, together with the DLA approximation (the full Bessel function) for the proton, we have been able to compute analytically the position of the peak for very small values of y . The result reads (compare to Eq. (2.23)) :

$$z_0(Y) \approx 0.435 + \frac{0.882}{\rho_A} + 0.862Y - 0.769\sqrt{\frac{Y}{\rho_A}}, \quad (5.42)$$

where the neglected terms are such that, when $Y \sim 1/\rho_A$, they are all of $\mathcal{O}(\rho_A^{-2})$.

To summarize the previous considerations, the ratio (1.1) can be suggestively rewritten as follows:

$$\begin{aligned} \mathcal{R}_{pA}(k_\perp, y) &\equiv \frac{\varphi_A(k_\perp, y)}{A^{1/3} \varphi_p(k_\perp, y)} = \frac{\Phi_A(k_\perp, y)}{\Phi_p(k_\perp, y)} \mathcal{R}_{pA}(k_\perp, y = 0), \\ \Phi_A(k_\perp, y) &\equiv \frac{\varphi_A(k_\perp, y)}{\varphi_A(k_\perp, y = 0)}, \quad \Phi_p(k_\perp, y) \equiv \frac{\varphi_p(k_\perp, y)}{\varphi_p(k_\perp, y = 0)}. \end{aligned} \quad (5.43)$$

The ratios Φ_A and Φ_p , which describe the relative evolutions of the nucleus and of the proton, respectively, play very different roles for the evolution at small y and momenta around $Q_s(A, y)$: Φ_p rises very fast with y , and is responsible for the rapid suppression of \mathcal{R}_{pA} at generic momenta. However, this factor varies only slowly with k_\perp , and thus cannot be responsible for the flattening of the peak. Φ_A , on the other hand, rises only slowly with y , but its evolution is quite asymmetric around $Q_s(A, y)$: the (relative) evolution is substantially larger at momenta above $Q_s(A, y)$ than below it, and because of this asymmetry, the peak gets progressively tilted (its ‘upper’ side at larger k_\perp rises faster than the lower one) and also flattens, until it eventually disappears.

6 High- k_\perp suppression in the nuclear gluon distribution at small x

In this section we shall extend our analysis of the evolution of the ratio $\mathcal{R}_{pA}(k_\perp, y)$ with increasing y to arbitrary values of the transverse momentum k_\perp . The various regimes of evolution in the $y - \ln k_\perp^2$ plane are illustrated in Figs. 1 and 10 for fixed and running coupling, respectively. In Sect. 5, we have followed the evolution along the nuclear saturation line $k_\perp = Q_s(A, y)$. Below, we shall consider all the physical regimes exhibited in Figs. 1 and 10, but our main focus will be on the high momentum region at $k_\perp \gg Q_s(A, y)$, which is the most interesting region for the phenomenon of “high- k_\perp suppression”. The natural way to follow this evolution is to increase simultaneously y and k_\perp , in such a way that the ratio $z \equiv k_\perp^2/Q_s^2(A, y)$ remains constant. This ensures that, with increasing y , the nucleus remains in the same physical regime, which could be either the saturation regime (for $z < 1$), or the (nuclear) BFKL regime (for $z > 1$).

In performing this analysis, it is useful to keep in mind the limitations of the analytic approximations that we shall use for the gluon occupation factor: The transition regions from saturation to BFKL, and also from BFKL to DLA, are not analytically under control, nor are the very early stages of the evolution. For the BFKL regime, as defined by Eq. (3.20), the saddle point approximation is justified provided $\bar{\alpha}_s y \geq 1$, while for the DLA regime at $\rho \gg \bar{\alpha}_s y$, the corresponding condition reads $\bar{\alpha}_s y \rho \gg 1$. We recall that $\rho \equiv \rho(A, k_\perp) = \ln k_\perp^2/Q_s^2(A)$ is much larger for the proton than for the nucleus (for the same value of k_\perp). Because of that, we shall be able to study the early ($\bar{\alpha}_s y \ll 1$) evolution of the proton (as described by DLA), but not also that of the nucleus (unless k_\perp is so large that the nucleus itself enters the DLA regime).

The analysis below will not only confirm the general arguments in Sect. 4 about the variation of the ratio \mathcal{R}_{pA} with y , k_\perp and A , but will also allow us to explicitly compute this ratio and, in particular, its limiting values at large y and/or large k_\perp . In the fixed coupling case, and for the linear regime, our results below will confirm and extend some of the conclusions originally obtained in Refs. [16, 24], with which the present analysis

has some overlap. Also, still for fixed coupling, our results will be seen to be consistent (within their limited range of validity and to the present accuracy) with the numerical analysis in Ref. [25] based on the Kovchegov equation.

6.1 Fixed coupling

In this section we shall explore the various regimes for the fixed coupling evolution exhibited in Fig. 1, and study the variation of the ratio $\mathcal{R}_{pA}(k_\perp, y)$ with y and k_\perp , as well as its parametric dependence upon A .

6.1.1 $k_\perp < Q_s(A, y)$: The nuclear saturation region

The nuclear distribution at saturation is not explicitly known (except for very small momenta $k_\perp \ll Q_s(A, y)$, where Eq. (3.1) applies), but this is some slowly varying function of $z \equiv k_\perp^2/Q_s^2(A, y)$ (because of geometric scaling), which moreover is simply a constant when the evolution is performed along a line parallel to the saturation line. As for the proton, it can be either at saturation, or in the linear regime above saturation, depending upon the value of k_\perp .

(I) $k_\perp < Q_s(p, y)$: Proton at saturation

In this regime, the gluon distributions in both the proton and the nucleus are universal functions of $k_\perp^2/Q_s^2(A, y)$ (with $Q_s(A, y) \rightarrow Q_s(p, y)$ in the case of the proton), which are only slowly varying. Thus, clearly, the ratio (1.1) is of order $1/A^{1/3}$, with only weak, logarithmic, dependencies upon A and k_\perp . This becomes explicit for sufficiently low momenta, $k_\perp \ll Q_s(p, y)$, where one can use Eq. (3.1) for both the proton and the nucleus, and thus find that $\mathcal{R}_{pA}(k_\perp, y)$ is monotonously increasing with k_\perp , and slowly, but monotonously, decreasing with y at fixed k_\perp . In particular, along the proton saturation line $k_\perp = Q_s(p, y)$, which defines the upper boundary of this region, one finds:

$$\mathcal{R}_{pA}(k_\perp = Q_s(p, y), y) \sim \frac{\rho_A}{A^{1/3}} \quad (\text{independent of } y). \quad (6.1)$$

(II) $Q_s(p, y) < k_\perp < Q_s(A, y)$: Proton in the linear regime

The corresponding analysis is very similar to that of the evolution along the nuclear saturation line, as discussed in Sect. 5. For $y < y_c$, cf. Eq. (5.1), the proton can be either in the DLA, or in the BFKL, regime (depending upon the value of k_\perp), while for larger y , it is always in the BFKL regime (see Fig. 1).

A straightforward analysis shows that the ratio is rapidly decreasing with y at any fixed k_\perp , due to the fast evolution of the proton. It is also interesting to consider the large y behavior at fixed z . Then, the proton is in the BFKL regime, so using Eq. (3.17) (with $Q_s(A, y) \rightarrow Q_s(p, y)$) and writing $\varphi_A(k_\perp, y) = (1/\alpha_s N_c) \bar{\varphi}_0(z)$, one obtains (with $\gamma \equiv \gamma_s \simeq 0.63$ from now on) :

$$\begin{aligned} \mathcal{R}_{pA}(k_\perp, y) &\sim \frac{\rho_A^\gamma}{A^{\frac{1-\gamma}{3}}} \frac{z^\gamma \bar{\varphi}_0(z)}{\rho_A - \ln 1/z + \Delta} \exp \left\{ \frac{(\rho_A + \ln z)^2}{2\beta \bar{\alpha}_s y} \right\} \\ &\rightarrow \frac{\rho_A^\gamma}{A^{\frac{1-\gamma}{3}}} \frac{z^\gamma \bar{\varphi}_0(z)}{\rho_A - \ln 1/z}, \quad \text{for } 2\beta \bar{\alpha}_s y \gg \rho_A^2, \end{aligned} \quad (6.2)$$

(in this regime $\rho_A > \ln 1/z$), which is indeed consistent with the previous result (5.11) on the nuclear saturation line $z = 1$.

6.1.2 $Q_s(A, y) < k_\perp < Q_g(A, y)$: The nuclear BFKL region

For $y < y_c$, the proton is in the DLA regime for any k_\perp , while for $y > y_c$, it can be either in the BFKL, or in the DLA regime, according to the value of k_\perp .

(I) $y < y_c$: Proton in the DLA regime

In this region, the ratio \mathcal{R}_{pA} is formed by using Eq. (3.17) for the nucleus and Eq. (3.15) for the proton. After straightforward manipulations, similar to those leading to Eq. (5.2), the result can be cast into the form:

$$\mathcal{R}_{pA}(z, Y) \sim \rho_A z^{1-\gamma} (\ln z + \Delta) \exp \left\{ cY - \sqrt{4Y(\ln z + cY + \rho_A)} - \frac{\ln^2 z}{2\beta Y} \right\}, \quad (6.3)$$

where $z \equiv k_\perp^2/Q_s^2(A, y)$ and $Y \equiv \bar{\alpha}_s y$. Note that the overall normalization is not under control. Eq. (6.3) applies for k_\perp in the nuclear scaling window (3.20), that is:

$$0 < \ln z < \ln \left[Q_g^2(A, y)/Q_s^2(A, y) \right] = \nu cY, \quad \text{and} \quad 1 \lesssim Y < Y_c \equiv \rho_A/\nu c. \quad (6.4)$$

It can be checked that, within this physical range¹⁵ the function $\mathcal{R}_{pA}(z, Y)$ is monotonously increasing with z , and also rapidly decreasing with Y at any fixed z . This behavior is in agreement with the general results in Sect. 4, and is illustrated in Fig. 8.

(II) $y > y_c$ & $Q_s(A, y) < k_\perp < Q_g(p, y)$: Double-scaling regime

¹⁵ The function in Eq. (6.3) develops a maximum at very large z , well outside the window (6.4). This is, of course, unphysical.

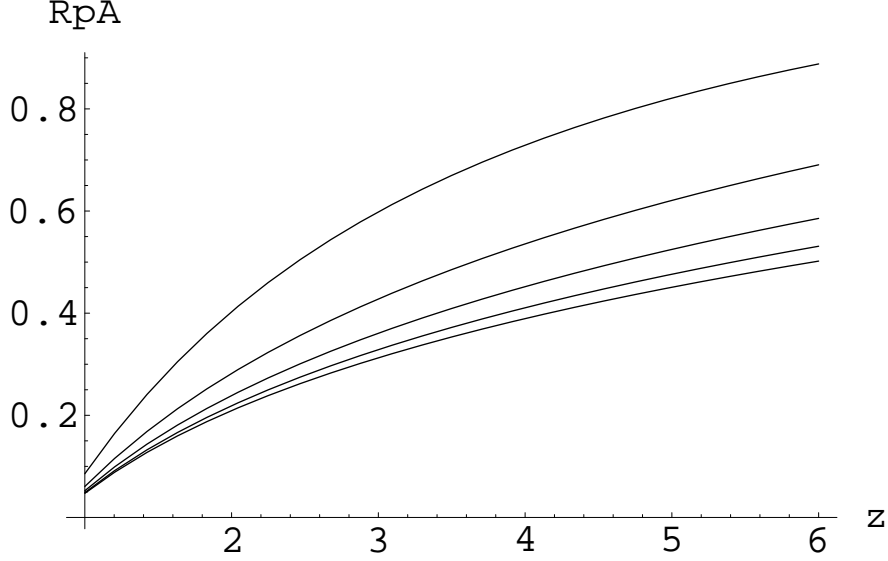


Fig. 8. The ratio $\mathcal{R}_{pA}(z, Y)$ in Eq. (6.3) as a function of $z = k_{\perp}^2/Q_s^2(A, y)$ for $\rho_A = 6$ (i.e., $Y_c \approx 0.75$) at different rapidities. The lines are for $Y = 0.1 + 0.15n$, with $n = 0, 1, \dots, 4$, from top to bottom. The bottom line corresponds to $Y = 0.7 \simeq Y_c$. The ratio \mathcal{R}_{pA} is measured in arbitrary units, since the normalization of Eq. (6.3) is not under control. Note the rapid decrease with increasing Y in the early stages of the evolution.

This region is interesting in that the proton and the nucleus are both in the same physical regime, namely in the window (3.20) for (approximate) geometric scaling, so they are described by the same approximation — the BFKL expression (3.17) —, and the normalization ambiguities cancel in the ratio \mathcal{R}_{pA} . Thus, in this regime, one can also predict the **amplitude** of this ratio, and not only its functional dependencies. Besides, this is also the regime for which the quantum evolution above the saturation line has been originally invoked, by Kharzeev, Levin and McLerran [16], as a possible mechanism to explain the high- k_{\perp} suppression observed in the RHIC data.

Using Eq. (3.17) for both the nucleus and the proton, one finds :

$$\mathcal{R}_{pA}(z, y) \simeq \frac{\rho_A^{\gamma}}{A^{\frac{1-\gamma}{3}}} \frac{\ln z + \Delta}{\ln z + \rho_A + \Delta} \exp \left[\frac{\rho_A}{2\beta Y} (2 \ln z + \rho_A) \right], \quad (6.5)$$

where we have used $\ln[k_{\perp}^2/Q_s^2(p, y)] \simeq \ln z + \rho_A$. Eq. (6.5) is valid within the range:

$$0 < \ln z < \nu c Y - \rho_A \quad \text{and} \quad Y > Y_c \equiv \rho_A/\nu c. \quad (6.6)$$

It is easily checked that the ratio (6.5) is an **increasing** function of z for arbitrary Y , and a **decreasing** function of Y for arbitrary $z > 1$. This behavior is illustrated in Fig. 9.

A noticeable difference with respect to the previous case, cf. Eq. (6.3), is that, in this double-scaling regime, the dominant y -dependencies of the nuclear and proton distributions, which are exponential, have cancelled in the ratio \mathcal{R}_{pA} . Indeed, according to Eq. (3.17), these dependencies are encoded in the respective saturation momenta, which however evolve in the same with y , cf. Eq. (3.14), and thus their ratio $Q_s^2(A, y)/Q_s^2(p, y) = Q_s^2(A)/Q_s^2(p) \simeq A^{1/3}\rho_A$ is independent of y .

The residual dependence on y in Eq. (6.5) comes from the diffusion term in Eq. (3.17), and is rather weak. (This is also in agreement with the discussion in Sect. 4; see especially Eq. (4.10).) Thus, for $Y > Y_c$, the suppression slows down, and for sufficiently large Y (such that the exponent in the second line of Eq. (6.5) become negligible), \mathcal{R}_{pA} stabilizes at a small value which depends slowly on z :

$$\mathcal{R}_{pA}(z, Y \rightarrow \infty) \simeq \frac{\rho_A}{(A^{1/3}\rho_A)^{1-\gamma}} \frac{\ln z + \Delta}{\ln z + \rho_A + \Delta}. \quad (6.7)$$

It can be verified that most of this suppression has been achieved already in the early stages of the evolution, while the proton was still in the DLA regime.

When approaching the nuclear saturation line from the above, Eq. (6.5) yields:

$$\mathcal{R}_{pA}(z \rightarrow 1, Y) \simeq \frac{1}{(A^{1/3}\rho_A)^{1-\gamma}} e^{\frac{\rho_A^2}{2\beta Y}} \xrightarrow{Y \rightarrow \infty} \frac{1}{(A^{1/3}\rho_A)^{1-\gamma}}. \quad (6.8)$$

As expected, this is the same function of A and y as obtained when approaching the saturation line from the below, cf. Eq. (5.9), with the noticeable difference that, now, also the **normalization** of this result is under control.

It is finally interesting to evaluate the ratio (6.5) on the proton geometric line (i.e., $k_\perp = Q_g(p, y)$, or $\ln z = \nu cY - \rho_A$), which is the upper boundary for the double-scaling regime considered here. In the large Y limit, one obtains:

$$\lim_{y \rightarrow \infty} \mathcal{R}_{pA}(k_\perp \sim Q_g(p, y), y) = \frac{\rho_A}{(A^{1/3}\rho_A)^\delta}, \quad \delta = 1 - \gamma - \frac{\nu c}{\beta} \simeq 0.21. \quad (6.9)$$

The dominant power of $1/A^{1/3}$ is lower on this upper boundary than on the lower one ($\delta \simeq 0.21$ as compared to $1 - \gamma \simeq 0.37$), since k_\perp is increasing faster along the geometric scaling line, and \mathcal{R}_{pA} is increasing with k_\perp .

(III) $y > y_c$ & $Q_g(p, y) < k_\perp < Q_g(A, y)$: Proton in the DLA regime

In this regime, the ratio $\mathcal{R}_{pA}(z, Y)$ is given again by Eq. (6.3), but which now applies to a different kinematical range : $\nu cY - \rho_A < \ln z < \nu cY$ and $Y > Y_c$.

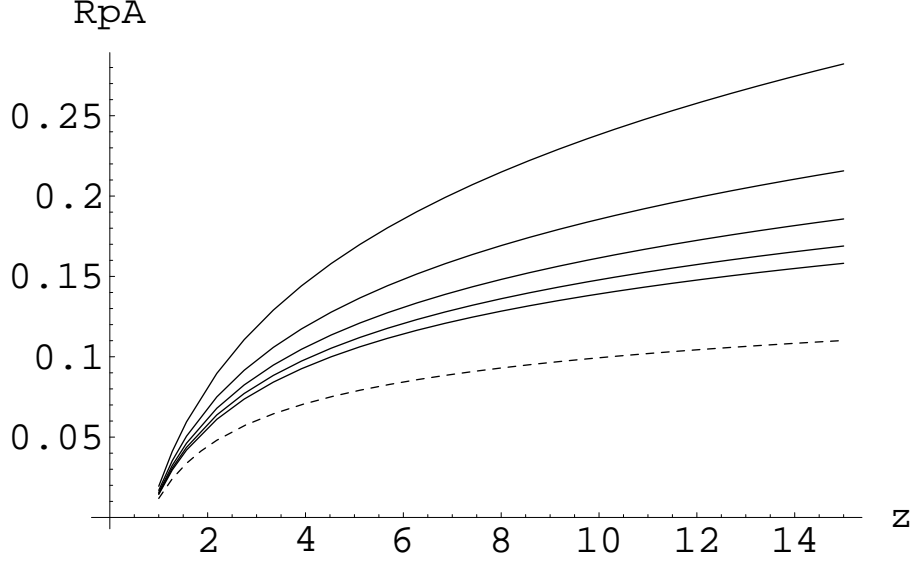


Fig. 9. The ratio $\mathcal{R}_{pA}(z, Y)$ in the double scaling window for $\rho_A = 6$ as a function of z at different $Y \gtrsim Y_c \approx 0.75$. The solid lines correspond to $Y = 0.75 + 0.3n$, with $n = 0, \dots, 4$ from top to bottom. The dashed line is the asymptotic ($Y \rightarrow \infty$) profile in Eq. (6.7). The upper limit of the double scaling window $z_{\max} = \exp\{\nu c(Y - Y_c)\}$ rapidly increases with increasing Y . For instance, $z_{\max} \approx 11$ for $Y = 1.05$ ($n = 1$), and $z_{\max} \approx 127$ for $Y = 1.35$ ($n = 2$).

6.1.3 $k_{\perp} > Q_g(A, y)$: The nuclear DLA region

This is the high momentum limit, in which both the proton and nucleus are in the DLA (or, more properly, DGLAP) regime, so the ratio can be again computed without uncertainties related to the normalization. One finds:

$$\mathcal{R}_{pA}(z, Y) = \exp \left[\sqrt{4Y(\ln z + cY)} - \sqrt{4Y(\ln z + cY + \rho_A)} \right], \quad (6.10)$$

valid for $\ln z > \nu cY$. It is clear that the extra term ρ_A in the exponential comes from the difference between two saturation scales. It is easy to check analytically that the ratio is an increasing function of z for any Y , but a decreasing function of Y for any fixed z . In particular, at very large z such that $\ln z \gg cY + \rho_A$, one obtains

$$\mathcal{R}_{pA} \simeq e^{-\rho_A \sqrt{Y/\ln z}}. \quad (6.11)$$

Therefore, when $z \rightarrow \infty$ the ratio approaches one from below.

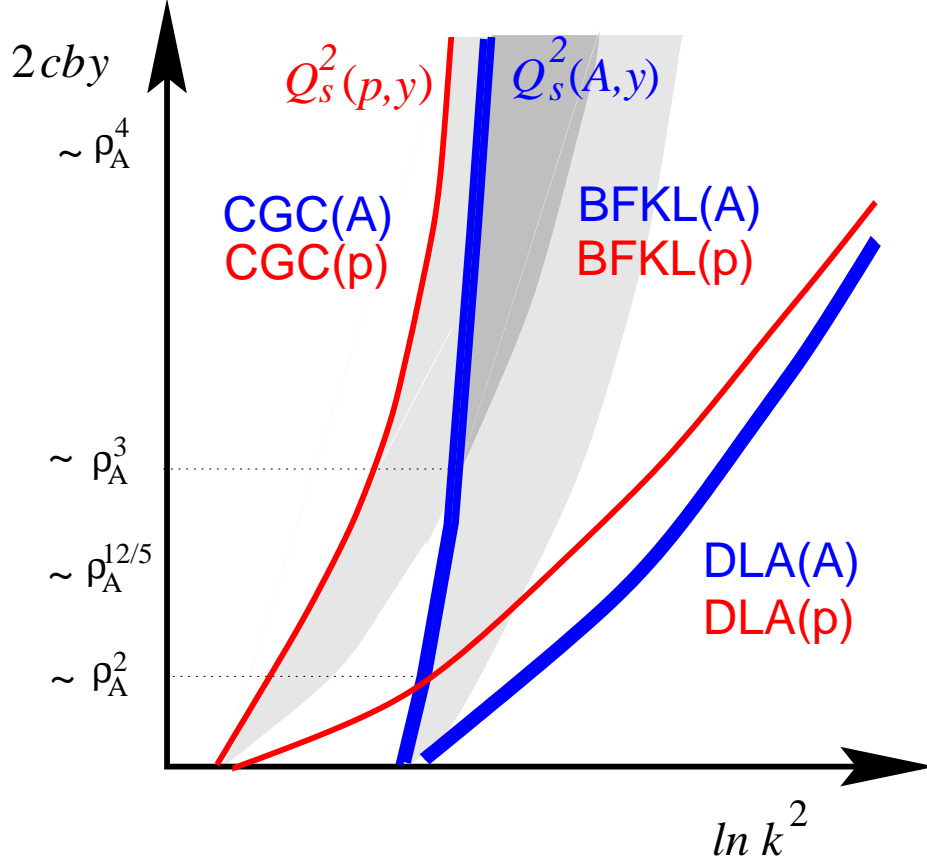


Fig. 10. *Various regimes of evolution for running coupling.* The boundaries which separate the three physical regimes (CGC, BFKL, and DLA) are shown by the red (thin) and blue (thick) curves for the proton and the nucleus, respectively. For each color (thickness), the left curve corresponds to the saturation line ($k_{\perp} = Q_s(p, y)$ or $k_{\perp} = Q_s(A, y)$), while the right curve is the boundary between BFKL and DLA regimes (which is less under control). The shaded bands on the right of the saturation lines are the respective geometric scaling regimes, which overlap with each other in the "double scaling" regime (the area with a darker shade).

6.2 Running coupling

The various physical regimes for evolution with running coupling are exhibited in Fig. 10, which should be compared to the corresponding map for fixed coupling, in Fig. 1. The differences between the two cases come from several sources:

First, the two saturation scales evolve differently with y (that for the proton growing faster) and eventually converge towards a common limit at very large y (cf. Eqs. (3.23)–(3.25)). A similar behavior holds for the corresponding lines for geometric scaling, and also for the boundaries separating BFKL from DLA behavior. This implies that, for sufficiently large y , the gluon distributions in the proton and in the nucleus become identical for all

the interesting momenta. (Differences between the two distributions persist only in the (common) DLA regime, which with increasing y is rapidly pushed towards asymptotic momenta.) This leads to the important conclusion that the ratio (1.1) approaches the universal constant $1/A^{1/3}$ at very large y , for all non-asymptotic momenta.

Second, in the case of a running coupling, the window for geometric scaling above saturation becomes narrower (cf. Eq. (3.33)), and, in contrast to the fixed coupling case, it does not coincide with the BFKL regime anymore : the latter is now defined by Eq. (3.30), and includes a domain where scaling violations are important. In Fig. 10, the regions of extended geometric scaling are the shaded bands lying on the right hand side of the nuclear and proton saturation lines, respectively.

Third, the precise boundaries of the BFKL and DLA regimes, and also the transition between these two regimes, are not under control. Whereas we expect the BFKL approximation (3.27) to be valid for $0 < \ln z < c_1 \tau_A^{2/3}(y)$ (with $z \equiv k_\perp^2/Q_s^2(A, y)$), and the DLA approximation (3.26) should apply at $\ln z > c_2 \tau_A(y)$, the constant factors $c_{1,2}$ in these conditions are not determined, and we do not dispose of analytic approximations for the intermediate region at $c_1 \tau_A^{2/3}(y) < \ln z < c_2 \tau_A(y)$.

To avoid cumbersome discussions and ambiguities associated with the location of the borderlines for the various regimes, in what follows we shall focus mainly on the situations in which both the proton and the nucleus find themselves in the same physical regime (which could be CGC, BFKL, or DLA). These situations are the most interesting ones, as they allow for a calculation of the ratio \mathcal{R}_{pA} which is free of renormalization ambiguities. Besides, they are the only ones to survive at large y : The other regimes visible on Fig. 10 are squeezed in between the proton and nucleus saturation lines, or in between the respective borderlines for BFKL behavior, and therefore shrinks to zero in the high energy limit.

The analysis to follow is particularly important because, with running coupling, we have no general arguments to understand the behavior of the ratio \mathcal{R}_{pA} , as we had for a fixed coupling. As we will see, in spite of interesting differences, the global behavior of \mathcal{R}_{pA} as a function of y , k_\perp and A is the same as in the fixed coupling case discussed in Sect. 4.

6.2.1 The double CGC region

On the left of the proton saturation line, both the proton and the nucleus are in the color glass condensate regime. For sufficiently low momenta $k_\perp \ll Q_s(p, y)$, one can compute the ratio \mathcal{R}_{pA} by using Eq. (3.2) for both hadrons. Then one can easily check that $\mathcal{R}_{pA}(k_\perp, y)$ has the same behavior as in the corresponding regime at fixed coupling. It is further interesting to follow the proton saturation line $k_\perp = Q_s(p, y)$, where Eq. (3.4) holds for the proton. One finds (see Eq. (3.23) for notations)

$$\mathcal{R}_{pA}(k_{\perp} = Q_s(p, y), y) \approx \frac{1}{A^{1/3}} \frac{(\tau_A(y) + \tau_p(y)) [a_0(\tau_A(y) - \tau_p(y)) + \kappa]}{2\tau_p(y)\kappa}, \quad (6.12)$$

where we have added a constant κ to the nuclear distribution in Eq. (3.2) in such a way to match the boundary condition (3.4) when $k_{\perp} \rightarrow Q_s(A, y)$. Of course, this is only a crude approximation — the approach towards the saturation line is not under control —, but this is interesting as it allows us to qualitatively study the behavior at large y , where the two saturation momenta converge to each other. For $2cby \gg \rho_A^2$, one finds:

$$\mathcal{R}_{pA}(k_{\perp} = Q_s(p, y), y) \approx \frac{1}{A^{1/3}} \left(1 + \frac{a_0}{\kappa} \frac{\rho_A^2}{2\sqrt{2cby}} \right), \quad (6.13)$$

which decreases with y , and for $2cby \gg \rho_A^4$ approaches the universal value $1/A^{1/3}$, as expected.

6.2.2 The nuclear BFKL region

Here we consider the region in between the two blue (thick) curves in Fig. 10. For relatively small rapidities $y < y_c$ with $2cby_c \sim \rho_A^2$, the proton is in the DLA regime for any k_{\perp} within this region. (See the discussion at the beginning of Sect. 5.2 for more details on the separating rapidities.) For larger rapidities, the proton BFKL regime starts to appear, but this is theoretically under control only for $y > y'_c$, with $2cby'_c \sim \rho_A^{12/5}$. The most interesting "double scaling" regime appears at the even larger rapidity $2cby''_c \sim \rho_A^3$.

(I) $y < y_c$: Proton in the DLA regime

Straightforward manipulations using Eq. (3.27) for the nucleus and Eq. (3.26) for the proton yield (with $z \equiv k_{\perp}^2/Q_s^2(A, y)$, as usual)

$$\begin{aligned} \mathcal{R}_{pA}(z, y) \sim & \left(\ln z + \tau_A(y) \right) \tau_A^{1/3}(y) \text{Ai} \left(\xi_1 + \frac{\ln z + \Delta}{D\tau_A^{1/3}(y)} \right) z^{1-\gamma} \\ & \times \exp \left\{ \tau_A(y) - \rho_A - \sqrt{4by \ln(\ln z + \tau_A(y))} - \frac{2 \ln^2 z}{3\beta\tau_A(y)} \right\}, \end{aligned} \quad (6.14)$$

where the normalization is not under control. This is valid provided the nucleus is in the BFKL window (3.30), which implies (c_1 is a constant of $\mathcal{O}(1)$):

$$0 < \ln z < c_1 \tau_A^{2/3}(y). \quad (6.15)$$

It can be checked that, within this physical range, the ratio $\mathcal{R}_{pA}(z, y)$ is monotonously increasing¹⁶ with z , and also rapidly decreasing with y at fixed z .

In particular, when approaching the nuclear saturation scale from the above, one recovers the same parametric dependencies upon A and y as in Eq. (5.16).

(II) $y > y'_c$: The double scaling regime

As before, this regime is interesting since the uncontrollable normalization factors cancel out in the ratio between the gluon distributions for the nucleus and the proton. Using Eq. (3.27), one finds :

$$\begin{aligned} \mathcal{R}_{pA}(z, y) \simeq & \frac{1}{A^{1/3}} \left(\frac{\tau_A}{\tau_p} \right)^{1/3} \frac{\text{Ai} \left(\xi_1 + \frac{\ln z + \Delta}{D\tau_A^{1/3}} \right)}{\text{Ai} \left(\xi_1 + \frac{\ln z + \tau_A - \tau_p + \Delta}{D\tau_p^{1/3}} \right)} \\ & \times \exp \left[\gamma(\tau_A - \tau_p) + \frac{2(\ln z + \tau_A - \tau_p)^2}{3\beta\tau_p} - \frac{2\ln^2 z}{3\beta\tau_A} \right], \end{aligned} \quad (6.16)$$

which is free of normalization ambiguities. Since now y is relatively large, one can replace in this and the subsequent equations $\tau_A - \tau_p \approx \rho_A^2/2\sqrt{2cby}$ and $\tau_p \approx \sqrt{2cby}$.

The upper limit for the validity range of this expression is fixed by the borderline for the proton BFKL regime (see Fig. 10). Therefore, Eq. (6.16) is valid for:

$$0 < \ln z < c_1 \tau_p^{2/3}(y) - (\tau_A(y) - \tau_p(y)). \quad (6.17)$$

It can be checked that, the ratio (6.16) is an **increasing** function of z , and a **decreasing** function of Y . This can be explicitly seen on the numerical plot of the ratio in Fig. 11. Note the rapid decrease of the ratio with increasing y . As compared to the corresponding plot for fixed coupling, in Fig. 9, one can see that with a running coupling the decrease of $\mathcal{R}_{pA}(z, y)$ is pursued up to larger values of y , until the ratio eventually stabilizes at the z -independent (and comparatively smaller) value $1/A^{1/3}$.

This evolution can be more explicitly studied by using the approximate form of Eq. (6.16) valid in the “double scaling” window, which is the regime where both the nucleus and the proton exhibit geometric scaling. This window opens at a rapidity $2cby_c'' \sim \rho_A^3$, and extends over the following interval in z (c_3 is a constant of $\mathcal{O}(1)$); see Eq. (3.33):

$$0 < \ln z < \ln \left[Q_g^2(p, y)/Q_s^2(A, y) \right] = c_3 \tau_p^{1/3}(y) - (\tau_A(y) - \tau_p(y)), \quad (6.18)$$

¹⁶ Although the ratio (6.14) develops a maximum at large z , it is well outside the physical region, similarly to the fixed coupling case. In fact, one can roughly estimate the position of the maximum to be $\ln z \sim a\tau_A(y)$ with $a \sim \mathcal{O}(1)$.

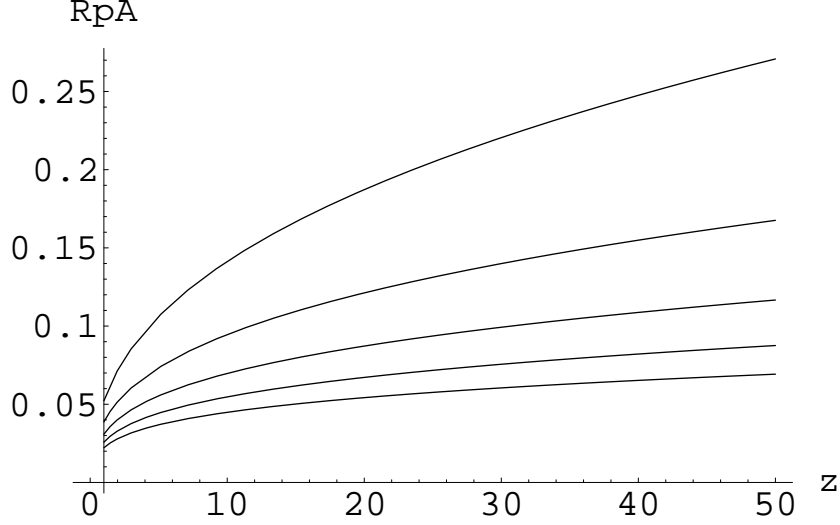


Fig. 11. The ratio $\mathcal{R}_{pA}(z, y)$ in the double BFKL regime for $\rho_A = 6$ as a function of z at different values of y . The lines correspond to $y = 1.1 + 0.3n$, with $n = 0, \dots, 4$ from top to bottom. The third line ($n = 2$) corresponds to $y = y_c'' = 1.7$. The range in z shown in the figure is in the physical range for all the lines, except for the top one. Indeed, the upper boundary of the physical regime is $z_{\max} = 22.8$ for $y = 1.1$, $z_{\max} = 50$ for $y = 1.4$, $z_{\max} = 97$ for $y = y_c''$, etc.

which is represented by the dark shaded area in Fig. 10. In this range, the ratio takes the simpler form (cf. Eq. (3.32)) :

$$\mathcal{R}_{pA}(z, y) \simeq \frac{1}{A^{1/3}} \frac{\ln z + \Delta}{\ln z + \rho_A^2/2\sqrt{2cby} + \Delta} \exp \left\{ \frac{\gamma}{2} \frac{\rho_A^2}{\sqrt{2cby}} \right\}, \quad (6.19)$$

which when approaching the saturation line from above ($\ln z \rightarrow 0$) is consistent with the previous estimate in Eq. (5.23).

For large y , such that $2cby \gg \rho_A^4$, the ratio (6.19) becomes independent of z , and approaches the universal limit $1/A^{1/3}$, as anticipated. This is also the limit of the full expression (6.16) for $2cby \gg \rho_A^4$ and any z in the range (6.17).

6.2.3 The nuclear DLA region

By using Eq. (3.26) for both the proton and the nucleus, one easily obtains:

$$\mathcal{R}_{pA}(z, y) = \exp \left[\sqrt{4by \{ \ln(\ln z + \tau_A(y)) - \ln \rho_A \}} - \sqrt{4by \{ \ln(\ln z + \tau_A(y)) - \ln \rho_p \}} \right], \quad (6.20)$$

which is valid, roughly, for $\ln z \gtrsim \tau_A(y)$. It is easy to check that the ratio is an increasing function of z for any y . We have numerically verified that, for $\ln z \gtrsim \tau_A(y)$ at least, the ratio is an decreasing function of y .

At very large z such that $\ln z \gg \tau_A(y)$, one obtains

$$\mathcal{R}_{pA} \simeq e^{-\ln \frac{\rho_A}{\rho_p} \sqrt{by/\ln \ln z}}. \quad (6.21)$$

Thus, when $z \rightarrow \infty$ the ratio approaches one **from the below** (but only very slowly). This concludes our analysis.

Acknowledgments

We are particularly grateful to Al Mueller for his careful and repeated reading of this manuscript, and many useful suggestions. We would like to thank Stephane Munier for many discussions and for sharing with us the results of a numerical calculation which helped us clarifying the argument for the flattening of the Cronin peak. During the elaboration of this work, we have benefited from vivid discussions, incisive questions, and insightful remarks from Jean-Paul Blaizot, François Gelis, Larry McLerran. One of the authors (K.I.) is thankful to Kirill Tuchin for informative discussions. This work has been completed while one of the authors (E.I.) was a visitor at Universidade Federal do Rio de Janeiro. He wishes to thank Eduardo Fraga for his hospitality and support during this visit.

A Appendix

Here we study in more detail the gluon occupation factor φ_A and the integrated gluon distribution function \mathcal{G}_A in the McLerran-Venugopalan model, both for fixed and running coupling. We first deal with the running coupling case, which turns out to be simpler, and then we continue with the fixed coupling one. At the end of the appendix we present some useful properties of the confluent hypergeometric function. Note that, in order to simplify writing, we shall often use different normalizations for the various quantities as compared to the main text. The differences will be indicated at the appropriate places.

The Running Coupling Case

The twist contribution to the gluon occupation factor, as given in Eq. (2.17), and with the constant factor $1/(b_0 N_c)$ omitted since it can be restored at the end of the calculation, reads

$$\varphi_A^{\text{twist}}(z) = \int_0^\infty dt J_0(\sqrt{4zt}) \frac{1 - e^{-t}}{t} \ln \frac{1}{t}. \quad (\text{A.1})$$

In principle, one should integrate up to $\sim t_{\text{max}} = e^{\rho_A}$, which corresponds to a dipole size $\sim r_{\text{max}} = 2/\Lambda$. However, it is harmless to extend the integration to infinity, so long as we are interested in momenta $k \gg \Lambda \Leftrightarrow z \gg e^{-\rho_A}$. We can do the above integration by replacing $\ln(1/t) \rightarrow t^{-a}$. Then we obtain an expression involving the confluent hypergeometric function ${}_1F_1(-a, 1, -z) \equiv \Phi(-a, 1, -z)$. Finally we take the derivative with respect to a at $a = 0$ to recover the quantity in Eq. (A.1), and we obtain

$$\varphi_A^{\text{twist}} = -\frac{1}{2} \ln^2 z - \gamma \ln z + \gamma \Gamma(0, z) + \frac{\pi^2}{12} - \frac{\gamma^2}{2} + \frac{1}{2} \Phi^{200}(0, 1, -z), \quad (\text{A.2})$$

where $\gamma \equiv \gamma_E = 0.577$ denotes the Euler–Mascheroni constant throughout this Appendix. In the small- z limit the hypergeometric term vanishes and one is left with

$$\varphi_A^{\text{twist}} = -\frac{1}{2} \ln^2 z - 2\gamma \ln z + \frac{\pi^2}{12} - \frac{3\gamma^2}{2} + \mathcal{O}(z). \quad (\text{A.3})$$

Notice that this is negative, but it never becomes larger in magnitude than the contribution of the saturation term $\varphi_A^{\text{sat}} = \rho_A \Gamma(0, z)$. Even at $k = \Lambda \Leftrightarrow z = e^{-\rho_A}$, one has

$$\varphi_A^{\text{twist}} \simeq -\frac{1}{2} \rho_A^2 \simeq -\frac{1}{2} \varphi_A^{\text{sat}}. \quad (\text{A.4})$$

and the gluon occupation factor is positive and well defined.

In the large- z region, we can use Eq. (A.21), given at the end of the appendix, to derive the asymptotic expansion of the index-differentiated hypergeometric function. This will have the form given in Eq.(A.23). It is straightforward to show that

$$\Phi^{200}(0, 1, -z) = \ln^2 z + 2\gamma \ln z + \gamma^2 - \frac{\pi^2}{6} + 2 \sum_{n=1} \frac{\Gamma(n)}{n} \frac{1}{z^n} + \mathcal{O}(e^{-z}). \quad (\text{A.5})$$

Then, Eqs. (A.2) and (A.5) imply that all the logarithmically divergent and constant terms in φ_A cancel, and as expected only the inverse powers of z survive. Therefore one has

$$\varphi_A = \varphi_A^{\text{twist}} = \sum_{n=1} \frac{\Gamma(n)}{n} \frac{1}{z^n} + \mathcal{O}(e^{-z}) = \frac{Q_s^2(A)}{k^2} + \frac{1}{2} \frac{Q_s^4(A)}{k^4} + \frac{2}{3} \frac{Q_s^6(A)}{k^6} + \dots, \quad (\text{A.6})$$

which exhibits the correct bremsstrahlung spectrum, accompanied by power corrections which are all positive.

Now we turn our attention to the integrated gluon distribution function, which we conveniently normalize as

$$\mathcal{G}_A = \int^Q \frac{d^2k}{\pi Q_s^2(A)} \varphi_A. \quad (\text{A.7})$$

For the saturation term of the gluon occupation factor the integration is trivial, and one obtains

$$\mathcal{G}_A^{\text{sat}} = [1 - e^{-Z} + Z \Gamma(0, Z)] \rho_A. \quad (\text{A.8})$$

In the above we have defined the scaled momentum variable $Z = Q^2/Q_s^2(A)$. For the twist contribution as given in (A.1), one can perform first the integration over k , which simply replaces $J_0(\sqrt{4zt})$ by $\sqrt{Z} J_1(\sqrt{4zt})/\sqrt{t}$. Then the integration over t can be done as before and gives

$$\begin{aligned} \mathcal{G}_A^{\text{twist}} = & -\frac{1}{2} Z \ln^2 Z + (1 - \gamma) Z \ln Z + \left(\frac{\pi^2}{12} - \frac{\gamma^2}{2} + \gamma - 1 \right) Z \\ & + \gamma [1 - e^{-Z} + Z \Gamma(0, Z)] + \frac{1}{2} Z \Phi^{200}(0, 2, -Z). \end{aligned} \quad (\text{A.9})$$

When $Q^2 \gg Q_s^2(A) \Leftrightarrow Z \gg 1$, the last two equations lead to

$$\mathcal{G}_A = \rho_A + \ln Z + 2\gamma - \sum_{n=1}^{\infty} \frac{\Gamma(n)}{n+1} \frac{1}{Z^n} + \mathcal{O}(e^{-Z}), \quad (\text{A.10})$$

where the first term comes from $\mathcal{G}_A^{\text{sat}}$ and the remaining from $\mathcal{G}_A^{\text{twist}}$. One can rewrite the above equation, in a more illuminating way, as

$$\mathcal{G}_A = \ln \frac{Q^2}{\Lambda^2} + 2\gamma - \frac{1}{2} \frac{Q_s^2(A)}{Q^2} - \frac{1}{3} \frac{Q_s^4(A)}{Q^4} + \dots, \quad (\text{A.11})$$

which shows that the higher twist corrections give a small negative contribution (shadowing) to the integrated gluon distribution function.

The Fixed Coupling Case

The twist contribution to the gluon occupation factor as given in Eq. (2.15) and multiplied by the constant factor $\rho_A \alpha_s N_c$, reads

$$\varphi_A^{\text{twist}}(z) = - \int_0^{\infty} dt J_0(\sqrt{4zt}) e^{-t} \sum_{n=1}^{n_{\text{max}}} \frac{t^{n-1} \ln^n t}{n! \rho_A^{n-1}}. \quad (\text{A.12})$$

The integration in the above equation needs to be cut at $\sim t_{\max} = e^{\rho_A}$ which corresponds to a dipole size $\sim r_{\max} = 2/\Lambda$. However, and in the “worst case” that z is small, each term gets its most contribution from the region $t \approx n$, with the “magnitude” of the n -th term being $\sim (\ln n/\rho_A)^n$. Therefore the integration in the terms with $n \lesssim n_{\max} = e^{\rho_A}$ can be extended to infinity, while terms with $n \gtrsim n_{\max}$ do not contribute, since their peak lies outside the region of integration. Thus, the cutoff in the MV model translates to a cutoff in the series in Eq. (A.12). Furthermore, this (asymptotic) series is rapidly convergent for $\rho_A \gg 1$, since $\ln n/\rho_A < 1$ for $n < e^{\rho_A}$. Thus, it is enough to keep a few terms in (A.12). They can be calculated by the same method we used in the running coupling case. The n -th term, apart from the overall suppressing factor ρ_A^{-n+1} , becomes constant when $z \ll 1$, and falls as z^{-n} (plus all possible higher inverse powers) for $z \gg 1$. The expressions become more and more complicated as n increases, and therefore we shall present only the first two terms. We have

$$\varphi_A^{n=1} = \gamma e^{-z} - \Phi^{100}(1, 1, -z), \quad (\text{A.13})$$

$$\begin{aligned} \varphi_A^{n=2} = & -\frac{1}{\rho_A} \left[\left(\frac{\pi^2}{12} + \frac{\gamma^2}{2} - \gamma \right) (1-z) e^{-z} \right. \\ & \left. + (1-\gamma) \Phi^{100}(2, 1, -z) + \frac{1}{2} \Phi^{200}(2, 1, -z) \right]. \end{aligned} \quad (\text{A.14})$$

Since $\Phi^{n00}(a, 1, -z)$ vanishes at small- z , the limiting value of φ_A^{twist} is finite. One easily finds that

$$\varphi_A^{\text{twist}} = \gamma - \frac{1}{\rho_A} \left(\frac{\pi^2}{12} + \frac{\gamma^2}{2} - \gamma \right) + \mathcal{O}(z). \quad (\text{A.15})$$

In the large- z limit, we need to expand the hypergeometric functions and we obtain

$$\varphi_A = \varphi_A^{\text{twist}} = \frac{Q_s^2(A)}{Q^2} + \frac{Q_s^4(A)}{Q^4} \left[1 + \frac{1}{\rho_A} \left(\ln \frac{Q^2}{Q_s^2(A)} + 2\gamma - 2 \right) \right] + \dots, \quad (\text{A.16})$$

where both the $n = 1$ and $n = 2$ terms contribute to the $1/z^2 = Q_s^4(A)/Q^4$ term. This correction is positive and the same will be true for all the $1/z^n$ ones.

Now let us calculate the integrated gluon distribution function. The saturation contribution is the same as the one we found in the running coupling case and is given in Eq. (A.8).

For the twist contributions we shall again present only the first two terms, which are

$$\mathcal{G}_A^{n=1} = \gamma - \gamma e^{-Z} - Z \Phi^{100}(1, 2, -Z) \quad (\text{A.17})$$

$$\begin{aligned} \mathcal{G}_A^{n=2} = & -\frac{1}{\rho_A} Z \left[\left(\frac{\pi^2}{12} + \frac{\gamma^2}{2} - \gamma \right) e^{-Z} \right. \\ & \left. + (1 - \gamma) \Phi^{100}(2, 2, -Z) + \frac{1}{2} \Phi^{200}(2, 2, -Z) \right], \end{aligned} \quad (\text{A.18})$$

and similar, but more complicated expressions can also be obtained for $n \geq 3$. Each term vanishes as Z becomes small, and all terms with $n \geq 2$ approach 0 as Z becomes large. Keeping the $n = 1, 2$ terms, we can obtain the first power law corrections in \mathcal{G}_A in the high momentum limit $Q_s^2(A) \gg Q^2$. We obtain

$$\mathcal{G}_A = \ln \frac{Q^2}{\Lambda^2} + 2\gamma - \frac{Q_s^2(A)}{Q^2} \left[1 + \frac{1}{\rho_A} \left(\ln \frac{Q^2}{Q_s^2(A)} + 2\gamma - 1 \right) \right]. \quad (\text{A.19})$$

As in the running coupling case the higher twist terms give a small negative contribution to the integrated gluon distribution function.

The Confluent Hypergeometric Function $\Phi(a, b, -z)$

Here we give some useful properties of the confluent hypergeometric function ${}_1F_1(a, b, -z) \equiv \Phi(a, b, -z)$. More precisely we examine its n -th derivative with respect to the first argument, that is $\Phi^{n00}(a, b, -z)$. The range of parameters that we are interested in is $a \geq 0$, $b \geq 1$ and $z \geq 0$.

The confluent hypergeometric function is defined as

$$\Phi(a, b, -z) = 1 - \frac{a}{b} z + \frac{1}{2!} \frac{a(a+1)}{b(b+1)} z^2 - \dots, \quad (\text{A.20})$$

and its large- z asymptotic expansion reads

$$\begin{aligned} \Phi(a, b, -z) = & \frac{\Gamma(b)}{\Gamma(b-a)} z^{-a} \\ & \times \left[1 + \frac{a(a-b+1)}{z} + \frac{1}{2!} \frac{a(a+1)(a-b+1)(a-b+2)}{z^2} + \dots \right], \end{aligned} \quad (\text{A.21})$$

where terms that fall as e^{-z} have been neglected.

We can find the behavior of $\Phi^{n00}(a, b, -z)$ in the small- z region from Eq. (A.20) and in the large- z region from Eq. (A.21). We obtain

$$\Phi^{n00}(a, b, -z) = \frac{\Gamma(b)}{\Gamma(b+n)} z^n + \mathcal{O}(z^{n+1}) \quad \text{for } z \ll 1, \quad (\text{A.22})$$

which vanishes when $n \geq 1$, and

$$\Phi^{n00}(a, b, -z) = z^{-a} \left[\sum_{k \geq 0} \frac{c_k}{z^k} \right] \left[\sum_{k=0}^n d_k \ln^k z \right] \quad \text{for } z \gg 1, \quad (\text{A.23})$$

where the coefficients c_k and d_k depend on the set of parameters (n, a, b) and can be determined from Eq. (A.21). The function $\Phi^{n00}(a, b, -z)$ diverges for large- z as a power of $\ln z$ when $a = 0$, while it approaches zero when $a > 0$.

References

- [1] “Quark Matter 2002”, Proceedings of the 16th International Conference on Ultra-Relativistic Nucleus-Nucleus Collisions, (Nantes, France 18-24 July, 2002), Nucl. Phys. A 715 (2003).
- [2] See for example, D. d’Enterria, “*Hard scattering at RHIC: Experimental review,*” arXiv:nucl-ex/0309015 and references therein.
- [3] B. B. Back *et al.* [PHOBOS Collaboration], *Phys. Rev. Lett.* **91** (2003) 072302 [arXiv:nucl-ex/0306025]; S. S. Adler *et al.* [PHENIX Collaboration], *Phys. Rev. Lett.* **91** (2003) 072303 [arXiv:nucl-ex/0306021]; J. Adams *et al.* [STAR Collaboration], *Phys. Rev. Lett.* **91** (2003) 072304 [arXiv:nucl-ex/0306024]; I. Arsene *et al.* [BRAHMS Collaboration], *Phys. Rev. Lett.* **91** (2003) 072305 [arXiv:nucl-ex/0307003].
- [4] I. Arsene [BRAHMS Collaboration], “*On the evolution of the nuclear modification factors with rapidity and centrality in d+Au collisions at $\sqrt{s_{NN}} = 200$ GeV,*” arXiv:nucl-ex/0403005.
- [5] R. Debbe and M. Murray, for the BRAHMS Collaboration, talks given at QM2004, Oakland, USA, January 2004.
- [6] T. Frawley and M. X. Liu, [PHENIX Collaboration], P. Steinberg and R. Nouicer, [PHOBOS Collaboration], and L. Barnby [STAR Collaboration], talks given at QM2004, Oakland, USA, January 2004.
- [7] L.V. Gribov, E.M. Levin, and M.G. Ryskin, *Phys. Rept.* **100** (1983) 1.
- [8] A.H. Mueller and J. Qiu, *Nucl. Phys.* **B268** (1986) 427.
- [9] J.-P. Blaizot and A. H. Mueller, *Nucl. Phys.* **B289** (1987) 847.

- [10] L. McLerran and R. Venugopalan, *Phys. Rev.* **D49** (1994) 2233; *ibid.* **49** (1994) 3352; *ibid.* **50** (1994) 2225.
- [11] A. H. Mueller, *Parton Saturation—An Overview*, hep-ph/0111244. Published in *QCD Perspectives on Hot and Dense Matter*, Eds. J.-P. Blaizot and E. Iancu, NATO Science Series, Kluwer, 2002.
- [12] E. Iancu, A. Leonidov and L. McLerran, *The Colour Glass Condensate: An Introduction*, hep-ph/0202270. Published in *QCD Perspectives on Hot and Dense Matter*, Eds. J.-P. Blaizot and E. Iancu, NATO Science Series, Kluwer, 2002;
E. Iancu and R. Venugopalan, *The Color Glass Condensate and High Energy Scattering in QCD*, hep-ph/0303204. Published in *Quark-Gluon Plasma 3*, Eds. R. C. Hwa and X.-N. Wang, World Scientific, 2003.
- [13] J. W. Cronin, et al. *Phys. Rev.* **D11** (1975) 3105; D. Antreasyan, et al. *Phys. Rev. Lett.* **38** (1977) 112; D. Antreasyan, et al. *Phys. Rev.* **D19** (1979) 764.
- [14] Yu.V. Kovchegov and A.H. Mueller, *Nucl. Phys.* **B529** (1998), 451.
- [15] A. Accardi and M. Gyulassy, “*Cronin effect vs. geometrical shadowing in $d + Au$ collisions at RHIC,*” arXiv:nucl-th/0308029.
- [16] D. E. Kharzeev, E. Levin, and L. McLerran, *Phys. Lett.* **B561** (2003) 93.
- [17] B.Z. Kopeliovich, J. Nemchik, A. Schafer, and A.V. Tarasov, *Phys. Rev. Lett.* **88** (2002) 232303; A. Accardi, “*Cronin effect in proton nucleus collisions: A survey of theoretical models,*” arXiv:hep-ph/0212148; I. Vitev, *Phys. Lett.* **B562** (2003) 36; X. N. Wang, *Phys. Lett.* **B565** (2003) 116; R. C. Hwa and C. B. Yang, “*Final-state interaction as the origin of the Cronin effect,*” arXiv:nucl-th/0403001.
- [18] For a review, see M. Gyulassy, I. Vitev, X. N. Wang and B. W. Zhang, “*Jet quenching and radiative energy loss in dense nuclear matter,*” arXiv:nucl-th/0302077. Published in *Quark Gluon Plasma 3*, editors: R.C. Hwa and X.N. Wang, World Scientific, Singapore.
- [19] M. Braun, *Eur. Phys. J.* **C16** (2000) 337; *Phys. Lett.* **B483** (2000) 105.
- [20] Yu. V. Kovchegov and K. Tuchin, *Phys. Rev.* **D65** (2002) 074026.
- [21] A. Dumitru and L. McLerran, *Nucl. Phys.* **A700** (2002) 492.
- [22] J.P. Blaizot, F. Gelis, R. Venugopalan, “*High energy $p A$ collisions in the color glass condensate approach. I: Gluon production and the Cronin effect,*”, hep-ph/0402256; “*High energy $p A$ collisions in the color glass condensate approach. II: Quark production,*” hep-ph/0402257.
- [23] R. Baier, A. Kovner and U. A. Wiedemann, *Phys. Rev. D* **68** (2003) 054009.
- [24] D. Kharzeev, Yu. V. Kovchegov, and K. Tuchin, *Phys. Rev.* **D66** (2003) 094013.
- [25] J. L. Albacete, N. Armesto, A. Kovner, C. A. Salgado and U. A. Wiedemann, *Phys. Rev. Lett.* **92** (2004) 082001.

- [26] E. Iancu, A. Leonidov and L. McLerran, *Nucl. Phys.* **A692** (2001) 583; *Phys. Lett.* **B510** (2001) 133; E. Ferreira, E. Iancu, A. Leonidov and L. McLerran, *Nucl. Phys.* **A703** (2002) 489.
- [27] D. Kharzeev, E. Levin and M. Nardi, *Nucl. Phys.* **A730** (2004) 448, erratum in arXiv:hep-ph/0212316.
- [28] J. Jalilian-Marian, “*Forward Rapidity Hadron Production in Deuteron Gold Collisions from Valence Quarks,*” arXiv:nucl-th/0402080.
- [29] Yu.V. Kovchegov, *Phys. Rev.* **D54** (1996), 5463; *Phys. Rev.* **D55** (1997), 5445.
- [30] J. Jalilian-Marian, A. Kovner, L. McLerran, H. Weigert, *Phys. Rev.* **D55** (1997) 5414.
- [31] J. Jalilian-Marian, A. Kovner, A. Leonidov and H. Weigert, *Nucl. Phys.* **B504** (1997) 415; *Phys. Rev.* **D59** (1999) 014014.
- [32] I. Balitsky, *Nucl. Phys.* **B463** (1996) 99; *Phys. Rev. Lett.* **81** (1998) 2024; *Phys. Lett.* **B518** (2001) 235; *High-energy QCD and Wilson lines*, hep-ph/0101042.
- [33] Yu. V. Kovchegov, *Phys. Rev.* **D60** (1999), 034008; *ibid.* **D61** (2000) 074018.
- [34] H. Weigert, *Nucl. Phys.* **A703** (2002) 823.
- [35] E. Iancu and L. McLerran, *Phys. Lett.* **B510** (2001) 145.
- [36] E. Iancu, K. Itakura and L. McLerran, *Nucl. Phys.* **A724** (2003) 181.
- [37] A. H. Mueller, *Nucl. Phys.* **B558** (1999) 285.
- [38] E. Iancu, K. Itakura, and L. McLerran, *Nucl. Phys.* **A708** (2002) 327.
- [39] A. H. Mueller and D.N. Triantafyllopoulos, *Nucl. Phys.* **B640** (2002) 331.
- [40] D.N. Triantafyllopoulos, *Nucl. Phys.* **B648** (2003) 293.
- [41] S. Munier and R. Peschanski, *Phys. Rev. Lett.* **91** (2003) 232001 [arXiv:hep-ph/0309177]; *Phys. Rev.* **D69** (2004) 034008 [arXiv:hep-ph/0310357]; “*Universality and tree structure of high energy QCD,*” hep-ph/0401215.
- [42] A. H. Mueller, *Nucl. Phys.* **A724** (2003) 223.
- [43] L.N. Lipatov, *Sov. J. Nucl. Phys.* **23** (1976) 338; E.A. Kuraev, L.N. Lipatov and V.S. Fadin, *Zh. Eksp. Teor. Fiz* **72**, 3 (1977) (*Sov. Phys. JETP* **45** (1977) 199); Ya.Ya. Balitsky and L.N. Lipatov, *Sov. J. Nucl. Phys.* **28** (1978) 822.
- [44] V.S. Fadin and L.N. Lipatov, *Phys. Lett.* **B429** (1998) 127; G. Camici and M. Ciafaloni, *Phys. Lett.* **B430** (1998) 349.
- [45] G.P. Salam, *JHEP* **9807** (1998) 19; M. Ciafaloni, D. Colferai, *Phys. Lett.* **B452** (1999) 372; M. Ciafaloni, D. Colferai, and G.P. Salam, *Phys. Rev.* **D60** (1999) 114036.

- [46] K. Rummukainen and H. Weigert, “*Universal features of JIMWLK and BK evolution at small x ,*” arXiv:hep-ph/0309306.
- [47] E. Iancu and A.H. Mueller, *Nucl. Phys.* **A730** (2004) 494.
- [48] A.H. Mueller and A.I. Shoshi, “*Small- x physics beyond the Kovchegov equation,*” arXiv:hep-ph/0402193.
- [49] N. Armesto and M. Braun, *Eur. Phys. J.* **C20** (2001) 517; *ibid.* **C22** (2001) 351.
- [50] K. Golec-Biernat, L. Motyka, and A.M. Staśto, *Phys. Rev.* **D65** (2002) 074037.
- [51] E. Levin and M. Lublinsky, *Phys. Lett.* **B521** (2001) 233; *Eur. Phys. J.* **C22** (2002) 647; M. Lublinsky, *Eur. Phys. J.* **C21** (2001) 513.
- [52] K. Golec-Biernat and A.M. Stasto, *Nucl. Phys.* **B668** (2003) 345.
- [53] F. Gelis and J. Jalilian-Marian, *Phys. Rev.* **D67** (2003) 074019.
- [54] J. Jalilian-Marian, Y. Nara and R. Venugopalan, *Phys. Lett.* **B577** (2003) 54.
- [55] E. Levin and K. Tuchin, *Nucl. Phys.* **B573** (2000) 833; *Nucl. Phys.* **A691** (2001) 779; *Nucl. Phys.* **A693** (2001) 787.
- [56] A.M. Staśto, K. Golec-Biernat, and J. Kwieciński, *Phys. Rev. Lett.* **86** (2001) 596.
- [57] V.N. Gribov and L.N. Lipatov, *Sov. Journ. Nucl. Phys.* **15** (1972) 438; G. Altarelli and G. Parisi, *Nucl. Phys.* **B126** (1977) 298; Yu. L. Dokshitzer, *Sov. Phys. JETP* **46** (1977) 641.
- [58] A. H. Mueller, *Nucl. Phys.* **B643** (2002) 501.
- [59] K. Golec-Biernat and M. Wüsthoff, *Phys. Rev.* **D59** (1999) 014017; *ibid.* **D60** (1999) 114023.
- [60] E. Iancu, K. Itakura and S. Munier, “*Saturation and BFKL dynamics in the HERA data at small x ,*” arXiv:hep-ph/0310338, to appear in *Phys. Lett. B*.